UNIVERSITY OF LONDON THESIS

Degree PhD Year 2006 Name of Author KRILLEKE Dominik

Structural and functional analysis of the heparin-binding domain of VEGF164

Dominik Krilleke

Endothelial Cell Biology Laboratory

Cancer Research UK, London

A thesis submitted for the degree of Doctor of Philosophy at the University of London

August 2006

ProQuest LLC
789 East Eisenhower Parkway
P.O. Box 1346
Ann Arbor, MI 48106-1346

Abstract

Several of the multitude of functions attributed to Vascular Endothelial Growth Factor-A (VEGF-A) are coordinated by its various isoforms, which are generated as a result of alternative splicing from a single gene. Despite the fact that the VEGF isoforms exhibit distinct biochemical properties, little has been done to clarify their functions and their contributions to physiological and pathological processes.

In this thesis I describe the biochemical and biological characterization of the heparin-binding domain of mouse VEGF164 through structure-function analysis. To investigate the functional significance of heparin binding, mutations were introduced into exon 7 of VEGF164 to identify essential residues for heparin binding. Three key amino acids involved in this interaction were identified. Mutants with alterations in these amino acids were unable to bind heparin and were compromised in their ability to bind to cell-surface heparan sulfate. These mutants, however, retained wild-type like potency in inducing tissue factor expression *in vitro* and microvessel growth *ex vivo*, and maintained the capacity to bind to the receptors neuropilin-1, VEGFR-1, and VEGFR-2.

A second goal of this work was to better define the role of VEGF164 in mediating inflammatory processes during pathological vascularization of the retina. Analysis of VEGF164-deficient ($VEGF^{120/188}$) mice subjected to neovascularization-inducing conditions and rats injected intravitreally with recombinant VEGF variants demonstrated that endogenous and exogenous VEGF164 increases leukocyte adhesiveness to retinal vessels compared to the non-heparin-binding isoform, VEGF120. Interestingly, the three basic residues that confer heparin binding of VEGF164, appear to be critical for its pro-inflammatory activity, but not for its angiogenic activity. In addition, both mutants (and VEGF120) exhibited a reduced affinity for VEGFR-1, a leukocyte-expressed receptor that mediates VEGF-induced migration. Results of *in vivo* experiments using PlGF, VEGF-E, as well as a VEGFR-1 neutralizing antibody, further demonstrate a role for VEGFR-1 in retinal leukostasis.

To my family

Acknowledgements

I wish to thank my supervisor Dave Shima who has been a magnificent teacher and whose enthusiasm and integral view on science has made a deep impression on me. I am also grateful to Greg Robinson and Eric Ng for stimulating discussions; Fiona Jucker for help with biochemical problems and for introducing me to the world of Structural Biology; Kazuaki Nishijima, Andrea de Erkenez, Michael Gee and Matthew Golding for skillful technical help. I would like to thank Anne Goodwin and Tracy Mitchell for critical reading of the manuscript. I also wish to express my gratitude towards the administrative teams at Cancer Research UK and (OSI) Eyetech for easing the transition of this work between two continents.

Financial support for this work was provided by Cancer Research UK and (OSI) Eyetech.

Table of contents

Chapter 5: *In vivo* functional analysis of the VEGF164 heparin-binding domain

Chapter 6: References

List of figures and tables

Abbreviations

BSA	bovine serum albumin
Con A	concanavalin A
E	embryonic day
ERK	extracellular signal-regulated protein kinase
FBS	fetal bovine serum
FGF	fibroblast growth factor
FGFR	fibroblast growth factor receptor
HBD	heparin-binding domain
HIF	hypoxia-inducible factor
HRP	horseradish peroxidase
HSPG	heparan sulfate proteoglycan
HUVEC	human umbilical vein endothelial cells
ICAM-1	intercellular adhesion molecule 1
IL	interleukin
MAPK	mitogen-activated protein kinase
MEK	mitogen-activated protein kinase kinase
MMP	matrix metalloproteinase
MCP-1	monocyte chemotactic protein
NMR	nuclear magnetic resonance
OIR	oxygen-induced proliferative retinopathy
P	postnatal day
PAE	porcine aortic endothelial cells
PBS	phosphate-buffered saline
PDGF	platelet-derived growth factor
PECAM	platelet endothelial cell adhesion molecule
PLC	phospholipase C
PCR	polymerase chain reaction
PlGF	placental growth factor
ROP	retinopathy of prematurity
SDS-PAGE	SDS-polyacrylamide gel electrophoresis
S-domains	sulfated domains
TF	tissue factor
TNFα	tumor necrosis factor α
UTR	untranslated region
VEGF	vascular endothelial growth factor
VEGFR	VEGF receptor
vHL	von Hippel-Lindau
VPF	vascular permeability factor

Chapter 1: Introduction

1.1 Vascular structure and development

The endothelium-lined vasculature is the first functional organ to form during embryonic development of vertebrates. A complex network of endothelial and supporting peri-endothelial cells perfuses all tissues in the body, satisfying the essential need for exchange of oxygen, nutrients and metabolic wastes between blood and tissues. Dysregulated formation of the vascular network is often lethal early in embryonic development, while abnormal vessel growth, particularly excessive angiogenesis, in the adult organism contributes to the pathogenesis of many disorders.

All blood vessels consist of at least two different cell types, endothelial cells and supporting mural cells. Endothelial cells form a single layer that lines the entire length of the vessel lumen and therefore serve as an interface between blood and the tissues. Because most of the exchange of particles between blood and tissue occurs in the capillaries, the capillary endothelial cells often exhibit remarkable morphological and functional heterogeneity in order to accommodate local physiological requirements [1]. For example, endothelial cells in the brain interact with astroglial cells, and the presence of tight junctions between continuous endothelial cells is essential for maintenance of the blood-brain barrier. On the other hand, capillaries of certain organs are discontinuous and highly fenestrated. This ensures efficient filtration in the kidney glomeruli, and allows exchange of metabolites and processing of toxins in the liver [2-5].

Vessel heterogeneity is also evident with regard to vessel wall coverage. Once endothelial cells have formed patent tubes, mural cells – that is, pericytes or smooth muscle cells – are

recruited to form the vascular wall. In large vessels, such as arteries and veins, multiple layers of vascular smooth muscle cells surround the endothelial tubes to provide structural support and contractile ability. In capillary beds, small vessels are covered by a single layer of specialized mural cells called pericytes. The association of smooth muscle cells and pericytes with newly formed vessels is essential for vascular maturation. These peri-endothelial cells control blood flow, regulate vascular branching and permeability, and protect vessels against rupture and regression [6]. Indeed, insufficient recruitment of mural cells results in leaky and fragile vessels, which are prone to bleeding and ultimately regress [7].

The endothelium is supported by a basal lamina, which separates the endothelial cell layer from the mural cells. The extracellular matrix provides necessary contacts between endothelial cells and the surrounding tissues and consists mainly of proteoglycans, collagen fibers, and multiadhesive matrix proteins. Remodeling of the extracellular matrix by proteinases plays a key role in regulating vessel sprouting and pruning. Matrix-bound growth factors and chemokines are released that can promote or inhibit angiogenesis. Furthermore, proteinases are able to expose cryptic epitopes or generate fragments of extracellular matrix components, which then regulate angiogenesis [8]. The endothelium and mural cells, together with the basement membrane, form the basic architecture of the vessel. Through reciprocal interactions between the cells of the vasculature and their local environment, including the extracellular matrix and parenchymal cells, vessels acquire specialized functions in different vascular beds [9].

The assembly of blood vessels is commonly thought to occur through two mechanisms: vasculogenesis, the *de novo* formation of blood vessels from angioblasts, which are

mesoderm-derived endothelial cell precursors that differentiate into endothelial cells and assemble a primary capillary plexus [10], and angiogenesis, the generation of new blood vessels via sprouting and branching from pre-existing capillaries [2, 11]. Vasculogenesis describes the establishment of the primary, albeit immature and poorly functional, vascular network, whereas the expansion and remodeling of this network is accomplished by angiogenesis. Because the vasculature is usually quiescent in the adult, growth of new blood vessels rarely occurs at this stage. The few adult tissues that do require ongoing angiogenesis include the female reproductive organs and injured tissues. In addition, physiological organ growth and increases in vascular density in cardiac and skeletal muscle also depend on angiogenesis [12-15]. As a whole, physiological angiogenesis in the adult is a highly regulated process in which the new vessels rapidly mature, becoming stable and quiescent. By contrast, uncontrolled angiogenesis often occurs in pathological conditions, with abnormal vessel patterns and morphology due to an imbalance of pro- and antiangiogenic signals [16]. Well-known examples of pathological angiogenesis occur in cancer, psoriasis, arthritis and diseases in the back of the eye, often associated with blindness [17].

While in humans most organs are vascularized before birth, vascularization of the mouse retina occurs postnatally and can therefore be used to model physiological angiogenesis. Immediately after birth the superficial vascular system starts to develop, originating from the optic nerve and extending radially along the vitreoretinal interface to fill the peripheral avascular retina. This vascularization is guided by vascular endothelial growth factor (VEGF)-secreting astrocytes [18]. Around postnatal day (P) 7, vessels then invade into the retina by sprouting to form the intermediary and deep capillary beds. This creates a three-

dimensional network consisting of three horizontal microvessel layers, as well as vertical connecting capillaries. Finally, selective pruning of retinal capillaries immediately following formation of the primary vascular plexus, in response to various factors such as hyperoxia and immune cells, leaves behind a remodeled, smaller-caliber vasculature with distinct hierarchy of vessel size [19, 20]. Because of its accessibility for manipulation, the neonatal retina has been increasingly used as a model for studying molecular and cellular mechanisms of blood vessel development, both during normal development and during progression of retinopathies [21, 22] (and references therein).

1.2 The multifunctional role of VEGF

VEGF and its receptors (VEGFR-1-3) form a paracrine system that is likely the most important in controlling vascular development and neovascularization. This system controls physiological and pathological vascularization, in both the embryo and the adult [23]. Several lines of evidence can be put forward in support of this view. Firstly, expression patterns of VEGF and its receptors correlate both temporally and spatially with areas of vascular growth in developing embryos [24-26]. Secondly, embryos lacking either VEGF or one of its receptors fail to develop functional vessels [27-31]. Thirdly, VEGF is haplo-insufficient; the lack of even one allele results in severe disruption of vessel development and embryonic lethality, suggesting that the correct dosage of VEGF is critical for normal vascular development [27, 28, 32]. Fourthly, VEGF levels are increased in conditions involving pathological angiogenesis [33]. Lastly, antagonists of VEGF or its receptors are potent inhibitors of pathological angiogenesis [34-38].

1.2.1 VEGF: history of the angiogenic "Factor X"

The quest for angiogenic factors in the last decades was mainly driven by the observation that neovascularization is involved in the progression of many pathologies, and by the hope that identification of angiogenic factors could lead to new treatments for these diseases. Based on early observations that some human tumors are highly vascularized and that the tumor environment has an influence on tumor vessel characteristics, Ide and coworkers found that the transplantation of tumors into the rabbit ear causes a strong neovascular response, which led them to propose that tumor cells release growth factors that promote blood vessel formation [33]. In 1945, this hypothesis was advanced in a study led by Glenn Algire, who for the first time used a quantitative approach to assess blood vessel growth in mice [39]. By counting blood vessels and comparing them to tumor size, Algire and colleagues found that rapid growth in size of transplanted tumors followed vascular growth; they concluded that the ability to promote vascular proliferation gives the tumor increased autonomy compared to normal tissues [39]. Isaac Michaelson was the first to hypothesize the existence of an angiogenic 'Factor X', which he thought was causal for pathologic neovascularization in the retina [39]. Efforts to find this factor culminated in the isolation of highly purified protein from conditioned medium and subsequent cDNA cloning of VEGF and vascular permeability factor (VPF) by two independent groups in 1989 [40, 41]. It soon became apparent that VEGF and VPF were the same molecule, which was able to mediate such seemingly unrelated activities as endothelial cell mitogenesis and vascular permeability. It is now clear that VEGF elicits an array of responses by vascular endothelial cells, including proliferation, migration, permeability, survival, and upregulation of proinflammatory gene expression [33].

1.2.2 The activities of VEGF

From the year of its discovery, the role of VEGF in regulating angiogenesis and vasculogenesis has been the subject of intense investigation. Studies have concentrated primarily on the roles of this factor during vascular development and in the etiology of diseases that are associated with abnormal angiogenesis. VEGF promotes both proliferation and survival of cultured endothelial cells [33]. It also induces growth and sprouting of blood vessels in a number of in vivo models, including the chick chorioallantoic membrane assay [40], the Matrigel plug in mice [42] and the corneal pocket assay [43]. Mitogenic signaling is mediated by the ERK/MAPK cascade, which can be activated in two ways: via Ras-dependent induction of the Raf-1/MEK/ERK cascade [44, 45] and via Ras-independent phosphorylation of phospholipase C (PLC)-γ and subsequent activation of the ERK pathway [46-48].

In cell culture assays, the prosurvival effects of VEGF are transduced via VEGFR-2, also known as Flk-1, and mediated mainly by the phosphatidylinositol (PI)-3 kinase/protein kinase B (Akt) pathway [49, 50]. Akt is highly expressed in endothelial cells, where it inhibits proapoptotic proteins such as Bad and caspase-9 [51]. *In vivo*, VEGF is essential for growth and survival in early postnatal life, but its role in endothelial cell survival in the adult animal has been controversial. One group recently reported that depletion of VEGF in adult mice by administration of a neutralizing antibody or soluble VEGFR-1 causes proteinuria and glomerular endothelial cell detachment [52]. However, other studies suggest that VEGF inhibition has no significant effect on glomerular function in fully developed healthy mice, though it may be important for the regeneration of injured glomerular endothelial cells [53, 54].

In addition to promoting proliferation and survival, VEGF induces the migration of endothelial cells and other cell types, including hematopoietic stem cells, monocytes, osteoblasts and, as recently shown, branchiomotor neurons [55-59]. Upon VEGF stimulation, endothelial cells migrate into perivascular areas, a process that requires cytoskeletal reorganization and localized degradation of the extracellular matrix. VEGF forms a chemotactic gradient to attract endothelial cells, and upregulates or activates proteolytic enzymes to promote tissue invasion. The chemotactic role of VEGF appears to be evolutionarily conserved. In *Drosophila,* VEGF controls the migration of VEGFR-expressing blood cells, indicating an ancestral role for this factor in hematopoiesis [60]. In a recent study, Ruhrberg et al. have shown that blood vessel tips extend along rising VEGF concentration gradients in the midline region of the developing mouse hindbrain [61, 62]. Disruption of these gradients clearly impaired the directed extension of vessel tip filopodia, resulting in vessel branching defects [61, 62]. VEGF is also a potent chemoattractant for monocytes, a cell type implicated in pathological angiogenesis, and can both activate monocytes and induce monocyte chemotaxis across endothelial cell monolayers [58].

Endothelial cells accommodate the specific needs of certain surrounding tissues by displaying specialized characteristics, and VEGF levels likely mediate these specific endothelial phenotypes. In particular, degrees of vascular permeability have been correlated with differing levels of VEGF expression. The permeability of the blood-brain-barrier endothelium must be low in order to ensure a tight barrier that prevents toxic substances from entering the brain. VEGF expression levels in the brain are dramatically decreased in the adult compared to levels during embryonic angiogenesis [63]. Conversely, the vessels of the kidney must maintain a high level of permeability to facilitate the

exchange of metabolites, and VEGF and its receptors are highly expressed in this adult tissue [64]. In the kidney glomerulus, where fluid filtration occurs, and in endocrine organs, which secrete particles into the blood, endothelial cells are discontinuous and fenestrated [65]. Fenestrae are circular membrane pores, usually containing a diaphragm, that span the entire thickness of highly attenuated endothelia and thus provide a route for transcellular permeability [66]. VEGF promotes the formation of fenestrae, either when added to cultured endothelial cells or when injected into certain tissues [65, 67]. While the molecular mechanisms for this process are almost completely unknown, the rapidness of the induction suggests that fenestrae formation relies on reorganization of pre-existing cytoskeletal components rather than *de novo* gene transcription.

1.2.3 Regulation of VEGF expression

In vitro, several mechanisms have been shown to regulate the expression of VEGF, including growth factors and cytokines, cellular transformation, and low oxygen tension [23, 68, 69]. Cytokines and growth factors that induce VEGF mRNA expression or VEGF release in cultured cells include epidermal growth factor (EGF), transforming growth factor-β (TGF-β), platelet-derived growth factor (PDGF), insulin-like growth factor (IGF)-1 and stromal-derived factor (SDF)-1 [70-74]. Certain pro-inflammatory cytokines, such as tumor necrosis factor-α (TNF-α), interleukin (IL)-6 and IL-1β, induce expression of VEGF, suggesting a role for VEGF as mediator in inflammatory disorders [75-77]. Although these pro-inflammatory cytokines lack direct angiogenic effects, many can indirectly induce angiogenesis through upregulation of VEGF. In addition, some of these factors are upregulated by VEGF, suggesting autocrine and paracrine loop mechanisms

that may potentiate VEGF effects. The relevance of these indirect angiogenic stimulants for normal and pathological angiogenesis has yet to be fully examined.

Certain transforming events can also modulate VEGF expression. The von Hippel-Lindau (*VHL)* tumor suppressor gene encodes the vHL protein, an inhibitor of hypoxia-regulated proteins. Mutations in *VHL* result in increased expression of VEGF in cerebellar hemangioblastomas and human renal carcinomas [78, 79]. VEGF expression is also increased following loss of the wild-type tumor suppressor gene *p53*, and as a result of mutation or overexpression of H-ras, v-src, or v-raf during transformation of fibroblasts or epithelial cells [80-82]. Because tumor growth usually depends on angiogenesis, genetic changes that favor VEGF expression promote rapid and sustained tissue growth.

The third type of signal that regulates VEGF expression, low oxygen tension or hypoxia, is the most important inducer of VEGF gene expression. Indeed, virtually all cell types increase VEGF expression under hypoxic conditions [83, 84]. Hypoxia-induced upregulation of VEGF is a fundamental physiological mechanism to adapt the vascular network to low tissue oxygenation both in the growing and physiologically hypoxic embryo, and in response to pathological circumstances in the adult organism such as chronic hypoxia or ischemic insults [85, 86]. A well-characterized example of hypoxia-induced VEGF production in developmental organogenesis is the formation of the retinal vascular network. As astrocytes and other neuroglial cells migrate away from existing blood vessels in the developing retina, they encounter increasingly hypoxic conditions and in response secrete increasing levels of VEGF. The VEGF concentration gradient thus resulting allows new blood vessels to grow toward the VEGF source, following the

migration of the astrocytes until the oxygen demand is accommodated [87]. Upregulation of VEGF under hypoxic conditions is achieved by activation of two transcription factors, hypoxia-inducible factor (HIF)-1 and -2, and by an increase in VEGF mRNA stability [88-91]. The protein levels of the HIF-1α subunit are downregulated in normoxic cells by ubiquitination and proteasomal degradation, a process that is mediated by the tumor suppressor vHL [92]. When activated by low oxygen tension, HIF-1 accumulates and translocates to the nucleus, where it binds to the hypoxia response element (HRE) located in the 5' and 3' untranslated region (UTR) of the VEGF gene, resulting in activation of VEGF gene transcription [85]. The important role of HIF-1 in mediating VEGF expression during embryonic development and tumor angiogenesis has been confirmed by targeted disruption of the HIF-1α gene [93, 94]. Loss of the HIF-1α gene in these mice reduces hypoxia-induced expression of VEGF. In addition to transcriptional control, VEGF levels under hypoxic conditions are increased via regulation of mRNA stability. This increased stabilization occurs when as yet unidentified proteins bind to the 3' UTR of the VEGF mRNA, thereby preventing normal turnover of the VEGF transcript [95, 96].

1.3 Biochemical and biological properties of VEGF

1.3.1 *VEGF* gene structure and splice forms

VEGF-A (henceforth referred to as VEGF) is the most prominent member of the PDGF/VEGF family of growth factors, a family that includes placental growth factor (PlGF), VEGF-B, VEGF-C, VEGF-D, the ORF virus-derived VEGF-E variants, and the recently identified VEGF-F [97-99]. VEGFs are present in all vertebrate species with a high degree of sequence homology. Homologues have been found in invertebrates,

including *Drosophila*, *C. elegans* and jellyfish, pointing to a role for VEGF in orchestrating elemental developmental functions [100-102]. The human *VEGF* gene spans approximately 14 kb and contains eight exons separated by seven introns [103, 104]. At least five isoforms of 121, 145, 165, 189 and 206 amino acids after signal peptide cleavage are produced from a single gene by alternative RNA splicing [103-107] (Figure 1.1). The corresponding murine splice products, VEGF120, VEGF144, VEGF164 and VEGF188 (the mouse homolog of human VEGF206 has not been identified) contain one less amino acid than their human counterparts but are thought to posses the same biochemical properties and exert similar activities. Recently, a subspecies of human VEGF165, VEGF165b, was identified in a PCR-screen examining the differential expression of VEGF isoforms in renal carcinoma cells [108]. This variant, which contains an alternative exon 8, was found to be downregulated in malignant cells. It was further shown to inhibit VEGF-induced proliferation and migration *in vitro* as well as angiogenesis *in vivo,* suggesting a role for this splice form as endogenous inhibitor of angiogenesis [108, 109]. Another RNA splice form, VEGF162, was detected in a human ovarian carcinoma cell line [110]. The purified protein bound heparin with high affinity due to the presence of exon 6A- and 6B-encoded peptides, and was mitogenic and angiogenic [110], but its specific biological role remains unidentified.

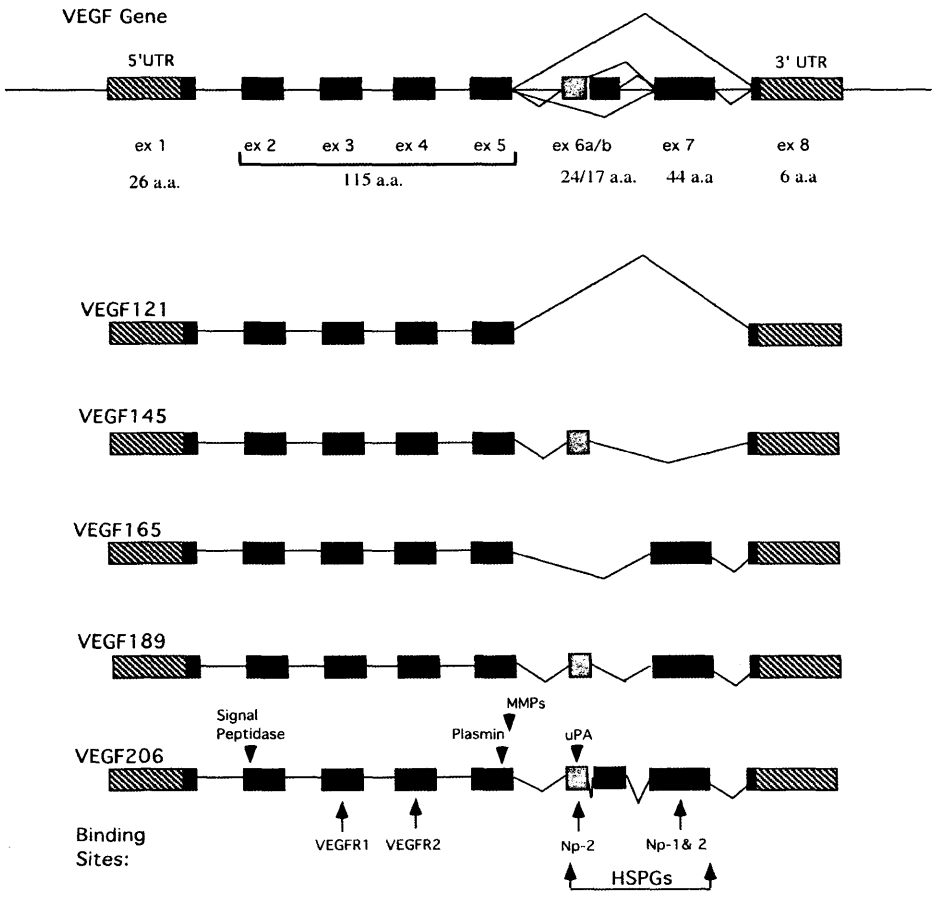

Figure 1.1 Exon structure of the splice variants of human VEGF. The eight exons of the human VEGF-A gene are alternatively spliced to produce at least five isoforms that differ in total amino acid number. The length of some individual exon-encoded polypeptides and the exon number from which they derive are shown at the top of the figure. 5'- and 3'-untranslated regions (UTR) are represented by diagonal lines and introns are represented by horizontal lines. Introns and exons are not drawn to scale. The signal peptide cleavage site in the exon 2-encoded domain and other enzyme cleavage sites are marked by arrowheads. Abbreviations: a.a., amino acids; ex, exon; MMP, matrix metalloproteinase; uPA, urokinase-type plasminogen activator; Np, neuropilin; HSPGs, heparan sulfate proteoglycans. Courtesy of Y.S. Ng.

1.3.2 VEGF protein structure

VEGF is a dimeric glycoprotein that belongs to the cysteine knot family of growth factors [111, 112]. Members of this family contain eight conserved cysteine residues in each monomer, forming the typical disulphide bonded knot motif that is thought to be a major determinant for the stability of these growth factors [111, 113]. In VEGF, two monomers are covalently linked by two interchain disulfide bridges between cysteine 51 and cysteine 60 to form an antiparallel homodimer [114]. A hydrophobic signal sequence, essential for dimerization and secretion, is encoded by exon 1 and four residues of exon 2 and is cleaved off during secretion [40, 41, 115]. All VEGF splice forms share the same amino (N) -terminal amino acid sequence encoded by exons 1 to 5, containing high-affinity binding sites for the receptor tyrosine kinases VEGFR-1 and VEGFR-2. Crystal structure studies and site-directed mutagenesis have identified symmetrical receptor binding sites located at each pole of the VEGF homodimer [114, 116]. Binding to these poles appears to be important for receptor dimerization and signaling [117]. While sharing the same N-terminus, the VEGF transcripts all differ by the presence or absence of sequences encoded by exons 6 and 7. This region encodes two heparin-binding domains (HBDs), each of which confers the ability to bind heparin [118]. The HBD of VEGF165 is located to the exon 7-encoded peptide (Figure 1.2). The structure of both the N- and the C-terminal binding domains of VEGF have been solved separately by X-ray crystallography and NMR, respectively [116, 119]. In addition, the HBD structure has been characterized [119, 120].

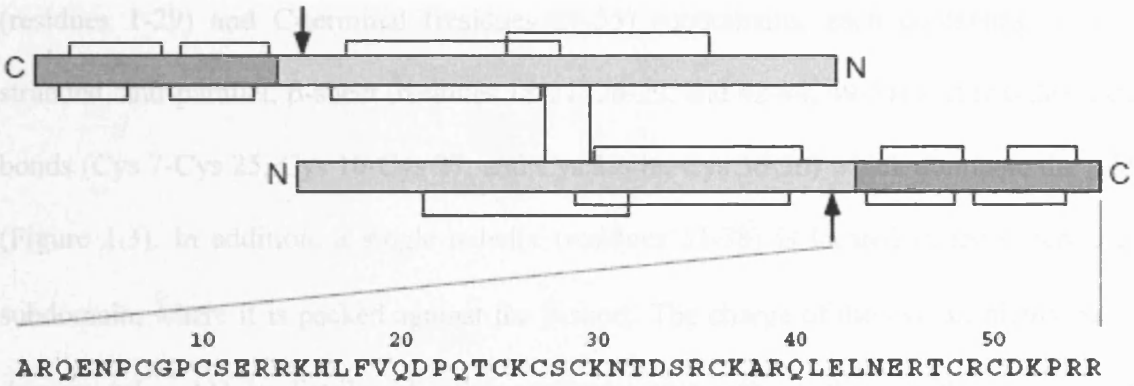

Figure 1.2 Schematic representation of VEGF165. The VEGF165 isoform is a homodimeric protein with a 55-residue HBD (VEGF111-165) located in the C-terminal region of each monomer. This domain is defined by the plasmin cleavage site (arrow) in the exon 5-encoded domain and includes the C-terminal part of exon 5 as well as exon 7 and 8 (dark-shaded regions). The amino acid sequence of the HBD is shown at the bottom. Intermolecular and intramolecular disulfide bridges are represented by lines. Adapted from W. Fairbrother et al. [119].

1.3.3 The HBD of VEGF165

Since the HBD plays such a critical role in determining VEGF isoform localization and function, it is important to understand the characteristics of this domain. The structure of the VEGF165 HBD produced by plasmin cleavage of the full-length protein has been determined by a group at Genentech [119, 120]. Neither the sequence nor structure of this 55-residue C-terminal fragment (VEGF111-165) bears any similarity to known heparin-binding proteins outside the VEGF family of growth factors, suggesting that the HBD has a novel fold [121]. This fragment binds heparin with the same affinity as the full-length isoform, demonstrating that all heparin-binding activity of VEGF164/165 is indeed

confined to this domain [118]. The HBD is comprised of clearly defined N-terminal (residues 1-29) and C-terminal (residues 29-55) subdomains, each containing a two-stranded, anti-parallel, β-sheet (residues 18-21, 26-29, and 42-44, 49-51) and two disulfide bonds (Cys 7-Cys 25, Cys 10-Cys 27, and Cys 29-48, Cys 36-50) which dominate the fold (Figure 1.3). In addition, a single α-helix (residues 33-38) is located in the C-terminal subdomain, where it is packed against the β-sheet. The charge of the overall highly basic domain (pI ~ 11) is distributed rather unevenly across the surface, with a surplus of positively or negatively charged amino acids on each side of the domain. It has been suggested that an area with a high density of positively charged side chains on one side of the N-terminal subdomain (Lys 30, Arg 35, Arg 39, and Arg 46) may represent a major heparin-binding site [119]. However, the loop region at the interface of the two subdomains (residues 11-17) and the relative orientation of the subdomains within the HBD remain poorly defined. The increased flexibility of this domain compared to the remainder of the protein complicates accurate prediction of heparin-binding sites within the HBD.

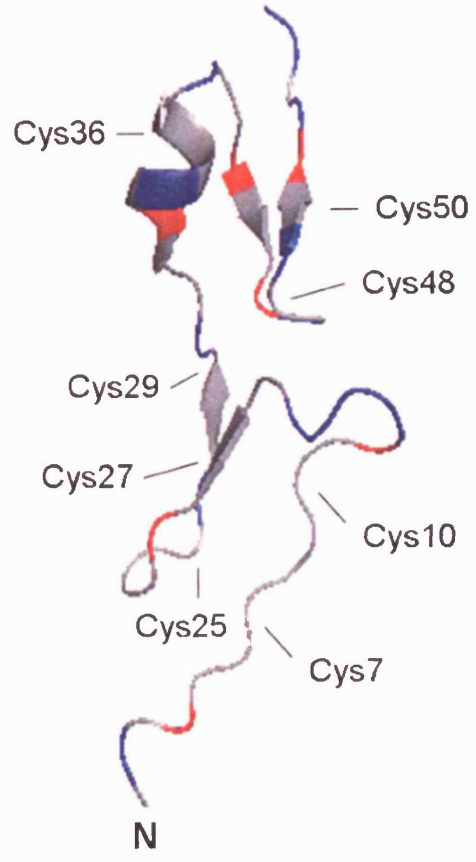

Figure 1.3 Structural fold of the VEGF165 HBD. Stereo ribbon diagram of the VEGF165 HBD with secondary structure elements. The cysteines shown are all involved in the formation of disulfide bonds. Charged residues are color coded, with basic residues depicted in blue and acidic residues depicted in red. Numbering of residues is according to the primary amino acid sequence shown in Figure 1.2. The diagram was produced using PyMOL (DeLano Scientific) based on published NMR data (PDB code: 1KMX).

1.3.4 The VEGF isoforms: extracellular distribution

Although at least five human VEGF isoforms have been identified to date, most VEGF-secreting cells appear to preferentially express VEGF121, VEGF165 and VEGF189. These variants have a wide tissue distribution, whereas the less common VEGF145 and

VEGF206 are only expressed in the female reproductive system [122, 123]. The VEGF isoforms have distinct biochemical properties. Perhaps the most striking feature is the differential binding affinity for heparin. *In vivo*, heparin affinity translates into the ability to interact with heparan sulfate and heparan sulfate proteoglycans (HSPGs) on cell surfaces and basement membranes, therefore representing a major determinant for the localization of the isoforms in the extracellular space [124]. VEGF121, the shortest isoform, lacks both the exon 6- and exon 7-encoded HBDs. This isoform is freely released from cells upon secretion and can therefore diffuse relatively long distances. The larger isoforms VEGF189 and VEGF206 are highly basic and bind heparin strongly due to the presence of two independent heparin-binding regions located in exon 6a and exon 7. Consequently, these proteins are almost completely sequestered in the extracellular matrix and on the cell surface [124, 125]. VEGF145 binds to the extracellular matrix but shows decreased heparin-binding activity relative to VEGF189 because it lacks the exon 7-encoded peptide sequence [106]. VEGF165, the prototypic and most abundant VEGF isoform, displays only a moderate affinity for heparin and differs from VEGF121 by the inclusion of a basic peptide encompassing 44 residues encoded by exon 7. This peptide also contains binding sites for neuropilin-1 and neuropilin-2 [126, 127]. The proportion of VEGF165 associated with the extracellular matrix was reported to be 50-70%, which enables this isoform to act in a dual fashion, as both a soluble and a cell-bound factor [128-130].

Through production of both soluble and matrix-bound forms of VEGF, bioavailability and spatial distribution of this factor around endothelial cells can be controlled. Indeed, a finely balanced VEGF concentration gradient consisting of isoforms with differential heparin-binding affinities seems to be necessary for proper blood vessel branching morphogenesis

in the mouse hindbrain [61]. It is important, however, that mechanisms exist to release VEGF from the extracellular matrix.

1.3.5 Processing of VEGF in the extracellular milieu

The cell surface-bound and extracellular matrix-associated isoforms are thought to constitute a reservoir of growth factors, which can be released into the extracellular milieu as active proteins without the need to initiate gene transcription. This can occur either by displacing the isoform with heparin or HSPGs, by exposure to heparinases; or more rapidly, by specific proteases such as plasmin and urokinase-type plasminogen activator [124, 131]. Plasmin cleavage of VEGF165 and VEGF189 releases a homodimeric, non-heparin-binding 34-kDa fragment that consists of amino acids 1-110 (VEGF110). Although this fragment contains the binding domains for VEGFR-1 and VEGFR-2, the endothelial cell mitogenic potential of VEGF110 was significantly less than that of VEGF165 *in vitro* [118].

Another example for the mobilization of cell-bound VEGF by proteolytic activity was reported in a study by Plouet et al. [131]. In this study, VEGF189 was shown to undergo a maturation process mediated by the serine protease urokinase. Cleavage by urokinase was required to convert VEGF189 from an inactive precursor state to a smaller, mature version, which was able to potently induce a mitogenic effect *in vitro*. By cleaving VEGF within the exon 6-encoded region, urokinase activity is thought to expose the VEGFR-2-binding site, which is obscured in the full-length version. Matrix metalloproteinases (MMPs) have also been implicated in the mobilization of extracellular

matrix-bound VEGF. The degradation of the basement membrane and extracellular matrix catalyzed by MMPs, which allows endothelial cells to proliferate and migrate toward an angiogenic stimulus, also releases matrix-bound VEGF isoforms. Recently, it has become evident that MMPs can precisely cleave extracellular matrix-associated molecules, thereby liberating bioactive fragments and growth factors [132]. Immobilized VEGF165 and VEGF189 can be cleaved intramolecularly by certain proteases of the metalloproteinase family, and the unprocessed and processed forms exert different activities in vascular morphogenesis [133].

1.4 The VEGF receptors

VEGF family members can bind to type III tyrosine kinase receptors, neuropilins, and HSPGs (Figure 1.4). Cellular responses to VEGF are primarily mediated by the binding of this factor to the type III tyrosine kinase receptors VEGFR-1 and VEGFR-2, to the semaphorin receptor neuropilin-1, and to HSPGs.

1.4.1 The VEGF tyrosine kinase receptors

VEGFR-1 and VEGFR-2 have been identified as high-affinity transmembrane receptor tyrosine kinases for VEGF [134, 135]. The two receptors share a 44% amino acid identity and both contain seven extracellular immunoglobulin-like domains, a single transmembrane region, and a conserved intracellular tyrosine kinase sequence interrupted by a kinase-insert domain [136, 137]. VEGFR-3 (also known as Flt-4), the third member of this receptor family, is a receptor for VEGF-C and VEGF-D, but not for VEGF [138, 139].

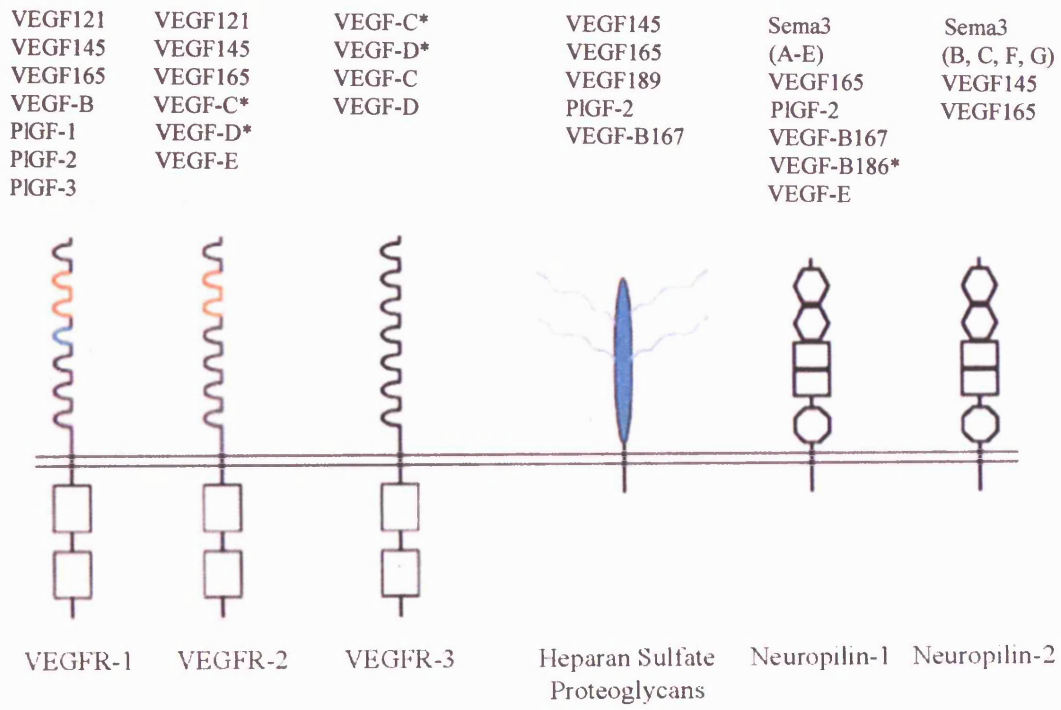

Figure 1.4 The cell-surface receptors for VEGF. The monomeric VEGF tyrosine kinase receptors (VEGFR-1, VEGFR-2 and VEGFR-3), membrane-associated heparan sulfate proteoglycans and the non-tyrosine kinase receptors neuropilin-1 and neuropilin-2 are displayed with their characteristic structural features and identified ligands listed above. Ig-like domains 2 and 3 of VEGFR-1 and VEGFR-2 (shown in orange) have been shown to be important for high-affinity ligand binding, and domain 4 (shown in blue) is believed to mediate receptor dimerization for VEGFR-1. Both the unprocessed and proteolytically processed (*) forms of VEGF-C and VEGF-D can bind to VEGFR-3. Only the processed forms of VEGF-C and –D bind to VEGFR-2, but their binding affinity is significantly weaker than that of VEGF-A for VEGFR-2. Ligands for heparan sulfate proteoglycans are thought to interact with specific sequences of sulfation within the heparan sulfate chains, which are attached to a core protein (shown in blue). Binding of the VEGF-B186 splice form to neuropilin-1 is regulated by proteolytic processing (*). VEGF-E is a collective term for a group of VEGF-like proteins that are encoded by certain strains of the *Orf* virus. Some members of this group, including $ORFV_{NZ10}VEGF$, $ORFV_{NZ2}VEGF$, and $ORFV_{D1701}VEGF$, were shown to bind to neuropilin-1 with varying affinities [357]. Adapted from Neufeld, G. et al. [68].

1.4.1.1 VEGFR-2: the major signaling receptor

VEGFR-2, also known as Flk-1 or KDR, has been identified as a major regulator of vasculogenesis and angiogenesis. It is considered to be the most important signaling receptor for VEGF, mediating most of its biological activities in endothelial cells. Binding of VEGF induces dimerization of the monomeric receptors, which results in autophosphorylation at several specific tyrosine residues of the cytoplasmic domains. The mode of ligand binding is similar for both receptors. Two receptor monomers bind one VEGF dimer, in such a way that each receptor molecule binds to the pole of each monomer at opposite ends of the ligand homodimer, in which the monomers are arranged in a head-to-tail orientation [68, 116, 140]. The immunoglobulin domains 2 and 3 are necessary and sufficient for VEGF binding [116, 140-142]. Ligand-induced dimerization of VEGFR-2 leads to efficient phosphorylation of tyrosine residues [135, 143, 144]. Upon activation of VEGFR-2, autophosphorylated tyrosines create binding sites for several Src homology-2 (SH2) domain-containing proteins, such as PLC-γ or Grb2, leading to the phosphorylation and activation of these proteins. This mechanism has been implicated in the activation of the Raf-1/MEK/ERK cascade, a crucial signaling pathway, resulting in endothelial cell proliferation and angiogenesis [45, 46, 145].

Expression of VEGFR-2 has been detected in endothelial and other mature vascular cells, as well as in endothelial and hematopoetic precursor cells [146, 147]. Mice deficient in Flk-1 (murine VEGFR-2) die between embryonic day (E) 8.5 and E9.5, exhibiting a lack of yolk sac blood islands and organized blood vessels [30], a phenotype that is not surprising given that the proliferation and migration of hematopoietic/endothelial progenitor cells requires signaling through Flk-1 [148]. Certain tumorigenic cell types also

express VEGFR-2, including human melanoma cells and cells from acute and chronic forms of leukemia [149, 150]. Interestingly, VEGFR-2 expression has also been described in neural progenitor cells of the retina, in neurons of the superior cervical and dorsal root ganglia, and in Schwann cells [151, 152]. These findings led to the hypothesis that VEGFR-2 may transmit neurotrophic and even neuroprotective signals [152].

1.4.1.2 VEGFR-1

The transmembrane receptor tyrosine kinase VEGFR-1, also known as Flt-1, was the first receptor identified for VEGF. Ligands for this receptor also include the related growth factors PlGF and VEGF-B. VEGFR-1 is expressed on vascular endothelium and in some non-endothelial cells, including hematopoietic stem cells, macrophages and monocytes [26, 153, 154]. Inactivation of the VEGFR-1 gene in mice leads to death *in utero* between E8.5 and E9.5, due to a failure of endothelial cells to organize in functional blood vessels. The lack of vessel formation in these animals has been linked to an abnormal increase in the number of endothelial progenitors, indicating that VEGFR-1 may act as a negative regulator of VEGF function during development [155]. In support of this view, activation of the VEGFR-1 kinase in wild-type endothelial cells does not appear to cause direct proliferative, migratory or permeability effects, and upregulation of putative downstream signaling molecules has only been observed in heterologous cell types or in cells overexpressing this receptor [143, 156-160]. In contrast to the critical role of tyrosine phosphorylation in VEGFR-2 function, deletion of the VEGFR-1 tyrosine kinase domain, with the ligand binding domain unaffected, was compatible with normal vascular development and angiogenesis [161, 162]. These observations suggest a role for VEGFR-1 in controlling VEGF availability by sequestering excess VEGF. Such a 'decoy' function

can also be performed by a truncated, soluble form of VEGFR-1 (sFlt-1), which has the same ligand binding affinity as the full-length version despite lacking the transmembrane and intracellular domains [163, 164].

While VEGFR-1 tyrosine kinase activity appears to be expendable for developmental vascular development, this activity is required for other physiological and pathological functions. For example, chemotaxis of monocytes and macrophages in response to both VEGF and PlGF depends on the tyrosine kinase activity of this receptor [161, 165, 166]. Both cell types are known to express VEGFR-1 as the sole VEGF receptor. Indeed, macrophage migration towards VEGF or PlGF was strongly suppressed in VEGFR-1 tyrosine kinase-deficient (VEGFR-1/Tk$^{-/-}$) mice [161]. These data were complemented by a recent study in which PlGF signaling via VEGFR-1 was reported to activate monocytes, leading to production of inflammatory cytokines and chemokines including TNF-α, IL-1β and monocyte chemotactic protein (MCP-1) [167].

There is mounting evidence indicating that VEGFR-1-mediated signaling may have a significant role in pathological angiogenesis. In a recent study, Carmeliet et al. observed that PlGF binding to VEGFR-1 specifically enhanced VEGF-induced angiogenesis through VEGFR-2 in a mouse model of ischemia [163]. Furthermore, injection of an anti-VEGFR-1 antibody into tumor-bearing mice suppressed neovascularization of tumors to an extent similar to that of anti-VEGFR-2 treatment [168]. Autiero and coworkers found evidence for a new mechanism of VEGFR-1 activity, in which PlGF can activate intermolecular cross-talk between VEGFR-1 and -2, thereby enhancing VEGF signaling through VEGFR-2. According to this study, PlGF - but not VEGF - stimulates the phosphorylation of

distinct VEGFR-1 tyrosine residues, resulting in transphosphorylation and activation of the VEGFR-2 kinase [169]. Interestingly, although PlGF and VEGF bind similar domains in VEGFR-1, each ligand induces a different pattern of gene expression and induces, at least in part, different biological responses [169-171].

The apparently contrasting activities of VEGFR-1, inhibition and enhancement of VEGF signaling via VEGFR-2, may be partly explained by correlations between VEGFR-1 function and cell type, developmental stage or pathological condition. While under certain pathological circumstances in the adult organism VEGFR-1 can act as a positive signal transducer and mediator of angiogenesis, its function in embryonic angiogenesis is primarily the depletion of excess ligand [172]. Furthermore, while the heparin binding isoform VEGF165 binds to VEGFR-1 with higher affinity than does VEGF121, it is not yet known whether this difference in binding affinity translates into distinct biological responses [118]. Another complication in elucidating VEGFR-1- and VEGFR-2-mediated signaling outcomes in response to VEGF is the presence of further interaction partners such as the neuropilins and the HSPGs. Association with these species, either directly or indirectly through binding to VEGF, may potentially modulate VEGF receptor behavior.

1.4.2 Neuropilin-1: a VEGF isoform-specific receptor

Another VEGF receptor, which is expressed on endothelial and tumor cells, as well as on neurons and vascular smooth muscle cells, specifically binds to the exon 7-encoded heparin-binding domain of VEGF165 and was found to be identical to neuropilin-1 [126, 179, 180]. Neuropilin-1 is a single-spanning transmembrane protein with a short

cytoplasmic domain of about 40 amino acids and five extracellular domains, a1/a2, b1/b2, and c. The a1/a2 domains and the b1/b2 domains contain the binding sites for class-III semaphorins and VEGF165, respectively, and the c domain mediates the formation of functional homodimers and heterodimers with neuropilin-2 [173, 174]. Neuropilin-1 was originally characterized as a neuronal receptor for axon repellent factors belonging to the class-III semaphorin subfamily [175, 176]. Both neuropilin-1 and neuropilin-2 control neuronal guidance at the growth cone of axons by forming ligand-independent complexes with receptors of the plexin family, which act as signal-transducers in response to semaphorin binding [177, 178].

The discovery of neuropilin-1 as a VEGF receptor was intriguing, as it substantiated previous observations in transgenic mice that indicated a role for this neuronal receptor in the vascular system. Overexpression of neuropilin-1 in mice causes excessive formation of dilated capillaries and blood vessels; ablation of the neuropilin-1 gene, on the other hand, results in insufficient vascularization of the yolk sac and neural tube, as well as cardiovascular defects, leading to embryonic death at E10.5-E12.5 [179, 180]. Morpholino-mediated knock-down of neuropilin-1 in zebrafish embryos results in impaired blood cell circulation in the intersegmental vessels, similar to the defect caused by inhibition of the VEGFR-2 kinase in this organism [181]. These observations suggest that VEGFR-2 cannot sufficiently transduce VEGF signals in the absence of neuropilin-1. Neuropilin-1 does not appear to mediate VEGF signals independent of other receptors. No direct effects have been observed after ligation of neuropilin-1 to VEGF165 or other VEGF-related neuropilin-1 ligands, including PlGF-2, VEGF-B and the VEGF-E variant $VEGF_{NZ2}$ [182-184]. Co-expression of neuropilin-1 and VEGFR-2, however, results in an enhanced VEGF-induced cell migratory response compared to cells expressing VEGFR-2

alone [126]. Similarly, VEGF165 is a more potent inducer of VEGFR-2 phosphorylation in HUVEC than is non-neuropilin-binding VEGF121 [185]. The role of neuropilin in mediating this effect was confirmed using a PlGF-derived peptide that specifically competes with VEGF165 for binding to neuropilin-1. The peptide antagonized VEGF signaling via VEGFR-2 in an isoform-specific manner, suggesting that the ability of VEGF165 to bind to the VEGFR-2/neuropilin-1 complex may explain the difference in potency between VEGF165 and VEGF121 [185].

Surprisingly, the increased potency of VEGF165 in the presence of neuropilin-1 does not seem to result from an increase in binding affinity to VEGFR-2, but rather is the consequence of increased complex formation between the two receptors [185]. Neuropilin-1 does not bind VEGFR-2 directly, but it can present VEGF to VEGFR-2. Since VEGFR-2 and neuropilin-1 binding sites are distinct, VEGF165 can bind both receptors simultaneously, allowing the formation of ligand-dependent receptor clusters [186, 187]. This hypothetical model will most likely have to be modified if cell-surface HSPGs are to be included in the equation, because all three components of this complex are themselves heparin-binding proteins [186, 188, 189]. In addition, neuropilin-1 binds VEGFR-1 and can form a ligand-independent complex with this receptor [186]. Neuropilin-1 may therefore also play a role in VEGFR-1-associated biological responses, such as cell migration [59, 190].

Despite numerous biochemical and *in vivo* studies, it remains unclear how, exactly, neuropilin-1 exerts its functional role during vascular development and in the adult organism. The vascular defects observed in neuropilin null mice were predominantly

attributable to a deficiency in VEGF-neuropilin-1 signaling, as the deletion of the semaphorin binding domain of neuropilin-1 did not significantly alter the severity of the null mutant phenotype [191]. It remains to be determined whether the role of neuropilin-1 on endothelial cells is simply to sequester VEGF165 and amplify signaling through VEGFR-2, thus resulting in a synergistic increase in migratory and proliferative effects, or whether it is able to trigger distinct signaling pathways within the vascular cells that are specific for the VEGF165 isoform.

1.4.3 HSPGs: low-affinity VEGF receptors

HSPGs are abundant, highly conserved components of the cell surface and extracellular matrix of all animal cells. These molecules play a critical role in modulating the activities of a wide range of growth factors, morphogens and chemokines, including VEGF [192]. HSPGs bind to certain VEGF isoforms with low affinity, but this interaction is critically important in determining VEGF isoform localization and function.

1.5 HSPGs as modulators of protein function

1.5.1 Structural characteristics of HSPGs

HSPGs are molecules composed of repeated sulfated disaccharides, which constitute unique glycosaminoglycan chains covalently linked to a protein core [193]. The most abundant glycosaminoglycan, heparan sulfate, is a repeat of alternating glucuronic acids and glucosamines, and is characterized by a high degree of modification of the sulfo and acetyl groups [194, 195]. The heparan sulfate chains are assembled in the Golgi apparatus

by glycosyl transferases while attached to a proteoglycan core protein. The membrane-bound core proteins are predominantly members of two major families of proteoglycans, the membrane-spanning syndecans and the glycosylphosphatidylinositol-linked glypicans (Figure 1.5). Other proteoglycans, namely perlecan, agrin, and collagen, are associated with but are not linked to the cell membrane [194, 196]. Heparin, also a glycosaminoglycan, is a highly sulfated type of heparan sulfate and is almost exclusively produced by mast cells. It is structurally and chemically similar to heparan sulfate and is frequently used in biochemical studies as a heparan sulfate analogue [197, 198].

HSPGs are highly negatively charged molecules by virtue of densely packed sulfate and carboxylate groups on the heparan sulfate chains. An important and unique characteristic of heparan sulfate chains that determines binding affinity and specificity is the existence of spatially discrete, highly sulfated domains (S-domains) of different length (2-8 disaccharides) and varying patterns of 6-O-sulfation [199].

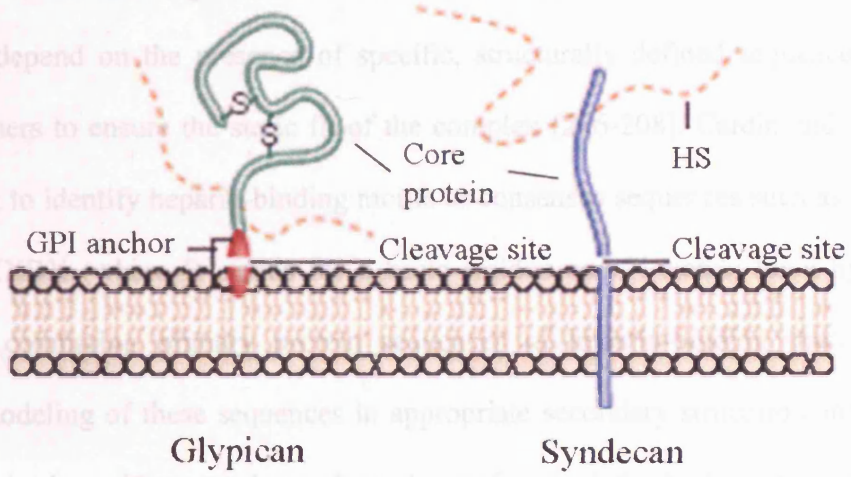

Figure 1.5 Structure of the two major cell-surface heparan sulfate proteoglycans (HSPGs). Glypicans (left) have a large globular domain and are linked to the cell membrane by a glycosylphosphatidylinositol (GPI) anchor. The transmembrane syndecans (right) can carry several heparan sulfate (HS) attachment sites near their extracellular N-terminus, whereas those in glypicans are located near the C-terminus close to the cell membrane. Both glypicans and syndecans can be proteolytically cleaved resulting in the release of the HSPG into the extracellular matrix. Adapted from Hacker, U. et al. [200].

These domains alternate with stretches of low sulfation, consisting mostly of unmodified N-acetylated and N-sulfated disaccharides [201] (Figure 1.6). Several proteins bind to individual or multiple S-domains simultaneously, depending on their oligomeric state and the number and positioning of the heparin-binding sites [202-204]. Because many proteins that bind heparin (and, by extrapolation, heparan sulfate) are basic or contain basic domains, binding is expected to occur mainly via electrostatic interactions [205]. Indeed, heparin-binding sites in proteins are characterized by clusters of arginines and lysines that bind to the highly anionic structures on glycosaminoglycan chains in a rather non-specific manner. However, crystallographic studies of heparin complexes with antithrombin,

annexin V, and fibroblast growth factor (FGF) have demonstrated that heparin-protein interactions depend on the presence of specific, structurally defined sequences on both binding partners to ensure the steric fit of the complex [206-208]. Cardin and Weintraub were the first to identify heparin-binding motifs or consensus sequences such as XBBXBX and XBBBXXBX (where B stands for a basic residue and X stands for a hydropathic residue) by comparing primary protein sequences of heparin-binding proteins [209]. Molecular modeling of these sequences in appropriate secondary structure conformations showed that basic residues are located on the surface and the hydropathic residues are pointing back into the protein core. Some heparin-binding proteins include the sequences described by Cardin and Weintraub, but many others do not contain any of these motifs, suggesting that heparin-binding ability and specificity might not primarily depend on a linear pattern of amino acids. Indeed, heparin-binding epitopes can also be defined by similar spatial motifs, in which basic residues that are distant in sequence but topologically close to each other form an optimal binding surface [210]. The affinity and specificity of the interaction can be further enhanced by the contributions of hydrogen bonds and hydrophobic interactions. Further structural characterization of protein-glycosaminoglycan complexes will be necessary to understand more fully the molecular details of these interactions. These studies would be greatly facilitated by technologies that allow the synthesis of size-defined, chemically homogeneous glycosaminoglycans, which are then used for x-ray crystallography and NMR spectroscopy [211, 212].

(a)

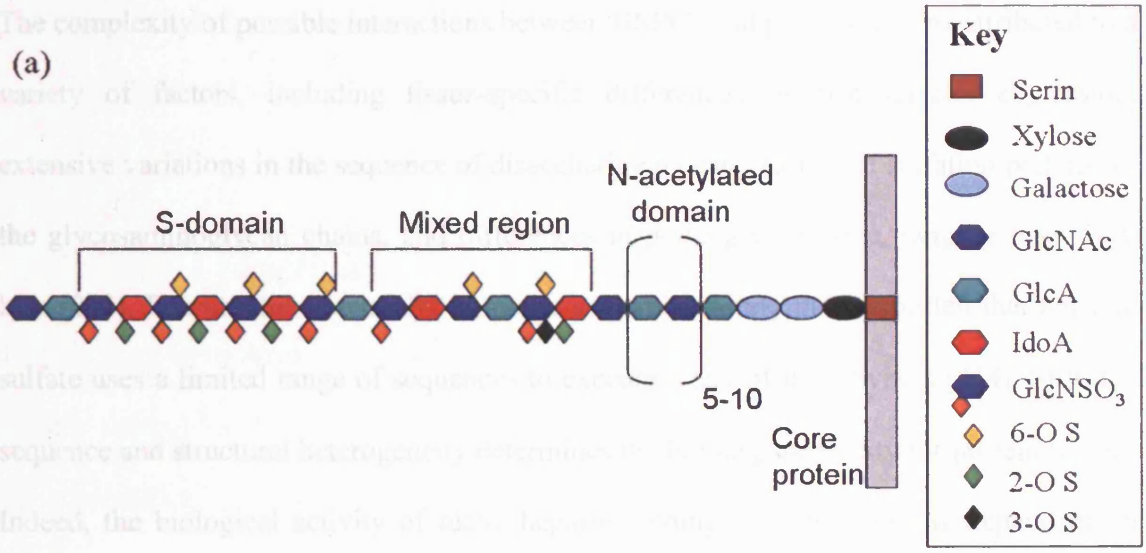

(b)

HS-binding factor classes	Examples
Growth factors and chemokines	FGF-2, HGF, VEGF, RANTES, MCP-1
Morphogens	Wnt/Wg, Shh/Hh, TGF-β/BMP/Dpp
ECM and cell adhesion factors	Laminin, Fibronectin, CAMs
Axon guidance factors and receptors	Netrin, Slit, Semaphorins, Np-1, EphB

Figure 1.6 Heparan sulfate chain structure and heparan sulfate-binding proteins. (a) Heparan sulfate (HS) chains are synthesized on the core protein by the sequential action of glycosyltransferases. The chain is attached to specific serin residues through a common tetrasaccharide linker region and consists of alternating disaccharide units comprising a hexuronic acid (glucuronic acid, GlcA, or iduronic acid, IdoA) and a D-glucosamine (GlcNAc). N-sulfated glycosamines ($GlcNSO_3$) may be O-sulfated at C3 (3-O S), C6 (6-O S) or both, or may carry no sulfates. Similarly, the N-acetylated glucosamines (GlcNAc) may be O-sulfated at C6 or unsulfated. Distinct domains of different charge densities are formed during biosynthesis of the polymer (micro-heterogeneity) and create a large potential for structural diversity. (b) An incomplete list of factors that bind to heparan sulfate (HS) and/or require heparan sulfate for activity.

The complexity of possible interactions between HSPGs and proteins can be attributed to a variety of factors, including tissue-specific differences in proteoglycan expression, extensive variations in the sequence of disaccharide repeats, variety of sulfation patterns of the glycosaminoglycan chains, and differences in proteoglycans size, ranging from 5-70 kDa [213]. Despite this potentially immense sequence variety, it is expected that heparan sulfate uses a limited range of sequences to execute many of its activities [214]. Still, the sequence and structural heterogeneity determines the binding specificity for protein ligands. Indeed, the biological activity of many heparin-binding growth factors is dependent on these 'fine structures' of HSPGs [215]. For example, 6-O-desulfated heparin can bind FGF-2 but, unlike non-modified heparin, fails to promote mitogenic activity of FGF-2 in heparan sulfate-deficient fibroblasts, probably due to inefficient signaling via FGF receptor (FGFR)-1 [216]. This idea was supported by a structural analysis of the FGF-2-FGFR-1 complex in the presence of a heparin fragment. In this structure, the 6-O-sulfate group was shown to make hydrogen bonds with both FGF-2 and its receptor [217, 218]. Although there is no agreement on a single, universal structure of the FGF-2-FGFR-heparin complex, this system remains one of the most well-studied examples of how heparin can control receptor-ligand engagement.

The structural components of heparin required for specific interaction with VEGF165 are different from those used for binding to many other proteins [219]. Whereas FGF binding to FGFR-1 was maximally potentiated in the presence of a dodecasaccharide, a heparin fragment with 22-24 sugars was required to potentiate VEGF receptor binding, suggesting that this fragment can occupy both HBDs in the VEGF homodimer [220, 221]. Furthermore, competition binding assays using heparin derivatives revealed that both N-

and O-sulfation of heparin is necessary for VEGF165 binding, indicating that VEGF interacts with both S-domain and non-S-domain sequences in heparan sulfate [219, 222].

1.5.2 HSPG function

HSPGs bind to numerous factors to influence cell function (Figure 1.6b), and exert their effects through a variety of mechanisms, including localization and sequestration of heparin-binding growth factors, facilitation of growth factor-receptor binding, and chemokine oligomerization. Genetic studies in *Drosophila* have identified specific functions for heparan sulfates in establishing gradients of signaling factors that are involved in morphogenesis and differentiation during pattern formation, such as wingless (Wg), hedgehog (Hh) or Notch [223-227]. In mice, brain-selective disruption of EXT1, an enzyme required for heparan sulfate biosynthesis, revealed a critical role for heparan sulfate in axon guidance, possibly due to altered function of heparin-binding guidance molecules [228]. Several mechanisms have been proposed for the role of heparin and heparan sulfates in growth factor regulation. It has been known for some time that heparin-bound growth factors are more resistant to proteolytic degradation and thermal denaturation. Moreover, heparin has the potential to restore bioactivity to damaged proteins. Notably, glypican-1 can act as an extracellular chaperone for VEGF165 and can restore its receptor binding ability after VEGF has been damaged by oxidation, thus enhancing its efficacy [229]. HSPGs can also maintain reservoirs for pro- and anti-angiogenic factors, including FGF, VEGF, platelet-derived growth factor (PDGF) or thrombospondins, thereby prolonging growth factor retention time and receptor engagement. During blood vessel remodeling, matrix-degrading proteases can either

release these factors to promote cell proliferation, or generate fragments from extracellular matrix proteins that are angiostatic [230-232].

More than a decade after the demonstration that heparan sulfate serves as an accessory molecule obligatory for the binding of FGF-2 to its receptor [233], and despite the progress that has been made in elucidating the various functions of HSPGs, the exact mechanism by which individual proteoglycans facilitate specific protein-protein interactions remains poorly understood [234]. Two mechanistic models, which are complementary rather than mutually exclusive, can be used to explain the potentiating functions of heparan sulfates. Firstly, negatively charged heparan sulfate chains can capture growth factors with high association rates and restrict their diffusion from three dimensions to the two-dimensional mobility of the HSPGs on the cell surface [235]. This lateral movement increases the frequency at which growth factors encounter unoccupied high-affinity signaling receptors. In the vicinity of these receptors, the ligand rapidly dissociates from the low-affinity binding site(s) and binds to the signaling receptor. This structure may be further stabilized by the formation of a ternary complex with heparan sulfate, resulting in a more durable activation of the receptor tyrosine kinase [235, 236]. The second model for heparan sulfate function involves enhancing receptor dimerization. It has been shown that FGF receptor dimerization induced by multivalent binding of a FGF-heparin complex is necessary for receptor activation. Active heparan sulfate chains are usually long enough to accommodate more than one FGF monomer, resulting in a higher-order structure that favors FGF receptor dimerization and activation [237, 238].

Higher-order oligomers can also provide directional cues to guide the migration of cells in physiological and pathological settings. For example, the ability of certain chemokines to

oligomerize on glycosaminoglycan chains to form chemokine gradients on cell surfaces was recently demonstrated to be important for the guidance of leukocytes *in vivo* [239]. During an inflammatory response, chemokine gradients are established and stabilized through interactions with HSPGs. Leukocytes are then chemotactically attracted by these gradients and move toward the endothelium, where they bind to selectins and integrins before transmigrating into the underlying tissue [240]. HSPGs may also add another level of specificity to cell migration and signal transduction processes beyond that defined by the interaction of chemokines with their G protein-coupled receptors (GPCR), when ligands specifically bind to certain types of glycosaminoglycans [241-243]. Whether these mechanisms are relevant to the modulation of VEGF activity remains to be investigated.

1.5.3 The modulation of VEGF behavior by heparan sulfates

HSPGs control various aspects of angiogenesis, e.g. by modulating FGF activity, as described above, and by influencing function of the different VEGF isoforms. The exact mechanisms by which heparin regulates the activity of heparin-binding VEGF isoforms has proved elusive, in part due to the potential complexity of interactions, since heparin can bind to all three VEGF receptors in addition to the ligand. Furthermore, the lack of crystal or NMR structures of protein-heparin complexes has made it difficult to gain insight into the structural specificity of the binding partners.

Endothelial cells predominantly express the membrane-bound glypican-1 and syndecans, as well as the extracellular matrix-associated perlecan [244-246]. Glypican-1 was the first native HSPG reported to bind to and modulate VEGF activity [229]. Glypican-1 binds

VEGF165 through its heparan sulfate chains with some specificity; this interaction can be inhibited by excess amounts of heparin, but not by other HSPGs. Exogenous glypican-1 also potentiates the binding of VEGF165 and oxidized VEGF165 to heparinase-digested human umbilical vein endothelial cells (HUVEC) and to soluble VEGFR-2, respectively [229]. In contrast, binding of VEGF121 to VEGFR-2 is not affected by removal of cell surface heparan sulfates, as detected by cross-linking to HUVEC, and neither glypican nor heparin can restore the receptor binding capability of VEGF121 treated with oxidizing reagents [247]. This function of glypican-1 may represent a mechanism to ensure VEGF activity by extending its half-life in situations where high levels of free radicals or other oxidizing agents are produced, such as wound healing, inflammation or hypoxia-induced angiogenesis [247].

An exact understanding of the effects of HSPGs on VEGF isoform activity is complicated by the fact that different studies have yielded seemingly contradictory results. Not surprisingly, the observed regulatory effects of heparin or HSPGs on receptor binding and activation by VEGF are affected by several factors, including the experimental set-up, the cell and receptor types involved, and the concentration, type and sulfation level of HSPGs [248, 249]. Whereas heparin strongly potentiates ^{125}I-VEGF165 binding to VEGFR-2 in a cell-free assay, the equivalent amount of heparin inhibited the binding to NIH-3T3 cells that overexpress VEGFR-2 [250]. Heparin did, however, augment VEGF binding to cells in which VEGFR-2 is endogenously expressed [248, 251]. In the case of VEGFR-1, both VEGF121 and VEGF165 binding are reduced by exogenous heparin [251, 252]. Ito et al. observed a dose-dependent decrease in VEGF165 binding to porcine aortic endothelial cells (PAEC) transfected with VEGFR-1 in the presence of different batches of heparin

[253]. Similar results were reported by Terman et al. [251]. These data suggest that heparin and HSPGs differentially modulate VEGF binding through direct interaction with the different receptor types. A heparin-binding peptide found in the extracellular domain of VEGFR-2 does not bind VEGF165, but it potently inhibits VEGF binding to the receptor and blocks endothelial cell proliferation [189]. Possible outcomes of a direct interaction of heparin with this receptor include an increase in the number of available binding sites, an increase in VEGF stability, and/or changes in receptor conformation [118, 248, 251, 253]. In the presence of HSPGs, VEGF165, VEGFR-2 and neuropilin-1 are thought to form an as-yet undefined signaling complex through intermediary heparan sulfate molecules [185, 249]. It can be assumed that heparin and HSPGs play an important role in enabling VEGF isoform-specific signaling responses in endothelial cells by orchestrating the differential association of VEGF isoforms with the various receptor components.

1.6 The roles of heparin-binding VEGF isoforms

1.6.1 Physiological angiogenesis

The VEGF isoforms exert specific functions based on their differential distribution in the extracellular milieu, as demonstrated in a study investigating vascular branch formation and its underlying mechanisms [61]. Although VEGF120 alone is able to support mouse embryonic vasculogenesis and angiogenesis to a certain extent [284], the balanced expression of both soluble and heparin-binding isoforms appears to be necessary to ensure proper vessel branching morphogenesis during vascular development in the hindbrain [61]. In the $VEGF^{120/120}$ mice, which lack heparin-binding isoforms, disruption of the naturally-occurring chemotactic VEGF gradient near the midline region resulted in defective

migration of sprouting vessel tips, decreased branching complexity and enlarged capillaries. On the other hand, the exclusive expression of the VEGF188 isoform ($VEGF^{188/188}$) promoted excess branching, producing small caliber vessels. Normal vessel parameters were fully restored in mice engineered to express VEGF120 and VEGF188 ($VEGF^{120/188}$), indicating that VEGF188 can compensate for the loss of VEGF164 during development. Thus, it has been hypothesized that the balance between the heparin-binding and non-heparin-binding variants determines whether vessels will undergo branching morphogenesis or luminal growth [61].

The longer VEGF isoforms are believed to provide positional cues to VEGFR-2-expressing endothelial tip cell filopodia due to their HBD-mediated retention near the VEGF-producing cells [61]. A similar role for the heparin-bound splice forms was found for the guidance of tip cells during retinal angiogenesis [62]. In $VEGF^{120/120}$ mice that survive until P9, the absence of the heparin-binding VEGF isoforms results in defective endothelial cell outgrowth and vessel remodeling [254]. Furthermore, VEGF164 not only supports the migration of endothelial cells but also contributes to neuronal patterning in vivo by acting as a guidance cue for neuropilin-1-expressing motor neurons [59].

The ability of VEGF188 and, to a lesser extent VEGF164, to be sequestered locally may trigger signaling events that modulate vessel morphogenesis. It has been shown that immobilized VEGF188 and VEGF164 remain functional and serve as substrates for endothelial cell adhesion and spreading through direct ligation with $\alpha v\beta 3$ integrins in vitro [255]. To induce proliferation, however, VEGF188 must undergo enzymatic processing to unmask its VEGFR-2-binding domain, suggesting that different mechanisms are involved

in proliferation and migration [131]. VEGF188 activities may also be modulated by the neuropilins. Binding of the VEGF188 to neuropilin-1/VEGFR-2 complexes through its exon-7-encoded sequence has yet to be verified, but this interaction may potentially induce a similar migratory response in endothelial cells to that observed for VEGF165 [126, 256].

1.6.2 Pathological conditions

1.6.2.1 Tumors

Deregulated VEGF expression contributes to the development of solid tumors by promoting tumor angiogenesis [36, 257]. In addition, the extracellular processing of VEGF isoforms has been implicated in the angiogenic switch, a process that renders hyperplastic tissue tumorigenic [258]. The regulation of expression of the three primary VEGF isoforms (VEGF121, VEGF165, and VEGF189) by tumor cells and the tumor-associated stroma, however, remains poorly understood. Moreover, the distinct pathophysiological roles of the isoforms appear to be affected significantly by the microenvironment, such as expression of VEGF receptors and extracellular matrix components, at the different anatomical sites of these tumors [259].

Overexpression of individual VEGF isoforms increases the angiogenic potential of tumor cells [260-262]. Various studies have shown that soluble VEGF is less effective than heparin-binding VEGF at supporting the neovascularization needed for tumor survival. For example, glioma cells transfected with VEGF121 fail to induce tumor progression when implanted in the sub-cutaneous space, whereas VEGF165- and VEGF189-overexpressing cells strongly augment neovascularization compared to parental cells [259]. VEGF120 is

incapable of supporting maximal growth of heterotypic tumor cells, as observed in a mouse xenograft model using transformed embryonic fibroblasts expressing individual isoforms on a VEGF nullizygous background [263]. In this seminal study, the diffusible VEGF120 recruited peripheral vessels but was incapable of vascularizing the tumor itself. In contrast, the high local concentration of the heparin-binding VEGF188 resulted in highly vascularized tumors with a retarded growth rate, as these tumors failed to connect to the systemic vasculature. Only VEGF164, with heparin-binding and diffusible properties, induced both internal and external tumor vascularization, fully rescuing growth of the angiogenesis-deficient tumor [263]. Analogous results have been observed with isoform-specific VEGF transgenic mice [61, 254]. Interestingly, tumors that form following injection of different combinations of immortalized, VEGF isoform-specific fibroblasts primarily contain VEGF164-expressing fibroblasts, indicating that this isoform confers a growth advantage in certain tumors [263]. A similar alteration of VEGF protein expression patterns in favor of the membrane-associated isoforms has been observed in lung and colorectal tumor tissues [264]. Finally, VEGF165 and VEGF188 expression has been associated with poorer outcomes in osteosarcomas and colon cancer, respectively [265, 266]. Taken together, these data suggest that soluble VEGF may be needed in the stages of tumor development in which the tumor has to recruit systemic vessels to ensure its blood supply. The heparin-binding forms appear to support the vascularization of the capillary bed within the tumor, inducing the formation of thin, highly branched and interconnected vessels [133, 263].

1.6.2.2 Intraocular disease and the predominant role of the VEGF164/165 isoform

Numerous studies suggest a causal role for VEGF activity in proliferative, neovascular pathologies of the eye [34, 267-269]. In diabetic retinopathy, retinopathy of prematurity (ROP), and the wet form of adult macular degeneration, VEGF not only causes uncontrolled neovascular growth that damages the retina, but also promotes vascular leakage of plasma proteins and vitreous hemorrhages that eventually lead to blindness [270]. During pathological proliferative retinopathy, hypoxia-induced VEGF production by ischemic retinal cells results in aberrant vessel growth that can extend beyond the retinal surface into the vitreous cavity [271]. Of the various isoforms, VEGF164 appears to be preferentially involved in pathologic retinal neovascularization and selectively accumulates in the ischemic retina in a commonly used animal model of human ROP [272, 273]. In this model, 1-week old mice are exposed to 75% oxygen for a 5-day period followed by a return to room air. Hypoxia-induced upregulation of VEGF expression results in abnormal vessel growth between P17 and P21 and is most prominent at the leading edge of the vascularized retina in the midperiphery [274]. Inhibition of the VEGF164 isoform in this model has been shown to be as effective as pan-VEGF blockade in preventing neovascularization [273].

Recent evidence indicates that VEGF164 is also the most pro-inflammatory isoform in the eye, capable of inducing leukocyte recruitment (leukostasis) to the limbal and retinal vascular endothelium [273, 275]. VEGF-induced retinal leukostasis and blood-retinal barrier breakdown is mediated, in part, through upregulation of intercellular adhesion molecule-1 (ICAM-1) expression on the endothelium [276]. VEGF may also directly act

on certain cells of the immune system, including monocytes, lymphocytes, and dendritic cells, as they have been shown to express active VEGF receptors [166, 277]. On an equimolar basis, VEGF164 was reported to be approximately 1.5 times more potent than VEGF120 in inducing retinal leukostasis, and about three times more potent in inducing corneal inflammation [275, 278]. The significance of this isoform-specific activity is considerable as inflammatory cells not only contribute to blood-retinal barrier breakdown and neovascularization, but also produce VEGF themselves [279]. In the ROP model, adherent leukocytes are commonly associated with pathological neovascularization. Because VEGF-induced pathological vessel growth is frequently preceded by an inflammatory response, it has been suggested that recruited leukocytes serve to mark the site of future neovascularization [273]. VEGF165/164 expression also predominates over other isoforms in human diabetic retinopathy and in an animal model of diabetes [279, 280]. Retinal inflammation and leakage in both early and established diabetes could be significantly reduced when VEGF164 activity was blocked by an isoform-specific, RNA-based aptamer antagonist [278]. This finding was surprising, given that the abnormal wound-healing response of diabetes involves a complex inflammatory process with changes in expression patterns of numerous factors [22].

Taken together, these observations suggest that VEGF164 is the major disease-causing isoform in models of neovascular eye disease. The above mentioned highlights the importance of understanding the specific contributions and the interplay of the VEGF isoforms regarding their normal physiologic role and in vascular pathologies. In particular, the expression, distribution and function of the major isoforms (i.e VEGF121, VEGF165 and VEGF189) in a spatial-temporal context must be better defined.

Chapter 2: Materials and methods

Sequencing reactions were separated and visualized by CRUK Sequencing Service and ACGT, Inc. Animal injections and perfusions, and *in vivo* acridine orange fluorography were performed by Kazuaki Nishijima (Eyetech Research Center). Real-time quantitative PCR was performed and analyzed by Michael Gee (Eyetech Research Center).Circular dichroism spectroscopy was performed by Indrajit Giri (OSI) Eyetech. The PAE cell-binding assay was performed by Andrea de Erkenez (Eyetech Research Center). Animal maintenance and mouse genotyping was provided by the Eyetech Animal Facility team.

2.1 Materials

2.1.1 Reagents

All chemicals were obtained from Sigma-Aldrich and Fluka, unless indicated otherwise. All mammalian tissue culture media and related products were purchased from Gibco (Invitrogen), unless stated otherwise. All restriction endonucleases were from New England Biolabs. Oligonucleotides were provided by Cancer Research UK (CRUK) oligonucleotide synthesis service or purchased from Proligo or Invitrogen. Human ^{125}I-VEGF and tritium-labeled heparin ([^{3}H]-heparin) were obtained from GE Healthcare and Perkin Elmer, respectively. All protease inhibitors were obtained from Roche, whereas heparinase I and III was obtained from Sigma-Aldrich. The expression vectors pPICZαC-VEGF120 and pPICZαC-VEGF164 were used for expression of full-length, untagged VEGF120 and VEGF164 in *Pichia pastoris* and were a gift of Dr. M. Golding (CRUK).

2.1.2 Oligonucleotides

For subcloning of human VEGF111-165 (HBD) into pPICZαC expression vectors:

VEGF-HBD (XhoI)

5'- CCGCTCGAGAAGAGAGCAAGACAAGAAAATCCCTGTGGGCCTTGC -3'

VEGF-HBD (XbaI)

5'- GCTCTAGATTATCACCGCCTCGGCTTGTCACATCTGCAAGT -3'

For generating VEGF164 HBD mutants:

164-R13/R14A

5'- TGTGAGCCTTGTTCAGAG**GCGGCA**AAGCATTTGTTTGTCC -3'

164-A13R (R13A reverse)

5'- GAGCCTTGTTCAGAG**CGG**GCAAAGCATTTGTTTGTCC -3'

K26A

5'- GTCCAAGATCCGCAGACGTGT**GCA**TGTTCCTGCAA -3'

164-K30A

5'- CGTGTAAATGTTCCTGC**GCA**AACACAGACTCG -3'

164-R35/R39A

5'- AACACAGACTCG**GCT**TGCAAGGCG**GCG**CAGCTTGAGTTAAACG -3'

164-R46/R49A

5'- TGAGTTAAACGAA**GCT**ACTTGC**GCA**TGTGACAAGCCGAGG -3'

164-R49A

5'- AACGAACGTACTTGC**GCA**TGTGACAAGCCGAGG -3'

(Nucleotides in bold indicate mutations)

For sequencing of pPICZαC constructs:

Forward

5'AOX-1	5'- GACTGGTTCCAATTGACAAGC -3'
α-Factor	5'- TACTATTGCCAGCATTGCTGC -3'

Reverse

3'AOX-1	5'- GCAAATGGCATTCGTACATCC -3'
PIC/BsmB I	5'- TCGAGGTACCGATCCGAGACG -3'

For genotyping of $VEGF^{120/188}$ mice:

VEGF120FOR	5'- CAGTCTATTGCCTCCTGACCTTCAGGGTC-3'
VEGF120REV	5'- CTTGCGTCCACACCGTCACATTAAGTCAC-3'
VEGF120COM	5'- TTCAGAGCGGAGAAAGCATTTGTTTGTCCA-3'
VEGF188FOR	5'- GATCAAACCTCACCAAAGCCAGCACATAG-3'
VEGF188REV	5'- TTGTCACATCTGCAAGTACGTTCGTTTAAC-3'
VEGF188COM	5'- GTGGGTAGAGAAAGGAGGAGAAAACAAG-3'

Real-time PCR (Taqman) primers and probes (ABI, sequences not disclosed):

human tissue factor	sequence reference: NM_001993 RefSeq, Exon3/4 (535bp)
human GAPDH	forward and reverse primer, probe (ABI 402869)

2.2 Methods

2.2.1 Bacterial culture

2.2.1.1 Preparation of electrocompetent bacteria

800 ml of LB medium inoculated with 5 ml of an overnight-culture of XL-1 Blue bacteria (Stratagene) was grown at 37 °C with shaking to an OD_{595} of 0.6. The culture was incubated on ice for 30 min and centrifuged at 5,000 rpm for 20 min at 4 °C using an Avanti JE centrifuge (Beckman Coulter) with a JA-10 rotor. The pellet was washed twice with 500 ml ice-cold water and once with 400 ml ice-cold 10% glycerol. The pellet was resuspended in 1 volume ice-cold 10% glycerol and tested for transformation efficiency.

Preparations that gave $\geq 10^8$ colonies/μg plasmid DNA in test transformations were stored at -80 °C.

2.2.1.2 Transformation of bacteria

50-500 pg DNA were added to 80 μl of competent cells in a 1 mm electroporation cuvette (Bio-Rad) and the mixture was incubated on ice for 10 min. Transformations were performed at 200 Ω, 25 μF, and 1.8 kV. Bacteria were incubated with 400 μl SOC medium at 37 °C for 1 hr and then centrifuged at 3,500 rpm for 1 min in a microfuge. The pellet was resuspended in 100 μl LB medium, plated on agar plates containing the appropriate selection agent and incubated for up to 18 hr at 37 °C.

2.2.1.3 Cryopreservation of bacteria

Bacterial cultures were stored as 40% glycerol stocks at -80 °C.

2.2.2 Yeast techniques

2.2.2.1 *Pichia pastoris* strains

Strain	Genotype	Phenotype
X-33	wild-type	Mut^+ (methanol utilization plus)
GS115	*his4*	His^-, Mut^+
KM71H	*arg4 aox1 :: ARG4*	Mut^S (methanol utilization slow), Arg^+
SMD1168H	*pep4*	Mut^+, deficient in protease A

2.2.2.2 Preparation of electrocompetent yeast cells

250 ml of YPD medium (1% (w/v) yeast extract; 2% (w/v) peptone; 2% (w/v) dextrose) was inoculated with 0.125 ml of a 3 ml overnight culture of the *Pichia pastoris* strain and incubated overnight at 30 °C to an OD_{600} of 1.3-1.5. The cells were centrifuged at 1500 x *g* for 5 min at 4 °C and then resuspended with 250 ml of ice-cold, sterile water. This washing step was repeated with 125 ml of ice-cold water before resuspending the pellet in 10 ml of ice-cold, 1 M sorbitol. After centrifugation, the pellet was resuspended in 0.5 ml of ice-cold 1 M sorbitol for a final volume of approximately 0.75 ml. The cells were kept on ice and used within 3 hr.

2.2.2.3 Transformation of yeast cells

Plasmids (10 μg) were linearized to completion with SacI and purified by phenol extraction. 80 μl of electrocompetent cells were mixed with 5-7 μg of the linearized DNA and transfered to an ice-cold, 2 mm electroporation cuvette (Bio-Rad). After incubation on ice for 5 min, the cells were pulsed at 200 Ω, 25 μF, and 1.5 kV using the Gene Pulser Xcell™ (Bio-Rad). 0.5 ml of ice-cold, 1 M sorbitol was immediately added to the cuvette before transfering the contents to a sterile 15 ml tube. The tube was incubated at 30 °C without shaking for 1 hr. 50 and 100 μl of culture were spread on separate, labeled YPDS agar (YPD; 1 M sorbitol, 2% (w/v) agar) plates containing 100 μg/ml, 200 μg/ml, or 500 μg/ml zeocin. The plates were incubated for 3-5 days at 30 °C.

2.2.2.4 Analysis of transformants for protein expression

Transformants were screened for high-secreting colonies using a modified colony blotting protocol [281]. A nitrocellulose filter (GE Healthcare) was placed over the colonies of the master plate for 1 min. The filter was carefully removed and placed upside-down onto a BMGY agar plate (1% (w/v) yeast extract; 2% (w/v) peptone; 100 mM potassium phosphate, pH 6; 1.34% (v/v) yeast nitrogen base; 4 x 10^{-5}% (v/v) biotin; 1% (v/v) glycerol; 2% (w/v) agar) and incubated overnight at 30 °C. To induce protein expression and secretion, the filter was then placed on a BMMY agar plate (1% (w/v) yeast extract; 2% (w/v) peptone; 100 mM potassium phosphate, pH 6; 1.34% (v/v) yeast nitrogen base; 4 x 10^{-5} % biotin; 0.5% methanol; 2% (w/v) agar) onto which 100 µl of BMMY medium had been spread out. The plate was returned to a 30 °C incubator overnight. The filter was transfered to a fresh BMMY agar plate and incubated again overnight. The nitrocellulose filter was removed and washed in tris-buffered saline (TBS; 20 mM Tris base and 150 mM NaCl, pH 7.5) to remove the yeast colonies. Subsequently, the filter was blocked in blocking buffer (PBSMT; 3.8 mM sodium phosphate monobasic, 16.2 mM sodium phosphate dibasic, 150 mM NaCl, pH 7.4, 5% (w/v) nonfat dry milk, 0.05% (v/v) Tween-20) for 2 hr and then incubated with a mouse monoclonal anti-VEGF antibody (C-1, Santa Cruz, 1:250 dilution) in blocking buffer for 1 hr. The filter was washed with PBST (phosphate-buffered saline (PBS) containing 0.05% Tween-20) for 20 min, incubated with blocking buffer containing a horseradish peroxidase (HRP)-conjugated anti-mouse secondary antibody (GE Healthcare) and washed with PBST for 20 min. Immunoreactivity was detected using enhanced chemiluminescence (ECL, GE Healthcare). Colonies that showed the strongest signal were selected for protein expression. Alternatively, *Pichia*

clones were tested for insertion of the gene of interest by direct PCR screening (Chapter 2.2.4.8.3).

2.2.2.5 Determination of the Mut (methanol utilization) phenotype

All zeocin-resistent transformants in KM71H are Mut^S because the AOX1 gene, which encodes one of the two methanol utilizing enzymes, is disrupted. Most of the transformants in X-33, GS115 or SMD1168H should have been Mut^+. To exclude the possibility that the cross-over recombination occured in the 3'- AOX1 region of the *Pichia* genome, thereby disrupting the wild-type AOX1 gene and creating a Mut^S transformant, a replica-plating assay was used. Ten colonies were patched on an MDH (1.34% (v/v) yeast nitrogen base, 4 x 10^{-5} % (v/v) biotin, 2% (v/v) dextrose, 0.004% (v/v) histidine) plate using sterile toothpicks. The plate was incubated at 30 °C for 2 days. The patches were then replica-plated from the MDH plate onto fresh MMH (same as MDH, except 0.5% methanol was used instead of dextrose) and MDH plates. The replica plates were incubated at 30°C for 2 days and growth on MDH and MMH plates was compared with the growth of Mut^S and Mut^+ control patches in order to determine the phenotype.

2.2.2.6 Cryopreservation of yeast cells

A single colony of each strain or transformant was cultured at 30 °C overnight in YPD (1% (w/v) yeast extract, 2% (w/v) peptone, 2% dextrose). The cells were harvested and suspended in 20% glycerol at a final OD_{600} of 30-50 (1.5-2.5 x 10^9 cells/ml). Cells were frozen in liquid nitrogen and stored at -80°C. Using a sterile pipette tip, approximately 20

µl of cells were taken from the frozen vial and were streaked out on YPD agar plates (for transformants, 100 µg/ml zeocin was added to the YPD medium) to obtain single colonies.

2.2.3 Tissue culture

2.2.3.1 Routine culture of mammalian cells

HUVEC (Cascade Biologics) were cultured in M200 media supplemented with 1x low serum growth supplement (Cascade Biologics), 2mM glutamine and 1x penicillin/streptomycin (Invitrogen). PAE cells were cultured in Ham's F12 medium supplemented with 10% FBS, 2 mM glutamine and 1x penicillin/streptomycin. All cells were grown at 37 °C in an atmosphere of 5% CO_2 / 95% air. All cell lines were trypsinized using a 1x trypsin/EDTA solution (Invitrogen). Cells were thawed by diluting the contents of a vial in 9 volumes of medium, sedimenting the cells at 500x *g* and resuspending the pellet in the appropriate volume of complete medium.

2.2.3.2 Cryopreservation of mammalian cells

Cells were frozen in 10% DMSO, 20% fetal bovine serum (FBS), 70% complete medium and were stored in liquid nitrogen using standard procedures.

2.2.3.3 Tissue factor (TF) induction in HUVEC

HUVEC cells were seeded at 8x 10^4 cells per well in a 12-well plate in complete medium. 24 hr later, the cells were serum-starved for 4 hr in M200 media containing 1% FBS and antibiotics. The cells were rinsed once with M200 media without serum before adding

VEGF variants (0.3 pmol) in 1 ml of serum-free medium or medium without VEGF. After incubation at 37 °C for 1 hr, the cells were rinsed once with PBS and processed for RNA isolation. The RNA was used to test for tissue factor expression (chapter 2.2.5.5)

2.2.3.4 Binding of VEGF variants to PAE cells

PAE cells were seeded at 3.0 x 10^5 cells/well in 12-well dishes and were cultured for 24 hr. Cells were washed once with binding buffer (Ham's F-12K medium containing 0.1% (w/v) bovine serum albumin (BSA), pH 7.5) Binding of purified mouse VEGF variants (7.14 nM) to the cell surface was carried out in binding buffer for 30 min at 37 °C and 5% CO_2. Unbound VEGF was removed with a pipette and the cells were washed three times with binding buffer before bound VEGF was enzymatically dissociated from cell-surface heparan sulfate proteoglycans. To this end, heparinase I and III were prepared immediately before each experiment by dissolving in 20 mM Tris-HCl (pH 7.5) containing 50 mM NaCl, 4 mM $CaCl_2$, and 0.01% (w/v) BSA. The enzymes were added to the cells at a final concentration of 0.5 U/ml and the mixture was incubated for 1 hr at 37 °C and 5% CO_2. The supernatant of each well was collected with a pipette and cells were washed one more time with binding buffer. The concentration of VEGF in the supernatant and the final wash was determined using the mouse VEGF Quantikine® ELISA kit (R&D) according to the instructions of the manufacturer.

2.2.4 DNA techniques

2.2.4.1 Quantitation of DNA

DNA was diluted in an appropriate buffer and placed in a quartz cuvette with a path length of 1 cm, and the absorbance was read at 260 nm and 280 nm using a spectrophotometer. An OD_{260} of 1 corresponds to 50 µg/ml double-stranded or 33 µg/ml single-stranded DNA. The $OD_{260/280}$ ratio was calculated to estimate the purity of the DNA preparation. A ratio of 1.7-1.9 was considered acceptable.

2.2.4.2 Phenol/chloroform extraction

To remove proteins from DNA preparations, DNA was mixed with 1 volume of a phenol/chloroform/isoamyl alcohol (25:24:1) mixture, vortexed and centrifuged in a microfuge at 14,000 rpm for 5 min at room temperature. The aqueous DNA solution was transfered to a fresh tube and residual phenol was removed by extracting the DNA with 1 volume chloroform. The DNA was then precipitated with ethanol.

2.2.4.3 Ethanol precipitation of DNA

The salt concentration of the DNA was adjusted by adding 1/10 volume of 3 M sodium acetate (pH 5.2). 2.5 volumes of ice-cold, 100% ethanol were then added and the resulting solution mixed and centrifuged at maximum speed in a microfuge for 30 min at 4 °C. The DNA pellet was washed twice with 70% ethanol, air-dried and resuspended in TE buffer (10mM Tris, pH 8.0, 1mM EDTA) or water.

2.2.4.4 Preparation of plasmid DNA

Plasmid DNA was prepared from overnight cultures of bacteria (1.5 ml for DNA mini preparations, 50-80 ml for DNA midi preparations) which were grown at 37 °C in LB medium containing Ampicillin (75 μg/ml) or Zeocin (25 μg/ml). DNA was purified using Qiagen plasmid mini kits or QiaFilter plasmid midi kits (Qiagen) according to the manufacturer's instructions.

2.2.4.5 DNA agarose gel electrophoresis

Agarose gels were prepared by dissolving 0.7%-2% agarose in TAE buffer (40 mM Tris base, pH 8.0, 20 mM glacial acetic acid, 1mM EDTA). Ethidium bromide was added to a final concentration of 0.5 μg/ml. DNA samples were mixed with 10x BlueJuice™ loading buffer (Invitrogen) and electrophoresed at 5-20 V/cm in running buffer (TAE). A 100 bp or 1 kb DNA ladder (Invitrogen) was run in parallel for comparison.

2.2.4.6 Gel purification of DNA fragments

DNA fragments were excised from agarose gels and purified using a gel extraction and nucleotide removal kit (Qiagen).

2.2.4.7 Restriction enzyme digestion

For small-scale diagnostic digests, 1 μg of DNA was incubated in the appropriate restriction enzyme buffer with 5-10 U of restriction endonuclease in a total volume of 20 μl. The reaction was incubated at the appropriate temperature for 1-2 hr. For large-scale

preparative digests, 10-20 μg of DNA was mixed with the appropriate buffer and 20-40 U of restriction endonuclease in a total volume of 100-150 μl, and incubated at the appropriate temperature for 3-6 hr. Following digestion, enzymes were inactivated by incubating at 65 °C for 20 min or by phenol/chloroform extraction.

2.2.4.8 Polymerase chain reaction (PCR)

2.2.4.8.1 Genotyping of $VEGF^{120/188}$ mice by PCR analysis

For each DNA sample, two PCR reactions were performed to screen for the deletion of exons 6 and 7 (VEGF120) and the presence of exons 4-8 (VEGF188), respectively. Reactions were carried out in the appropriate buffer containing 150ng genomic DNA, 100μM of each primer (chapter 2.1.2), 10mM dNTP, 0.75μl $MgCl_2$ (50 mM), and 0.2μl Taq Polymerase in a total volume of 25μl using the following conditions:

VEGF120:

Segment 1	1 cycle	denaturation at 94°C for 90 sec
Segment 2	4 cycles	denaturation at 94°C for 1 min
		annealing at 55°C for 45 sec
		extension at 72°C for 90 sec
Segment 3	24 cycles	denaturation at 94°C for 1 min
		annealing at 60°C for 1 min
		extension at 72°C for 1 min
Segment 4	1 cycle	extension at 72°C for 15 min

VEGF188:

Segment 1	1 cycle	denaturation at 95°C for 90 sec
Segment 2	27 cycles	denaturation at 95°C for 1 min
		annealing at 62°C for 45 sec
		extension at 72°C for 90 sec
Segment 3	1 cycle	extension at 72°C for 10 min

2.2.4.8.2 PCR-cloning of VEGF111-165 (HBD)

For subcloning of the cDNA encoding the C-terminal, 55-residue fragment of VEGF165 (HBD), primers were designed so that they were in frame with the *Pichia* α-factor signal peptide, which is removed proteolytically from the protein in the yeast cell. The reaction was carried out in the appropriate buffer containing 1 ng of VEGF165 cDNA encoding pPICZαC-VEGF165 vector, 0.5 μM of each primer, 200 μM dNTP (Roche) and 5 U high-fidelity Pfu DNA polymerase (Stratagene). The PCR amplification was performed by using the hot-start method and the following cycling conditions:

Segment 1	1 cycle	denaturation at 95 °C for 1 min
Segment 2	30 cycles	denaturation at 95 °C for 1 min
		annealing at 65 °C for 1 min
		extension at 72 °C for 1 min
Segment 3	1 cycle	extension at 72 °C for 5 min

The resulting PCR product was digested with XhoI and XbaI restriction endonucleases to generate cohesive ends for the subsequent ligation with XhoI- and XbaI-digested and purified pPICZαC expression vector (Invitrogen).

2.2.4.8.3 Direct PCR screening of *Pichia* clones

Pichia transformants were screened for the presence of the gene of interest using a PCR protocol by Linder *et al.* [282]. A single yeast colony was suspended in 10 µl of water and the cells were lysed by adding 25 U of Lyticase. After 10 min at 30 °C the sample was frozen at -80 °C for 10 min. Three µl of the lysate containing the genomic DNA, was mixed with 20 pmol primer 1 (5'- AOX1), 20 pmol primer 2 (3'- AOX1), and 15 µl of Mega Mix Blue (Helena Biosciences). The resulting PCR products were visualized after gel electrophoresis. The cycling conditions for were as follows:

Segment 1	1 cycle	denaturation at 94 °C for 1 min
Segment 2	32 cycles	denaturation at 94 °C for 40 sec
		annealing at 64 °C for 1 min
		extension at 72 °C for 1 min
Segment 3	1 cycle	extension at 72 °C for 3 min

2.2.4.9 Cohesive-end ligation

Following digestion of vector and insert, the linearized vector was dephosphorylated with 0.5 U/µg DNA of alkaline phosphatase (CIP, New England Biolabs) at 37 °C for 1 hr, to

prevent recircularisation. Vector and insert were gel-extracted and precipitated. Ligations were performed using 200-300 ng total DNA and 400U T4 DNA ligase (New England Biolabs) in a final volume of 15 µl. The vector to insert molar ratios were 1:2, 1:6, and 1:12. The reaction was carried out overnight at 16 °C. 1 µl of the ligation reaction was transformed into electrocompetent *E. coli* as described above.

2.2.4.10 Site-directed mutagenesis

In vitro site-directed mutagenesis was performed using the QuikChange™ multi site-directed mutagenesis kit (Stratagene). Oligonucleotide primers containing the desired mutation flanked by unmodified nucleotide sequence were synthesized, then purified by HPLC and ethanol precipitation. Primers were designed to bind to adjacent sequences or to separate regions on the same strand of the template plasmid and were usually 32-43 bp in length with a minimum GC content of 40% and a melting temperature (T_m) of $\geq$ 75 °C. The primers terminated in one or more C or G bases at the 3'- end and were 5'-phosphorylated for better mutagenesis efficiency. Reactions were carried out in the appropriate buffer in 25 µl using 100 ng of each primer, 50 ng double-stranded DNA template, 1 µl dNTP mix, and 1 µl of *Pfu* Turbo DNA polymerase enzyme blend (Stratagene). The following PCR conditions were used:

Segment 1	1 cycle	denaturation at 95 °C for 1 min
Segment 2	30 cycles	denaturation at 95 °C for 1 min
		annealing at 55 °C for 1 min
		extension at 65 °C for 2 min/kb of plasmid length

The reaction was placed on ice for 2 min before adding 10 U of *DpnI*-restriction enzyme for 1 hr at 37°C to digest the parental (nonmutated) DNA template. 1.5 µl of the *DpnI*-treated DNA was transformed into XL10-Gold ultracompetent cells (Stratagene) by incubating at 42 °C for 30 seconds. SOC medium (0.5% yeast extract, 2.0% tryptone, 10 mM NaCl, 2.5 mM KCl, 10 mM $MgCl_2$, 20 mM $MgSO_4$, 20 mM glucose) was added and the tubes were incubated at 37 °C for 1 hr. Different amounts of each transformation reaction were spread on low salt LB agar plates containing 25 µg/ml Zeocin. The mutagenesis efficiency of a control plasmid was determined as a positive control for each experiment.

2.2.4.11 DNA sequencing

Primers of 21 nucleotides in length were designed to amplify a region within the gene of interest or the vector sequence adjacent to the 5' and 3'- end of the gene. Reactions were carried out in a volume of 20 µl containing 300-500 ng DNA, 3 pmol of primer and 8 µl of fluorochrome labeling mix (Cancer Research UK) using a thermal cycler. The PCR conditions were as follows:

Segment 1	25 cycles	denaturation at 96 °C for 10 sec
		annealing at 50 °C for 5 sec
		extension at 60 °C for 4 min

Samples were ethanol-precipitated, electrophoresed and visualized. SDS-polyacrylamide gel electrophoresis (SDS-PAGE) and visualization were performed by the Cancer Research UK Sequencing Service. Alternatively, sequencing was performed by ACGT, Inc. DNA sequence analysis and alignment was performed using the software programs MacVector (Accelrys) and Sequencher (Gene Codes Corporation).

2.2.5 RNA techniques

2.2.5.1 RNA isolation

Total RNA was isolated from cells using the RNeasy mini kit (Qiagen). 3-5 x 10^5 HUVEC were lysed in 350 µl RLT buffer (Qiagen). The lysate was passed through a QIAShredder spin column and then loaded on an RNeasy mini column. Further purification steps were carried out according to the manufacturer's instructions. RNA was eluted in water, visualized on an agarose gel, quantified and stored at -80 °C.

2.2.5.2 RNA quantitation

RNA solutions were placed in a quartz cuvette (1 cm path length) and the absorbance of the sample was determined at 260 nm and 280 nm using a spectrophotometer. An OD_{260} value of 1, which corresponds to 40 µg/ml RNA, was used as a reference for calculations. An $OD_{260/280}$ ratio of 1.9-2.1 indicated a pure preparation.

2.2.5.3 RNA agarose gel electrophoresis

1.2% agarose gels were prepared in TBE buffer (45 mM Tris-borate, pH 8.0, 1mM EDTA) containing ethidium bromide at a final concentration of 0.5 μg/ml. RNA was mixed with 10x BlueJuice™ gel loading buffer (Invitrogen) and electrophoresed at 5-20 V/cm in running buffer (TBE). Distinct ribosomal RNA bands with the 28S rRNA band of double intensity relative to the 18S rRNA band were an indication of intact RNA. Alternatively, RNA samples were loaded on an RNA 6000 Nano Chip (Agilent Technologies) and run on a Bioanalyzer 2100 (Agilent Technologies) according to the manufacturer's instructions.

2.2.5.4 Reverse transcriptase PCR (RT-PCR)

Reverse transcription of RNA was performed using 100-200 ng RNA and TaqMan reverse transcription reagents (Applied Biosystems, ABI). The final concentration of the reaction was 1x Taqman Reverse Transcriptase buffer, 5.5 mM $MgCl_2$, 500 μM of dNTPs, 2.5 μM random hexamer primers, 0.4 U/μl RNase inhibitor, and 1.25 U/μl Multiscribe reverse transcriptase in a total volume of 60 μl. cDNA synthesis was carried out in a thermal cycler according to the following program:

Segment 1	1 cycle	25 °C for 10 min
Segment 2	1 cycle	42 °C for 60 min
Segment 3	1 cycle	95 °C for 5 min

2.2.5.5 Real-time quantitative PCR (Taqman) for TF expression

Taqman cocktails were prepared using 1x PCR master mix (Applied Biosystems, ABI), 1x Tissue Factor Assay-on-Demand/FAM (ABI), and 2 µl of cDNA in a total volume of 10 µl. GAPDH served as the internal control for all reactions, and was amplified with human GAPDH primers and probe (ABI), using 1x PCR master mix (ABI), 10 µM of each forward and reverse GAPDH primer, and 20 µM of GAPDH probe in a total volume of 10 µl. Reactions were loaded on a 384-well plate and run in the ABI Prism 7900HT System using the following cycling conditions:

Segment 1	1 cycle	50 °C for 2 min
Segment 2	1 cycle	95 °C for 10 min
Segment 3	40 cycles	melting at 95 °C for 15 sec
		annealing and extension at 60 °C for 1 min

Gene expression was analyzed using the SDS 7900HT software version 2.2 (ABI). Results were quantified using the comparative threshold (C_t) method [283]. Briefly, relative expression levels were calculated in comparison to the non-treated control using arithmetic formulae. The amount of target, normalized to the endogenous GAPDH housekeeping gene and relative to the non-treated control, was then given by $2^{-\Delta\Delta Ct}$, representing the normalized expression of the target gene in the unknown sample, relative to the normalized expression of the non-treated sample.

2.2.6 Protein techniques

2.2.6.1 Protein quantitation

Protein concentrations were determined using the bicinchoninic acid (BCA)-based protein assay (Pierce). Samples and the BSA standards were diluted in sample diluent to a total volume of 25 µl and mixed each with the BCA working reagent (200 µl) in a 96-well plate. After incubation at 37 °C for 30 min, the absorption was measured at 562 nm using a spectrophotometer. Standard curves were generated based on the absorbance of BSA standards and were used to determine the protein concentrations of the samples.

2.2.6.2 Protein precipitation with trichloroacetic acid (TCA)

Protein samples were mixed with 0.1 volumes of 100% TCA, incubated on ice for 30 min and centrifuged at 14,000 rpm for 15 min at 4 °C in a microfuge. Supernatants were completely removed and pellets washed with 300 µl acetone (-20 °C), dried and resuspended in SDS-PAGE sample buffer.

2.2.6.3 Endotoxin detection

To determine the endotoxin levels in recombinant protein samples prior to animal injection, a Pyrosate test kit (Associates of Cape Cod) with a sensitivity of 0.25 endotoxin units (EU) per ml was used according to the instructions of the manufacturer. A positive control was run in parallel. The absence of clot formation in the protein samples indicated that all samples contained less than 0.25 EU/ml.

2.2.6.4 SDS-PAGE

Gels were poured at a thickness of 1-1.5 mm using the Bio-Rad Mini-PROTEAN® 3 Cell assembly kit or the Bio-Rad Criterion™ Cell system and solutions from National Diagnostics. The separating gel was prepared as follows:

Final acrylamide concentration (%)	ProtoGel (ml)	Resolving buffer (ml)	Deionised water (ml)
8	2.67	2.5	4.72
10	3.33	2.5	4.06
12	4	2.5	3.39
15	5	2.5	2.39

100 µl of 10% ammonium persulfate (APS) and 10 µl TEMED were added per 10 ml of gel solution to initiate polymerisation. The stacking gel was prepared by mixing 1.3 ml ProtoGel, 2.5 ml ProtoGel Stacking Buffer, 6.1 ml deionised water and adding 50 µl APS and 10 µl TEMED. SDS sample buffer was prepared as a 6x stock solution, containing 0.35 M Tris-HCl (pH 6.8), 10% SDS, 0.6 M DTT, 30% glycerol, and 0.012% bromphenol blue. Protein samples were boiled in 1x SDS sample buffer at 100 °C for 5 min prior to loading. For detection of protein dimers, proteins were denatured in SDS sample buffer without dithiothreitol (DTT). Gels were run in Tris-glycine buffer (25 mM Tris, 250 mM

glycine (pH 8.3), 0.1 % SDS) at 100-170 V. The gels were stained in Coomassie R-250 using Imperial™ Protein Stain (Pierce) for 1 hr and destained in water until bands were clearly visible.

2.2.6.5 Western blotting

Following electrophoretic separation, proteins were blotted onto nitrocellulose membranes (Hybond™, GE Healthcare) using a semi-dry blotter (Bio-Rad). Membranes and pieces of Whatman paper were soaked in transfer buffer (8ml 5x Tris-glycine buffer, 20 ml methanol, and 72ml water). The gel and the membrane were sandwiched between six pieces of Whatman paper, with the membrane facing the anode of the electroblotter. The transfer was carried out at 120 mA per gel for 1 hr. Membranes were rinsed with PBS and then incubated in blocking buffer (5% non-fat dry milk in PBS with 0.05% Tween-20) for 2 hr at room temperature, or overnight at 4 °C. Blots were incubated in blocking buffer containing a primary antibody for 1-2 hr at room temperature. The following primary antibodies were used: mouse anti-VEGF (C-1, 1: 250, Santa Cruz Biotechnology), rat anti-$VEGF_{164}$ (1: 250, R&D Systems). The blots were washed with PBS containing 0.05% Tween-20 for 20 min, and incubated with a horseradish peroxidase (HRP)-conjugated secondary antibody diluted in blocking buffer for 1 hr at room temperature. The following secondary antibodies were used: sheep anti-mouse IgG (1:1000, GE Healthcare), goat anti-rat IgG (1:1000, GE Healthcare). Blots were washed for 20 min in PBS containing 0.05% Tween-20 and processed for detection of immunoreactivity using enhanced chemiluminescence (ECL, GE Healthcare).

2.2.6.6 Expression and purification of recombinant VEGF proteins

2.2.6.6.1 Secreted expression of recombinant VEGF proteins

Recombinant wild-type and mutant VEGF variants were produced in the methylotrophic yeast *Pichia pastoris*. Three ml of YPD medium containing 25μg/ml zeocin was inoculated with a single colony of *Pichia pastoris* transformants and cultured overnight at 30 °C in a shaking incubator. 800 μl of the saturated overnight culture was inoculated into 400 ml of BMGY growth medium and grown at 30 °C until the culture reached an OD_{600} of around 3, which indicated that the cells were in log-phase growth. The cells were then harvested by centrifuging at 2500 x *g* for 5 min. To induce expression, pellets of transformants with a Mut^s phenotype were resuspended in 100 ml of BMMY induction medium containing 0.01% Antifoam 204 (Sigma), whereas transformants of the Mut^+ phenotype were resuspended to an OD_{600} of 1 in the same medium. Cultures were grown at 29-30 °C for 36-42 hr and methanol was added to a final concentration of 1% every 12 hr to maintain induction of gene expression. The cultures were centrifuged at 7000 rpm for 12 min at 4 °C and the supernatants were filtered through a vacuum-driven, 0.22 μm Durapore® membrane filter (Millipore) and kept on ice. The supernatants were analyzed for protein expression by SDS-PAGE and Coomassie staining.

2.2.6.6.2 Purification of recombinant VEGF111-165 (HBD) by affinity chromatography

For purification of VEGF111-165 (HBD), the cleared supernatant was first concentrated from 150 ml to 5 ml using Vivaspin-20 centrifugation filter units with a 3 kDa molecular weight cut-off (Sartorius). The concentrate was equilibrated by adding two volumes of

heparin-affinity chromatography binding buffer (20 mM Tris (pH 7.4), 150 mM NaCl), centrifuged at 10,000 rpm for 10 min in a microcentrifuge to remove any precipitates, and loaded automatically onto a preequilibrated, 1 ml HiTrap Heparin HP column (Amersham Biosciences) at a flow rate of 0.5 ml/min using the AKTA FPLC™ system (Amersham Biosciences). The column was washed with 3 column volumes, then bound HBD was eluted from the column using a step gradient (0.15 M – 1.5 M NaCl) over 15 column volumes. The fractions containing the protein were pooled and analyzed by SDS-PAGE and Coomassie staining. Method programming as well as analysis and evaluation of runs were performed using the Unicorn 4.1 Software (Amersham Biosciences).

2.2.6.6.3 Purification of recombinant VEGF proteins by Ni-NTA chromatography

For purification of recombinant VEGF120, VEGF164 and VEGF164 HBD mutants, the cleared cell supernatant was first concentrated from 150 ml to 3 ml using Vivacell-70 ultracentrifugation filter units with a 30 kDa molecular weight cut-off (Sartorius). The concentrate was equilibrated by diluting with 2 volumes of Ni-NTA chromatography binding buffer ((pH 7.4), 2.7 mM KCl, 2 mM KH_2PO_4, 8 mM Na_2PO_4, 300 mM NaCl, and complete protease inhibitor without EDTA (Roche)), and incubated with 0.5 ml of pre-equilibrated Ni-NTA agarose (Qiagen) for 60 min at 4 °C. Ni-beads were centrifuged at 1700 rpm for 3 min and washed twice with 5 ml of binding buffer. Proteins were eluted with elution buffer (PBS containing 150 mM NaCl and 40 mM imidazole) in 1 ml steps and analyzed by SDS-PAGE and Coomassie staining.

2.2.6.6.4 Size-exclusion chromatography

Eluates from both purification procedures were concentrated to 100-200 µl using Centricon™ or Microcon™ centrifugal filter devices with the appropriate molecular weight cut-offs (Millipore). Concentrated proteins were centrifuged at 10,000 rpm for 10 min and then loaded automatically onto a preequilibrated Superdex 75 10/300 GL column (Amersham Biosciences) using an AKTA FPLC™ system (Amersham Biosciences) for buffer exchange and isolation of protein dimers. Proteins were eluted in storage buffer (PBS or TBS) at a flow rate of 0.3 ml/min and collected in 1 ml fractions using an automatic fraction collector (Amersham Biosciences). Fractions containing dimeric proteins were concentrated and filter sterilized using Ultrafree®-MC sterile centrifugal filter units (Millipore). Protein concentrations were determined using a BCA protein assay (Pierce), then proteins were snap frozen in liquid nitrogen and stored in aliquots at -80 °C.

2.2.6.7 Analytical heparin-affinity chromatography

To determine the heparin-binding affinity of VEGF variants, 200 µl of heparin-binding buffer (20 mM Tris, 100 mM NaCl, pH 7.4) containing 50 µg of protein was loaded onto a preequilibrated, 1 ml HiTrap Heparin HP column (Amersham Biosciences) at a flow rate of 0.25 ml/min using the AKTA FPLC™ system (Amersham Biosciences). Unbound material was removed and the column was washed with 3 column volumes of binding buffer. Proteins were then eluted with a linear salt gradient (100 mM - 1 M NaCl) over 15 column volumes at a flow rate of 0.5 ml/min. Alternatively, proteins were loaded in heparin-binding buffer containing 0.15 M NaCl and eluted with a salt gradient (0.15 M – 1.5 M NaCl) over 11 column volumes. The columns were reconstituted by washing with binding buffer, then

with H_2O, and were finally stored in 20% ethanol. Conductivity, pH and UV absorbance (280 nm) were measured at 4 °C. All fractions were subjected to trichloroacetic acid precipitation. Protein pellets were diluted in SDS sample buffer, boiled, separated on a 12% SDS-PAGE gel and analysed by Coomassie staining. Method programming as well as analysis and evaluation of runs were performed using the Unicorn 4.1 Software (Amersham Biosciences).

2.2.6.8 Nitrocellulose filter trapping assay

As an additional heparin-binding screen, binding of VEGF164 HBD mutants to heparin was assessed using a saturation binding assay in solution. 0.05 μM of [^{3}H]-heparin (Perkin Elmer) was incubated in microcentrifuge tubes with increasing concentrations of VEGF mutant in binding buffer (25 mM Tris, pH 7.5, 150 mM NaCl, 0.1% BSA) for 1 hr at 37 °C. Nitrocellulose filters (0.45 μm pore size, Millipore) were preequilibrated in BSA-free binding buffer and were placed into separate pockets of a vacuum manifold (Millipore). The samples were transfered onto the filters and unbound [^{3}H]-heparin was removed by applying vacuum and washing 3 times with 1 ml of BSA-free binding buffer. The filters were placed on Whatman paper for drying and then transfered to scintillation vials each containing 3 ml of scintillation liquid. The amount of [^{3}H]-heparin retained by the filter as complexes was determined by counting in a β-scintillation counter (Micro Beta Trilux, Perkin Elmer). Saturation and competition binding analysis were performed using GraphPad Prism 4 software (GraphPad).

2.2.6.9 Competition binding assays with soluble VEGF receptors

96-well microtiter plates (Wallac HB Isoplate, Perkin Elmer) were coated with 100 µl of anti-human IgG (F_c -specific) antibodies (Calbiochem) at a concentration of 5 µg/ml in PBS (pH 7.4) at 4 °C overnight. The wells were blocked 3 x 5 min with 300 µl of blocking buffer (Super Block, Pierce). The blocking buffer was removed and 100 µl of a solution containing receptor/F_c chimeric proteins (R&D systems) in binding buffer (PBS, 0.1% BSA, 0.02% Tween-20) at a final concentration of 400 pM (Flt-1/F_c), 2 nM (Flk-1/F_c), or 1.8 nM (Np-1/F_c) was added to each well. After 90 min of incubation at room temperature, unbound receptors were removed by washing the plate 3 times with 200 µl of binding buffer. Next, 0.01 µCi (for Flt-1) or 0.02 µCi (for Flk-1 and Np-1) of ^{125}I-labeled VEGF165 in binding buffer was added to the plate together with increasing concentrations of cold competitor in a final volume of 100 µl. Non-specific binding of ^{125}I-VEGF was assessed by adding 400 nM of VEGF164 to the well. Binding to equilibrium was carried out at 37 °C for 2-3 hr, after which the plate was washed 3x with 200 µl of binding buffer. Binding of ^{125}I-VEGF was quantitated in a β-scintillation counter (Micro Beta Trilux, Perkin Elmer). Inhibitory concentrations 50% (IC_{50}) values were calculated using the one-site competition binding analysis program of GraphPad Prism 4 (GraphPad Software).

2.2.7 Circular dichroism (CD) spectrophotometry

CD spectra of VEGF164 and the VEGF164 HBD mutants K30A/R35A/R39A, R14A/R49A, and R13A/R14A/R49A were recorded in the wavelength range 198-260 nm with a Jasco J-810 spectropolarimeter (Jasco, UK) and a 0.1 cm path-length stain-free cell. The proteins were analyzed at a concentration of 0.15 mg/ml in TBS (10 mM Tris, pH 7.4,

0.15 M NaCl) at room temperature. Due to the absorbance of NaCl, spectroscopic data below 200 nm were not used for structural interpretation. The spectra were recorded in millidegrees of ellipticity (θ). The solvent spectrum (TBS) was subtracted from the sample spectra and the subtracted spectra were converted to mean residue ellipticity (CD signal per amino acid residue, $[\theta]$) in degrees x cm^2 x $dmol^{-1}$ by the following equation:

$$[\theta]_{mrw} = \theta \times M_{mrw} / 10 \times c \times l$$

where c is the protein concentration in mg/ml, l is the cell path length in cm, and M_{mrw} is the mean residue molecular weight of the VEGF164 dimer. All measurements were done twice, with identical results.

2.2.8 Animal handling

All mice and rats examined were treated in accordance with the Association for Research in Vision and Ophthalmology Statement for the Use of Animals in Ophthalmic and Vision Research. Before intravitreal injection, the animals were anesthetized by intramuscular injection of a mixture of ketamine and xylazine. A drop of Tropicamide® was administered to dilate the pupil of each eye to be injected and liquid tears were administered to prevent desiccation. Animals were sacrificed by CO_2 narcosis.

2.2.9 Rat aortic ring assay for angiogenesis

Thoracic aortas were dissected from male Fisher rats (6-10 weeks) and placed into a dish containing EB medium (Cambrex) supplemented with 2 mM glutamine and

penicillin/streptomycin (100 μg/ml). The aortas were carefully cleaned of all surrounding adventitial tissues under a dissecting microscope and cut into 1 mm wide rings. Each of the rings was embedded in a rat collagen mix (2 mg/ml collagen I, 4 ml H_2O, 1x DMEM, 2.34 mg/ml $NaHCO_3$) in 4-well multidishes (Nunc) and the collagen gel was then overlaid with 450 μl of EBM medium. The plates were incubated at 37 °C and 5% CO_2 in a humidified atmosphere for 7 days and EBM medium was replaced every 48 hr with control medium or medium containing purified VEGF variants (4.4 nM). Rings that did not show any signs of vessel growth after 48 hr were discarded.

2.2.10 Generation of VEGF164-deficient ($VEGF^{120/188}$) mice

VEGF164-deficient ($VEGF^{120/188}$) mice were generated by mating $VEGF^{+/188}$ female mice and $VEGF^{+/120}$ male mice, both of which were produced via targeted mutagenesis with Cre/*lox*P-mediated site-specific recombination in embryonic stem cells [254]. Genotyping was performed by PCR.

2.2.11 Mouse model of oxygen-induced proliferative retinopathy

Oxygen-induced proliferative retinopathy (OIR) was induced in $VEGF^{120/188}$ mice and wild-type litter mates using the protocol described by Smith *et al.* [274]. P7 mice and their nursing mothers were exposed to 75% oxygen/25% nitrogen for 5 days to induce retinal vaso-obliteration and were then returned to room air (21% oxygen). Retinal leukostasis was observed at P14 and retinal neovascularization was observed at P17, using the techniques described below. $VEGF^{120/188}$ control mice of similar age were kept in room air.

2.2.12 Animal injections

For analysis of leukocyte recruitment, a single injection of 2 pmol or 20 pmol of VEGF164, inactivated VEGF164, VEGF120, VEGF164 HBD mutants, PlGF-1, PlGF-2 (R&D Systems), or VEGF-E (Cellsciences) in 2.5 µl PBS was performed by inserting a 33-gauge needle (Ito Seisakusyo) into the vitreous of an anesthetized male Long Evans rat (200-225 g, Charles River). For blocking experiments using purified HBD, various concentrations of recombinant HBD (2.5 µl) were injected intravitreally 2 min before injecting VEGF164 (2 pmol/2.5 µl). The dosage was determined based on a previous study describing leukostasis in the retinal vasculature after VEGF injection [276]. Insertion and infusion were performed under a surgical microscope. At 24, 48, and 72 hr after vitreal injection, leukocyte recruitment was analyzed using acridine orange fluorography.

To assess the effect of VEGFR-1 neutralization on leukostasis, mice were randomized to receive intraperitoneal injections of 0.3, 1.5, or 3.0 mg/kg anti-VEGFR-1 neutralizing antibody (R&D Systems) 3 hr before intravitreal injection of VEGF164 (2 pmol/0.8 µl) using a 33-gauge dual needle. Control animals received an equivalent amount of a pre-immune, control goat IgG (R&D Systems). To test the effect of recombinant HBD on the OIR-induced inflammatory response, 2 nmol of purified and sterilized HBD, 5 mg/kg of anti-VEGF-neutralizing antibody (R&D Systems) and goat IgG control (R&D Systems) were injected systemically into the penetrial space of P12 OIR mice every 24 hr for 2 days, using a 33-gauge needle (Ito Seisakusyo). To examine leukostasis, P14 OIR mice were perfused with FITC-coupled concanavalin A (Con A) from the heart as described below.

2.2.13 Cell labeling

2.2.13.1 Immunohistochemistry of rat aortic ring vessels

After 7 days in culture, aortic rings were washed with PBS and fixed in 1 ml/well of paraformaldehyde (10% (v/v) in PBS) for 1 hr at room temperature, followed by a triple wash (3 x 10 min) with PBS and blocking of non-specific binding sites with blocking buffer (6% (v/v) goat serum in PBS containing 0.3% (v/v) Triton X-100) for 8 hr. Blood vessels were stained with biotinylated isolectin B4 (Sigma, 1:300 in blocking buffer) overnight at 4 °C followed by multiple washes (4 x 15 min) in blocking buffer and incubation with HRP-conjugated Alexa 546 secondary antibody (Invitrogen, 1:250 in blocking buffer) for 2 hr at room temperature. Finally, rings were washed 4 x 20 min in blocking buffer and 2 x 20 min in PBS. Images of aortic rings were captured using a DMIR epifluorescence microscope (Leica) equipped with a digital camera (Qimaging).

2.2.13.2 Platelet endothelial cell adhesion molecule (PECAM)-staining of retinal endothelial cells

Mice were killed at P17 and frozen sections (10 μm-width) were made from eye cups embedded in optimal cutting temperature compound (Sakura Finetek). Samples were fixed with 4% paraformaldehyde in PBS for 10 min, then incubated in methanol/H_2O_2 for 15 min at 4 °C, washed with PBS, and incubated for 30 min in 10% normal goat serum. Slides were incubated for 2 hr with biotinylated anti-mouse PECAM-1 antibody (0.5 mg/ml, BD Biosciences) and, after washing with PBS, incubated with avidin coupled to peroxidase (Vector Laboratories) for 30 min at room temperature. After a final wash for 10 min, slides were incubated with diaminobenzidine to give a brown reaction product and were mounted

with Vectashield. The sections were examined under a microscope (DMRA2, Leica) and images were digitized using a 3CCD color video camera (ORCA-ER, Opelco).

2.2.13.3 Lectin labeling of retinal vasculature and adherent leukocytes in mice

C57BL/6J male mice (20-22g, Charles River) and VEGF transgenic mice were deep-anesthetised with intramuscular xylazine hydrochloride and ketamine hydrochloride. The chest cavity was then carefully opened and a 22-gauge cannula introduced into the aorta. The animals were perfused with 500 ml of PBS per kg of body weight to remove erythrocytes and non-adherent leukocytes. Perfusion with Con A coupled to fluorescein isothiocyanate (FITC, 40 μg/ml in PBS, pH 7.4; 5 mg/kg body weight; Vector Laboratories) was then performed to label adherent leukocytes and vascular endothelial cells, followed by PBS perfusion to remove residual unbound lectin. The eyes were enucleated and fixed with 4% paraformaldehyde for 1 hr before retinas were separated and flat mounted. Each retina was imaged with an epifluorescence microscope, and the total number of adherent leukocytes per retina was determined.

2.2.13.4 Labeling of macrophages with F4/80 immunofluorescence

Adherent leukocytes were first labeled *in vivo* with FITC-coupled Con A as described above. Eyes were removed and eye cups containing the retina were fixed overnight at 4 °C in 4% paraformaldehyde. Following fixation, eye cups were permeabilized with 0.5% Triton X-100 in PBS for 24 hr and non-specific binding was reduced by incubation in blocking buffer (10% goat serum in PBS). The eye cups were then incubated with a

purified rat anti-mouse antibody directed against F4/80 (1:250 dilution, eBiosciences) in blocking buffer for 2 hr at room temperature, washed for 2 hr in wash buffer (PBS containing 0.1% Triton X-100) and incubated with Alexa Fluor-488 goat anti-rat IgG secondary antibody (1:500 dilution, Molecular Probes) for 1 hr in blocking buffer. After a final wash for 3 hr, retinas were flat mounted and imaged with an epifluorescence microscope.

2.2.13.5 Acridine orange leukocyte fluorography

Leukocyte recruitment in the retina was studied *in vivo* by acridine orange leukocyte fluorography, using rats injected intravitreally with VEGF family member proteins and/or purified HBD as described above. At 24, 48, and 72 hr after vitreal injection, animals were injected intravenously with acridine orange, which causes leukocytes and endothelial cells to fluoresce through the noncovalent binding of the molecule to double-stranded DNA. Immediately before fluorography, each rat was anesthetized and the pupil dilated with 1% tropicamide. Acridine orange (Sigma) was dissolved in sterile saline (1 mg/ml), and 3 mg/kg were injected through the tail vein catheter at a rate of 1 ml/min. Static leukocytes in the capillary bed were observed *in vivo* 30 min later for 1 min by fundoscopy, using a scanning laser ophthalmoscope with an argon blue laser as illumination source and the standard fluorescein angiography filter in the 40° field setting. Thirty min later, the fundus was again observed to evaluate retinal leukostasis. Images were recorded on a digital videotape. To evaluate retinal leukostasis, 8 areas of 200 pixel^2 each at a distance of 5 disc diameters from the edge of the optic disc were assessed to determine the number of fluorescent dots in the retina. These numbers were converted to leukocytes/mm^2 by using

the formula: 1 pixel = 3.2 μm^2. Leukocytes were considered static if their position did not change for 3 min.

2.2.14 Morphometric analysis

2.2.14.1 Analysis of vessel outgrowth from aortic rings

To quantify blood vessel growth in the aortic ring assay, RGB images of the rings were converted to 8-bit grayscale images in Photoshop (Adobe) and blood vessels were traced in a new layer using a 9-point pencil tool. All images were traced by a masked researcher. The new image layer was then binarized and the traced lines skeletonized using the Image-J software (NIH). All white pixels in the skeletonized image were counted and expressed relative to the circumference of the aortic ring in order to normalize the total number of new blood vessels to the aortic ring size.

2.2.14.2 Analysis of vascular development and density in the retina

Vascular development was quantified by measuring the length of eight vessels from the optic nerve to the edge of the vascular area, each going in a different direction. The length of a vessel was then expressed as a percentage of the radius of the retina. The eight values were then analyzed statistically. To determine the vascular density of retinal flat mounts the total length of vessels in each of four different vascular areas (each 200 $pixels^2$) were measured using NIH image. The vessel length was expressed in $pixels^2$ and the vascular density was expressed as a percentage by dividing the total vessel length by the area using NIH image.

2.2.15 Statistical analysis

All values were expressed as mean ± SEM unless otherwise indicated. For statistical analysis of *in vivo* studies, the unpaired Student t-test was used when two groups were compared. Data were analyzed by using post-hoc comparison test (Bonferroni) when three or more groups were compared. Differences were considered statistically significant when P-values were <0.05.

Chapter 3: *In vitro* mutagenesis of the heparin-binding domain of VEGF164

3.1 Introduction

The significance of the heparin-binding VEGF isoforms was emphasized by the finding that 50% of the mice engineered to express exclusively the non-heparin-binding VEGF120 die of postnatal angiogenesis defects shortly after birth [284]. On the other hand, mice that solely produce VEGF164 appear normal and healthy [254]. VEGF165, the major isoform in humans, shows moderate affinity for heparin and neuropilin-1, as a result of binding determinants encoded by exon 7 [126]. It has been suggested that this region conveys distinct functions to VEGF165 and the longer isoforms [61, 118]. However, the functional significance of the heparin- and neuropilin-1-binding abilities of VEGF165 has remained elusive.

To better understand the role of heparin binding in the mouse homolog VEGF164, I started by identifying amino acid residues that are critically involved in mediating this function. To this end, I introduced mutations into the exon 7-encoded domain of full-length VEGF164 using alanine-scanning mutagenesis. This chapter describes the mutagenesis approach and the purification of wild-type and mutant VEGF species, as well as their characterization with regard to heparin and neuropilin-1 binding.

3.2 Results

3.2.1 Sequence alignment of the VEGF164 HBD

The HBD of VEGF165 lacks significant sequence homology to other heparin-binding proteins outside the VEGF family [121], indicating that VEGF-heparin binding occurs via binding regions distinct from the heparin-binding consensus sequences or motifs that exist in other proteins [209]. The novelty of the HBD and the highly basic character of the domain have made it difficult to identify critical amino acids involved in heparin interaction.

Sequence alignment analysis of the VEGF164 C-terminal region revealed a high degree of sequence homology among residues of the long VEGF isoforms and other members of the VEGF family of growth factors (Figure 3.1). Sequence homology was also observed between species as phylogenetically distant from mammals as frog and zebrafish, suggesting that heparin binding may be an evolutionarily conserved function of VEGF. All eight cysteine residues involved in the formation of intra-chain disulfide bridges within the VEGF165 HBD are conserved among all variants (Figure 3.1), resembling the highly conserved cysteine knot motif in the VEGF/PDGF homology domain (VHD) of VEGF [111]. Based on this cysteine homology, it is conceivable that the disulfide bond linkages are the same among these variants, raising the possibility of a conserved backbone structure.

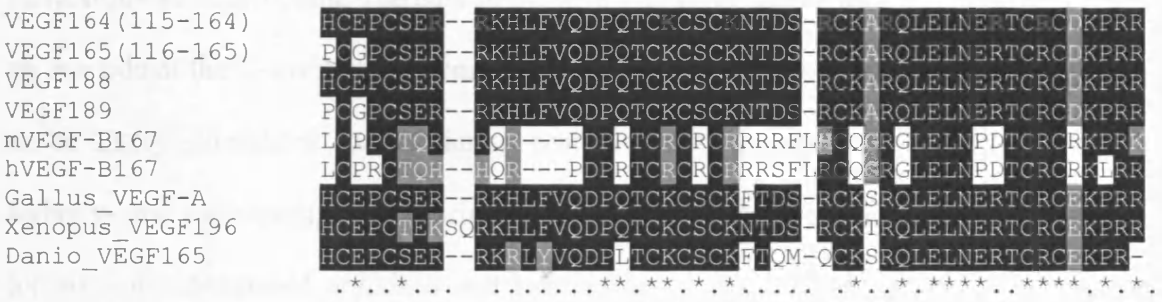

Figure 3.1 Multiple sequence alignment of the VEGF164 C-terminal region with selected VEGF variants. Comparison of VEGF164 exon 7- and 8-encoded amino acid sequence (SWISS-PROT accession No. Q00731-2) with corresponding regions of VEGF165 (SWISS-PROT accession No. P15692), VEGF188 (SWISS-PROT accession No. Q00731-1), VEGF189 (SWISS-PROT accession No. P15692-2), mouse VEGF-B167 (SWISS-PROT accession No. P49766-2), human VEGF-B167 (SWISS-PROT accession No. P49765-2), *Gallus* (chicken) VEGF-A (DDBJ/EMBL/GenBank accession No. AB011078), *Xenopus* (frog) VEGF196 (SWISS-PROT accession No. 042572), and *Danio* (zebrafish) VEGF165 (SWISS-PROT accession No. 073682-1). The sequence alignment was generated using the Clustal W program and was further optimized manually. Amino acids that are identical are shaded in black and amino acids that are similar are shaded in grey. The asterisk (*) denotes a column with fully conserved amino acids (100% identity), whereas a period (.) denotes a column in which the molecular weight or the hydropathy of amino acids has been preserved in at least 50% of the aligned sequences. Residues that were subjected to mutagenesis in this study are highlighted in green.

3.2.2 Site-directed mutagenesis of the VEGF164 HBD

The published NMR solution structure of the 55-residue HBD of human VEGF165 provided the basis for a structure-guided mutagenesis approach [119]. The HBD contains the five C-terminal residues of exon 5 in addition to the peptide encoded by exons 7 and 8. Analysis of the solvent-accessible molecular surface of HBD revealed a marked polarity in

surface charge distribution. The bulk of positively-charged amino acid residues are located on one side of the C-terminal subdomain. Basic residues in this region have been suggested to be likely candidates for mediating ionic interactions with the negatively-charged carboxy- and sulfo-groups of heparin [119]. To test this hypothesis, I exchanged alanine for six solvent-exposed arginines and two lysines, individually or in double, triple or quadruple combinations (Table 3.1).

Mutant	C-terminal HBD (11-55)
K30A	SERRKHLFVQDPQTCKCSC**K**NTDSRCKARQLELNERTCRCDKPRR
K35A/R39A	SERRKHLFVQDPQTCKCSCKNTDS**R**CKA**R**QLELNERTCRCDKPRR
K30A/R35A/R39A	SERRKHLFVQDPQTCKCSC**K**NTDS**R**CKA**R**QLELNERTCRCDKPRR
K30A/R35A/R39A/R49A	SERRKHLFVQDPQTCKCSC**K**NTDS**R**CKA**R**QLELNERTC**R**CDKPRR
K26A	SERRKHLFVQDPQTC**K**CSCKNTDSRCKARQLELNERTCRCDKPRR
R46A/R49A	SERRKHLFVQDPQTCKCSCKNTDSRCKARQLELNE**R**TC**R**CDKPRR
R13A/R14A	SE**RR**KHLFVQDPQTCKCSCKNTDSRCKARQLELNERTCRCDKPRR
R14A/R49A	SER**R**KHLFVQDPQTCKCSCKNTDSRCKARQLELNERTC**R**CDKPRR
R13A/R14A/R49A	SE**RR**KHLFVQDPQTCKCSCKNTDSRCKARQLELNERTC**R**CDKPRR
R13A/R14A/R46A/R49A	SE**RR**KHLFVQDPQTCKCSCKNTDSRCKARQLELNE**R**TC**R**CDKPRR

Table 3.1 VEGF164 HBD mutants and their targeted residues within the primary amino acid sequence. Residues highlighted in blue were replaced with alanine by site-directed mutagenesis. Residues 1-10 of the HBD (1-55) were not mutated and are not shown. Both the VEGF164 HBD and VEGF165 HBD consist of 55 amino acids and the mutated residues share the same numbering in both proteins.

The majority of these candidate amino acids can be grouped into three positively-charged clusters located on the same side of the N-terminal (R13, R14) and the C-terminal subdomain (K30, R35, R39, and R46, R49). Alanine mutagenesis was also applied to one lysine (K26) for control purposes. In total, 10 mutants were constructed (Figure 3.2). To generate the mouse VEGF164 HBD mutants, a PCR-based site-directed mutagenesis approach was performed using the cDNA of full-length VEGF164 as template.

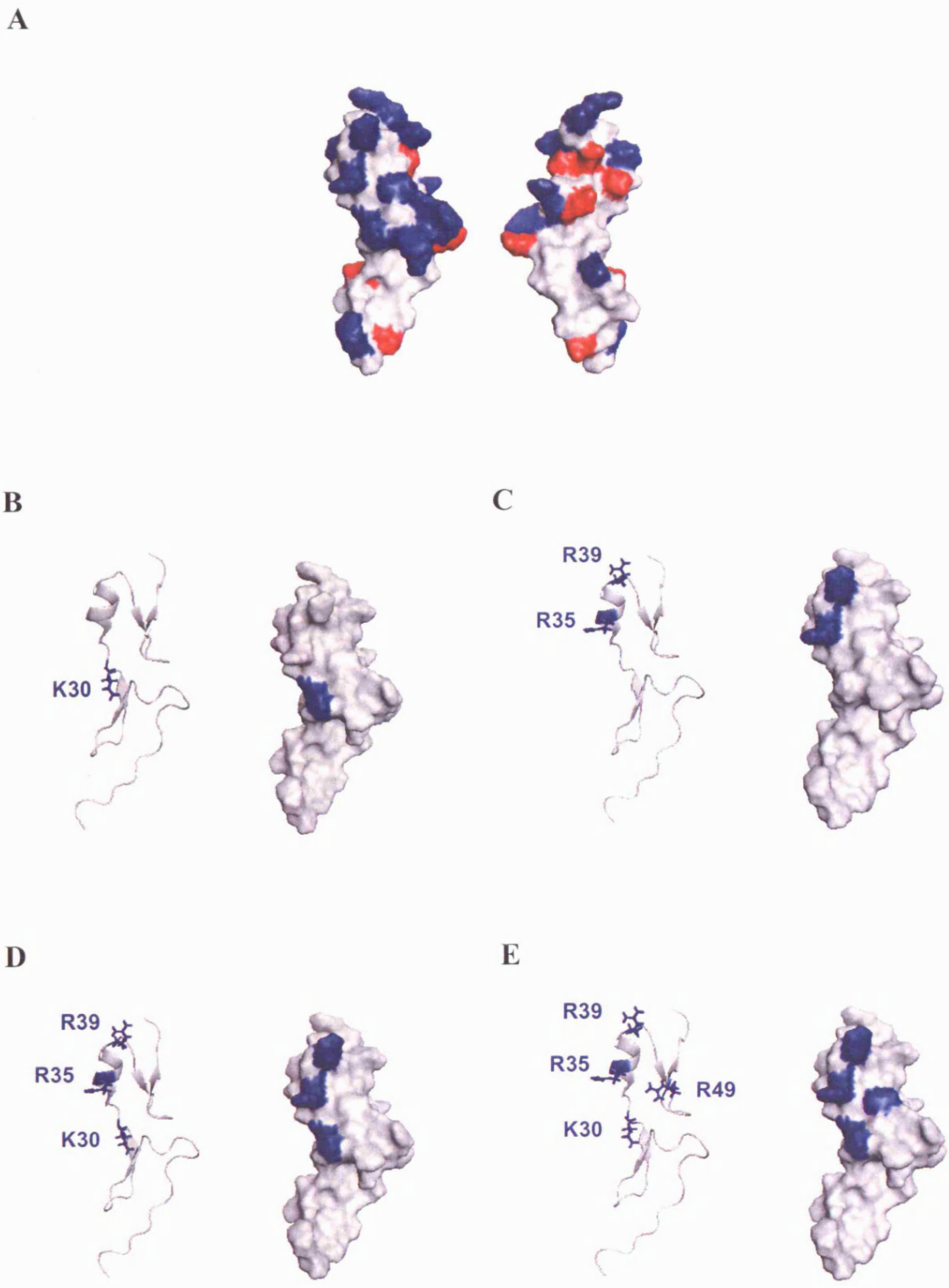
A
B
K30
C
R39
R35
D
R39
R35
K30
E
R39
R35
R49
K30

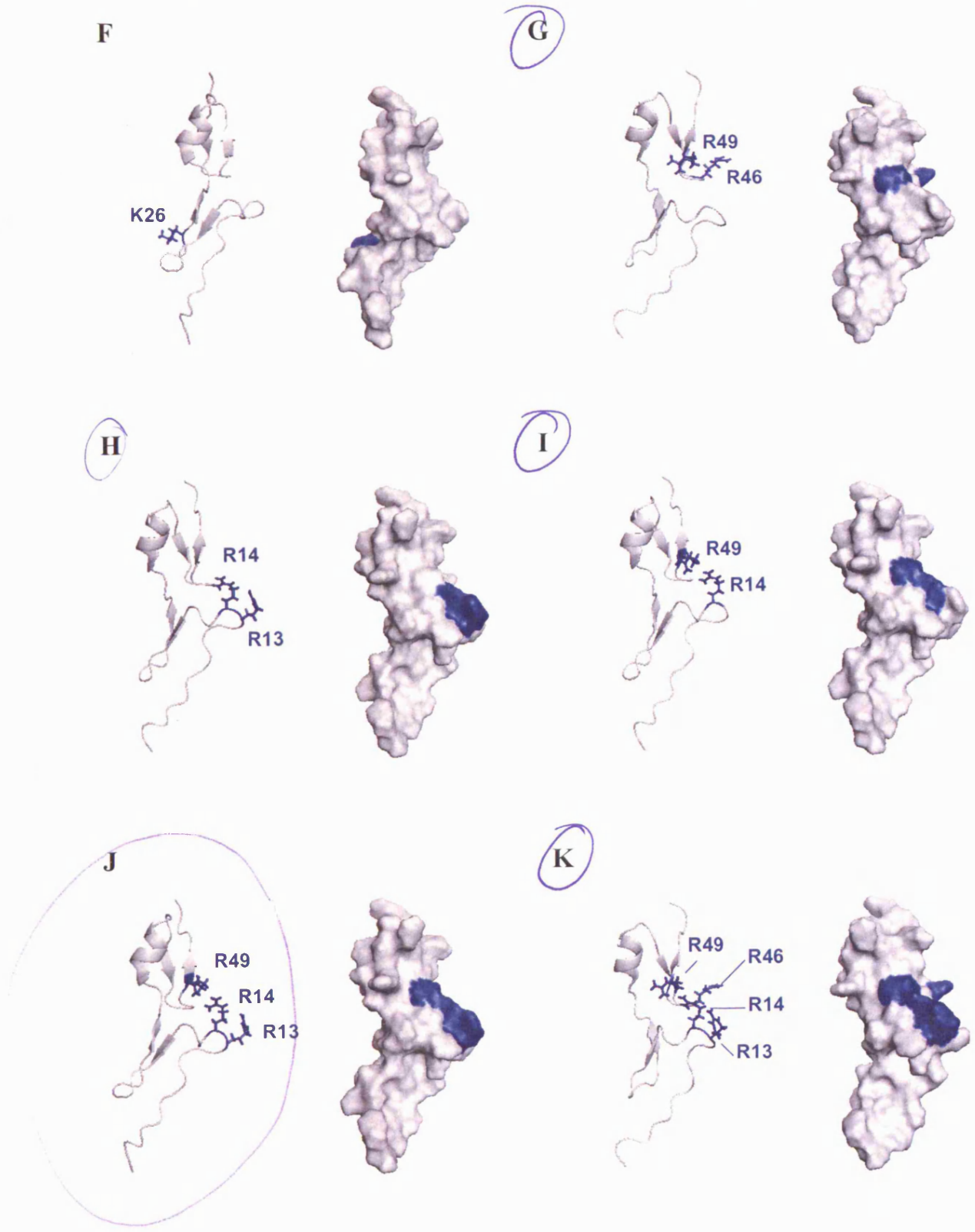
F
K26
G
R49
R46
H
R14
R13
I
R49
R14
J
R49
R14
R13
K
R49
R46
R14
R13

Figure 3.2 Structural representation of the VEGF165 HBD and illustration of the amino acids mutated in this study. (A) Surface topology model of the VEGF165 HBD (1-55) showing the distribution of electrostatic potential on the molecule surface. Charged residues are color coded with basic and acidic amino acids shown in blue and red, respectively. The structural model is shown at two angles rotated by 180° about the vertical axis. (B-K) Illustration of the mutated HBDs as ribbon diagram (left) and surface topology model (right). Lysine and arginine residues selected for mutagenesis are labeled and highlighted in blue. The numbering of amino acids is based on the primary sequence shown in table 3.1. (B) K30A, (C) R35A/R39A, (D) K30A/R35A/R39A, (E) K30A/R35A/R39A/R49A, (F) K26A, (G) R46A/R49A, (H) R13A/R14A, (I) R14A/R49A, (J) R13A/R14A/R49A, (K) R13A/R14A/R46A/R49A. Diagrams were generated with PyMOL (DeLano Scientific, Inc.) based on the NMR solution structure (Protein Data Bank code: 1KMX).

3.2.3 Expression and purification of VEGF proteins

To produce recombinant wild-type (VEGF120, VEGF164, and HBD) and mutant VEGF proteins, the *Pichia pastoris* yeast expression system was chosen. This system allows the inducible secretion of proteins into the yeast culture medium with the additional advantage of high heterologous protein expression levels. Proteins produced in this organism do not require refolding and, with regard to posttranslational modifications, resemble more closely those produced by higher eukaryotic organisms. All wild-type and mutant proteins appeared to be released into the medium of transformed *Pichia pastoris* cultures after secretion, as resuspension of yeast pellets in high-salt buffer did not result in significantly higher protein yields (data not shown). The protein yield obtained from cell supernatants was estimated by SDS-PAGE and Coomassie staining and was found to be comparable to

that of native VEGF164, suggesting that the mutations did not significantly interfere with proper folding.

Proteins were purified from conditioned media by using two purification strategies. In the first, medium containing HBD was applied to a heparin-sepharose column and eluted with a step gradient of increasing NaCl concentration. The fragment eluted at 0.6-0.8 M NaCl. In the second strategy, VEGF120, VEGF164 and all HBD mutants were purified by exploiting the nickel-binding affinity of histidine residues located in the N-terminus of VEGF. To better refine comparison of the different VEGF variants in both *in vitro* and *in vivo* studies, dimeric forms were separated from higher-order oligomers using size-exclusion chromatography. The purity of all protein preparations was approximately 95%, as estimated by SDS-PAGE and Coomassie staining (Figure 3.3). The identity of VEGF120 and VEGF164 was confirmed by probing the purified proteins with a mouse monoclonal antibody raised against the N-terminus (Figure 3.3 B). VEGF immuno-positive bands were detected at 18 kDa and 23 kDa, the expected molecular weights of monomeric VEGF120 and VEGF164, respectively. Recombinant HBD, for which no antibody was available, runs as an approximately 7 kDa-protein under reducing conditions. The ability of VEGF120 and VEGF164 to form disulfide-linked homodimers is a prerequisite for their bioactivity and was not compromised by heterologous expression or by the purification procedure, as dimerization of both proteins was preserved under non-reducing conditions.

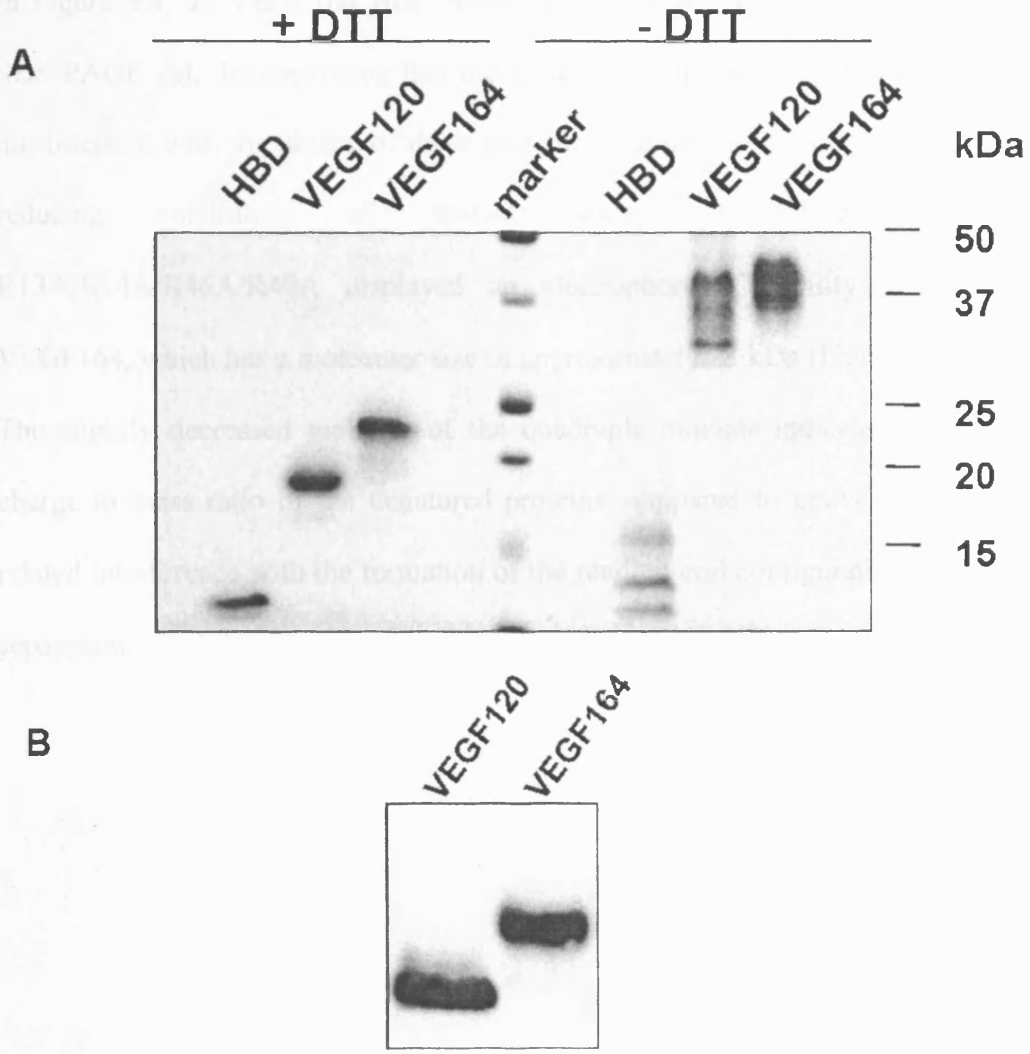

Figure 3.3 Purification of recombinant VEGF wild-type variants. VEGF proteins were expressed in *Pichia pastoris* and purified by nickel-agarose chromatography (VEGF120, VEGF164) or heparin-affinity chromatography (HBD), followed by size-exclusion chromatography. (A) Coomassie-stained SDS-PAGE gel of purified protein dimers and the HBD monomer (1 μg) electrophoresed under reducing (left) and non-reducing (right) conditions. The aggregation of HBD monomers may have been a heating artifact in the absence of DTT. (B) Western analysis of purified VEGF120 and VEGF164, which were probed with a monoclonal pan-VEGF antibody.

VEGF164 HBD mutants, too, were purified by nickel-agarose chromatography As shown in Figure 3.4, all VEGF164 HBD mutants showed the expected size on a non-reducing SDS-PAGE gel, demonstrating that the mutations within the heparin-binding domain did not interfere with the ability of these proteins to dimerize (Figure 3.4, top panel). Under reducing conditions, all mutants except K30A/R35A/R39A/R49A and R13A/R14A/R46A/R49A displayed an electrophoretic mobility similar to that of VEGF164, which has a molecular size of approximately 23 kDa (Figure 3.4, bottom panel). The slightly decreased mobility of the quadruple mutants indicates either a decreased charge to mass ratio of the denatured proteins compared to native VEGF or mutation-related interference with the formation of the random-coil configuration necessary for size separation.

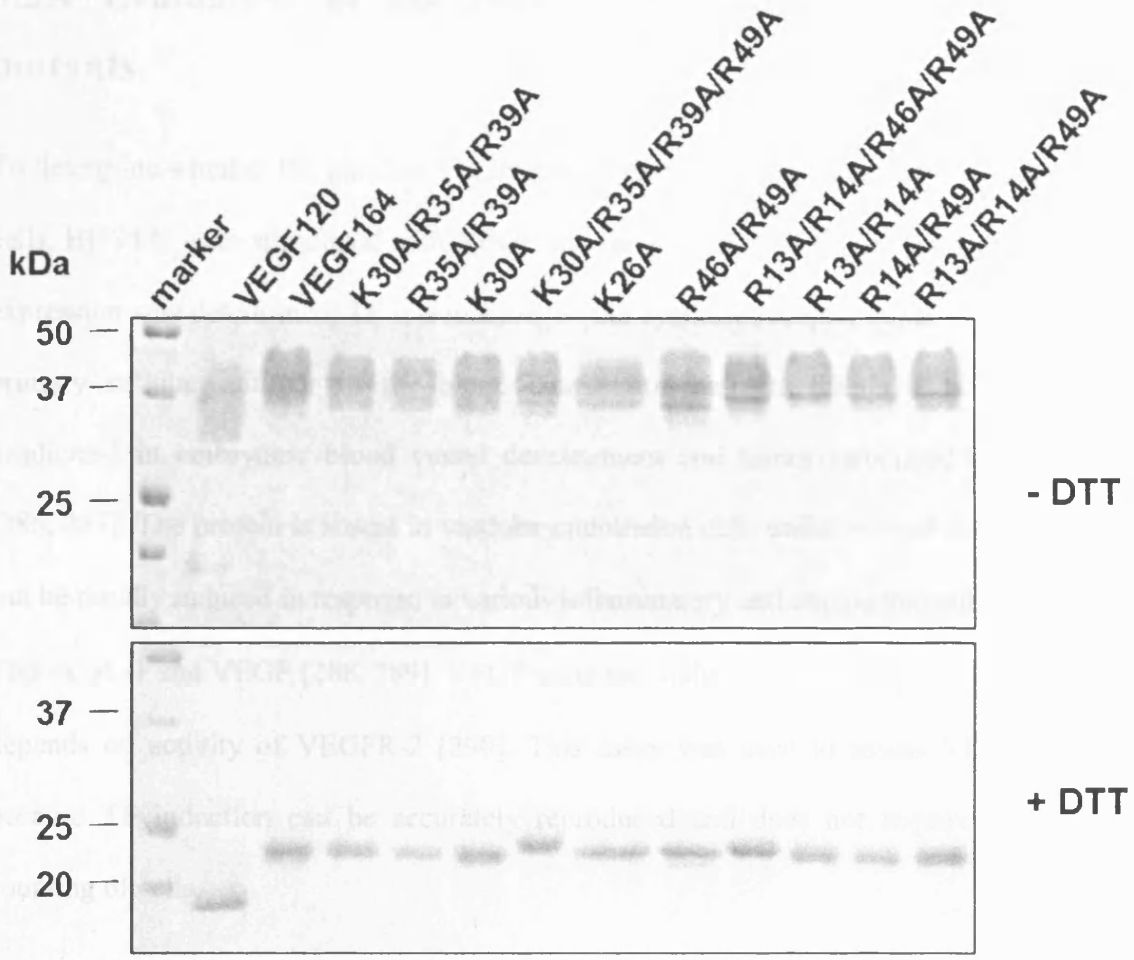

Figure 3.4 Purification of recombinant VEGF164 HBD mutants. VEGF164 HBD mutant proteins were expressed in *Pichia pastoris* and purified by nickel-agarose chromatography and size-exclusion chromatography. Coomassie-staining of gels after reducing (lower panel) and non-reducing (upper panel) SDS-PAGE of purified protein dimers (1 μg) are shown in comparison to purified VEGF120 and VEGF164 (1 μg). The additional faint band observed with some mutants under reducing conditions is believed to be unglycosylated VEGF [124].

3.2.4 Evaluation of the bioactivity of the VEGF164 HBD mutants

To determine whether the purified VEGF species exhibit biological activity in endothelial cells, HUVEC were stimulated with VEGF and the induction of tissue factor (TF) mRNA expression was determined. TF is a member of the cytokine-receptor super-family and the primary cellular initiator of the blood coagulation cascade [285]. It has also been implicated in embryonic blood vessel development and tumor-associated angiogenesis [286, 287]. The protein is absent in vascular endothelial cells under normal conditions, but can be rapidly induced in response to various inflammatory and angiogenic stimuli, such as TNF-α, IL-1 and VEGF [288, 289]. VEGF-mediated induction of TF expression by VEGF depends on activity of VEGFR-2 [290]. This assay was used to assess VEGF activity because TF induction can be accurately reproduced and does not require labeling or counting of cells.

Subconfluent HUVEC were treated with recombinant VEGF variants for 1 hr. The optimal VEGF concentration of 0.3 nM was determined in a dose-response experiment (data not shown). Compared to the buffer control, TF mRNA was induced 5.6-fold in response to VEGF164, whereas VEGF120 was slightly less potent, causing a 3.9-fold induction. All VEGF164 HBD mutants were active and their potency in stimulating TF gene expression was comparable to that of VEGF164. These results suggest that the mutations did not significantly affect the ability of VEGF164 to activate VEGF receptor-mediated signaling pathways leading to TF expression.

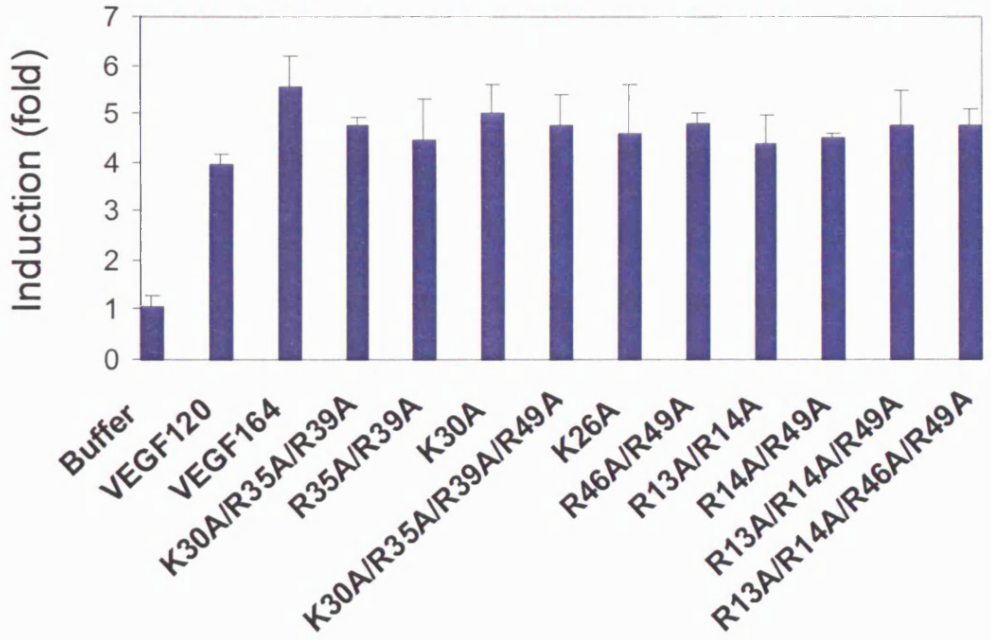

Figure 3.5 VEGF164 HBD mutants induce TF mRNA upregulation in HUVEC. HUVEC were treated for 1 hr with medium containing PBS or 0.3 pmol/ml of purified VEGF protein. Total RNA was isolated and reverse transcribed to yield cDNA, which was subjected to real-time PCR analysis using GAPDH as internal control. Levels of TF gene expression were determined using the comparative threshold method. The data represent the mean ± SEM of three independent experiments.

3.2.5 Qualitative analysis of heparin binding by VEGF164 HBD mutants

Next, I employed heparin-sepharose chromatography as a method for screening the heparin-binding affinity of the mutants. A heparin-sepharose column was loaded with purified protein dimers and washed, then the bound proteins were eluted with a linear NaCl gradient. The relative affinities for heparin were assessed by determining the amount of

salt required to elute the proteins from the column. As expected, VEGF164 completely bound to the heparin column in the presence of 0.1 M NaCl (Figure 3.6). Binding of VEGF to heparin occurs through binding determinants located in the HBD. VEGF120, which lacks this domain, did not bind to the column and was found in the flow-through and wash fractions. The HBD fragment alone exhibited similar heparin-binding behavior as VEGF164, resulting in a similar elution profile. These data confirm that the heparin-binding activity of VEGF164 is fully mediated by its C-terminal domain. Notably, VEGF164 did not elute from the column in one distinct peak but rather over a wide range of the salt gradient (0.58 M – 1 M NaCl). This made it impossible to determine a specific salt concentration for each protein that would be representative for its heparin-binding affinity. Instead, the concentration of NaCl in the elution buffer required to displace approximately 50% of the protein from the column was used as an indicator for its affinity.

With regard to their spatial arrangement, the basic amino acids K30, R35, R39, and R49 are located in relatively close proximity to each other and may thus form a cluster that acts as a docking site for heparin. The quadruple mutant K30A/R35A/R39A/R49A and the triple mutant K30A/R35A/R39A presented similar elution profiles. In both cases a significant amount of protein was found in the wash and early elution fractions and a second portion of the sample bound more tightly to the column and eluted at 0.46-0.7 M (Figure 3.6). A similar pattern was also observed with the double mutant R35A/R39A, albeit to a lesser degree. Next, the binding of the single mutant K30A was investigated in order to determine the relative contribution of this residue to the heparin-binding activity observed in the triple and quadruple mutant. The elution characteristics of K30A were comparable to those of VEGF164 (Figure 3.6). Therefore, Lys30 does not appear to be

critically involved in heparin interaction. Similar results were observed for Lys26 (Figure 3.6), which is located on the backside of the N-terminal subdomain (Figure 3.2 F).

Arg46 and Arg49 form a basic cluster that is part of the two-stranded antiparallel β-sheet structure within the HBD. Targeting of these residues resulted in a slightly decreased binding capacity of the protein, as shown in Figure 3.6. The NaCl concentration required to displace approximately 50% of this mutant from the column was approximately 0.82 M. Heparin binding was further impaired in the double mutant R13A/R14A (0.52 M NaCl). Arg13 and Arg14 are major components of a disordered and poorly-defined loop region adjacent to Arg46 and Arg49, and the combined quadruple mutant R13A/R14A/R46A/R49A displayed very little heparin-binding activity. Because the replacement of four residues may have caused major alterations in the local structure, the number of mutations was reduced to three (R13A/R14A/R49A) and two (R14A/R49A). Both variants bound to the column and eluted in one peak. However, R14A/R49A (0.49 M NaCl) and R13A/R14A/R49A (0.4 M NaCl) showed a marked reduction in their ability to bind to heparin.

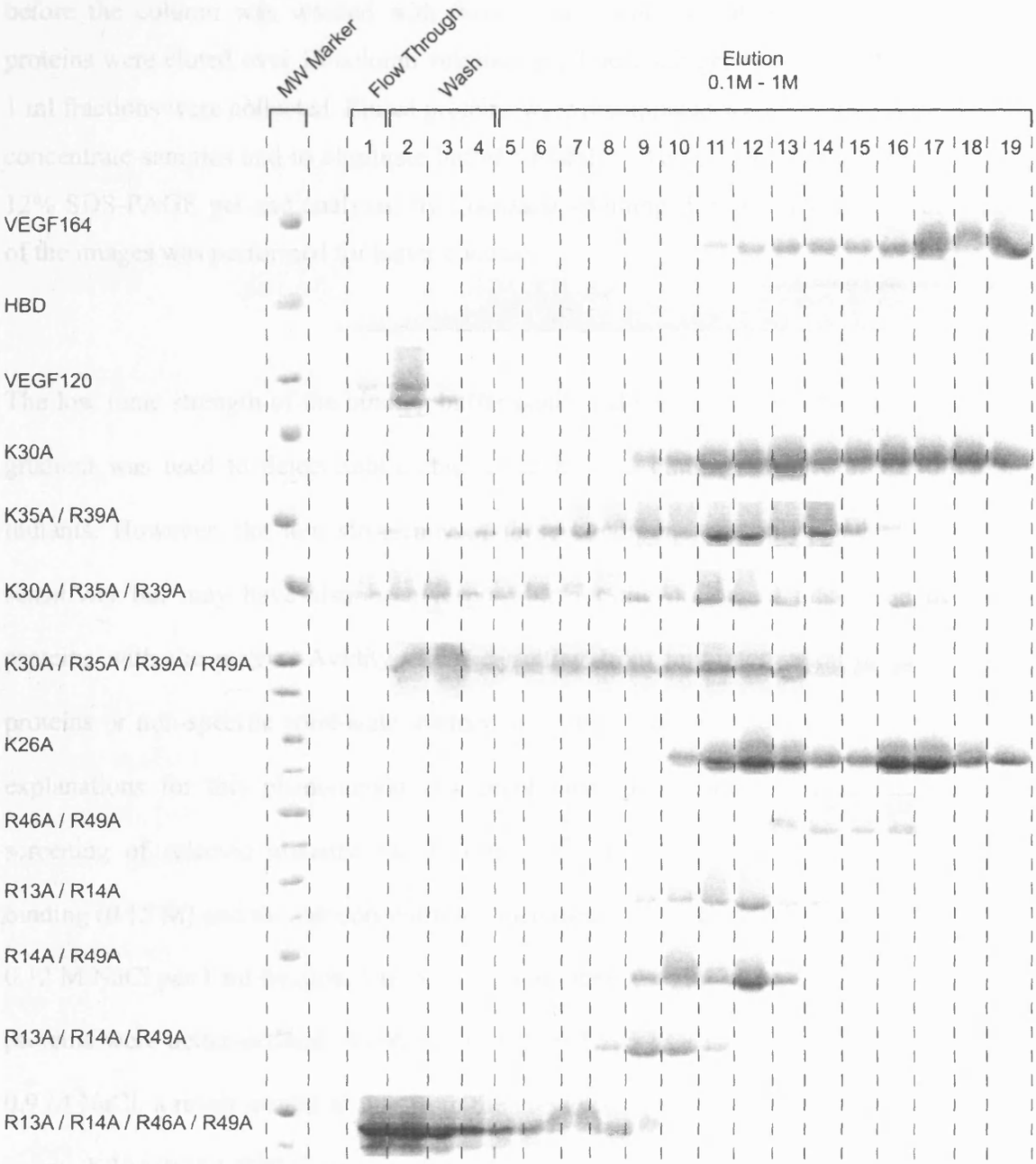
MW Marker
Flow Through
Wash
Elution
0.1M - 1M
1 2 3 4 5 6 7 8 9 10 11 12 13 14 15 16 17 18 19
VEGF164
HBD
VEGF120
K30A
K35A / R39A
K30A / R35A / R39A
K30A / R35A / R39A / R49A
K26A
R46A / R49A
R13A / R14A
R14A / R49A
R13A / R14A / R49A
R13A / R14A / R46A / R49A

Figure 3.6 Comparison of heparin-binding affinities of VEGF wild-type and mutant proteins. Purified protein dimers (50 μg) in binding buffer containing 0.1 M NaCl were applied to a heparin-sepharose affinity column. Flow through fractions were collected before the column was washed with three column volumes of binding buffer. Bound proteins were eluted over 15 column volumes in a linear salt gradient (0.1-1 M NaCl) and 1 ml fractions were collected. Eluted proteins were precipitated with trichloroacetic acid to concentrate samples and to eliminate buffer variability. The samples were separated on a 12% SDS-PAGE gel and analyzed by Coomassie-staining. Linear background correction of the images was performed for better contrast.

The low ionic strength of the binding buffer combined with the relatively shallow elution gradient was used to detect subtle changes in heparin binding activity of the different mutants. However, the low stringency of these conditions not only resulted in higher sensitivity but may have also been responsible for the prolonged interaction of some proteins with the matrix. Avidity effects resulting from multimerization of the dimeric proteins or non-specific solid-state interactions with the column matrix/resin are possible explanations for this phenomenon. To avoid these potential artifacts, a less-sensitive screening of selected mutants was performed by increasing the ionic strength during binding (0.15 M) and the salt concentration increments in the elution phase from 0.06 M to 0.12 M NaCl per 1 ml fraction. Under these conditions, the elution profiles of the indicated proteins were better-defined. As shown in Figure 3.7, VEGF164 eluted at approximately 0.9 M NaCl, a result similar to that from the previous experiment. As observed in the first assay, K30A/R35A/R39A contained two protein fractions which differed in heparin binding. One fraction did not bind heparin whereas the other fraction bound to heparin as strongly as did VEGF164. This differential binding behavior suggests the presence of a folded and misfolded protein population

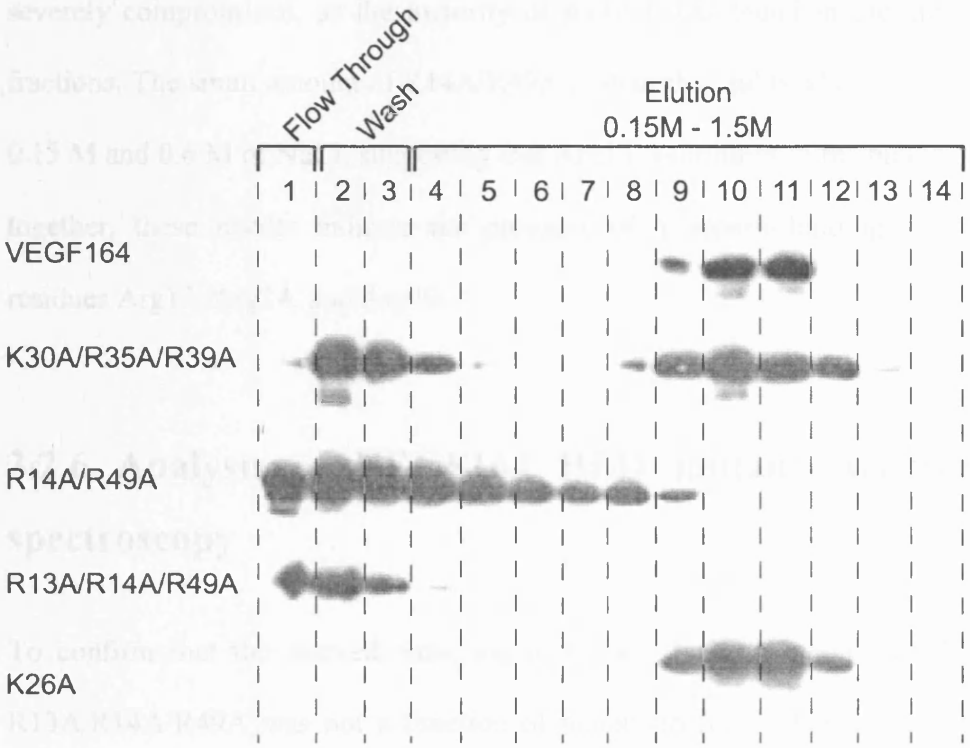

Figure 3.7 Comparison of heparin-binding affinities of wild-type VEGF164 and selected VEGF mutants at physiological salt concentration. Purified protein dimers (10 μg) were injected onto a heparin-sepharose affinity column in the presence of 0.15 M NaCl. The column was washed and bound proteins were eluted over 11 column volumes in a linear salt gradient (0.15-1.5 M NaCl) and 1 ml fractions were collected. Eluted proteins were precipitated with trichloroacetic acid and separated on a 12% SDS-PAGE gel. Western blotting was performed using a monoclonal pan-VEGF antibody, and immuno-positive bands were visualized with a chemiluminescence system (ECL).

caused by the mutations. Strikingly, mutant R13A/R14A/R49A lost its ability to bind to the heparin-sepharose column at the physiological salt concentration of this experiment, suggesting that the binding observed in the previous experiment may have been non-specific. Analysis of the double mutant R14A/R49A revealed that heparin binding was

severely compromised, as the majority of protein was found in the unbound and wash fractions. The small amount of R14A/R49A protein that did bind eluted gradually between 0.15 M and 0.6 M of NaCl, suggesting that Arg13 contributes to the binding energy. Taken together, these results indicate the presence of a heparin-binding site containing the residues Arg13, Arg14, and Arg49.

3.2.6 Analysis of VEGF164 HBD mutant structure by CD spectroscopy

To confirm that the marked reduction in heparin binding by mutant R14A/R49A and R13A/R14A/R49A was not a function of major structural changes, secondary structure analyses of these mutants and VEGF164 were performed using CD spectroscopy in the far-ultraviolet spectral region (190-260 nm). Changes in the tertiary structure of VEGF could not be analyzed with this method due to the low absorption in the near-UV spectral region (250-350 nm). The method is based on the differential absorption of left- and right-circularly polarized light by the protein sample. In far-ultraviolet CD, the spectra are dominated by the spatial arrangements of amide groups. Structural elements such as α-helix, β-sheet and random-coil each give rise to a characteristic shape and magnitude of the CD spectrum, thus allowing the comparison of these elements between mutant and wild-type protein species [291]. Figure 3.8 shows that the normalized far-UV CD spectrum obtained for the triple mutant R13A/R14A/R49A was essentially identical to that of wild-type VEGF164 (top panel). Both spectra were characterized by a negative trough near 210 nm and a strong positive ellipticity at 200 nm, both of which are indicative of a high

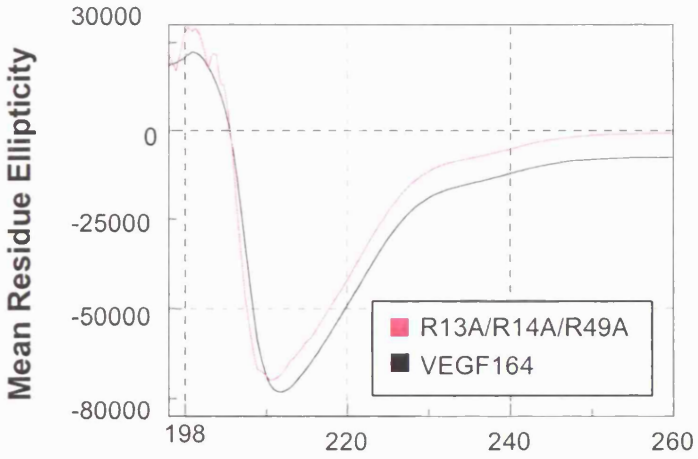
30000
0
-25000
-50000
-80000
Mean Residue Ellipticity
198
220
240
260
R13A/R14A/R49A
VEGF164

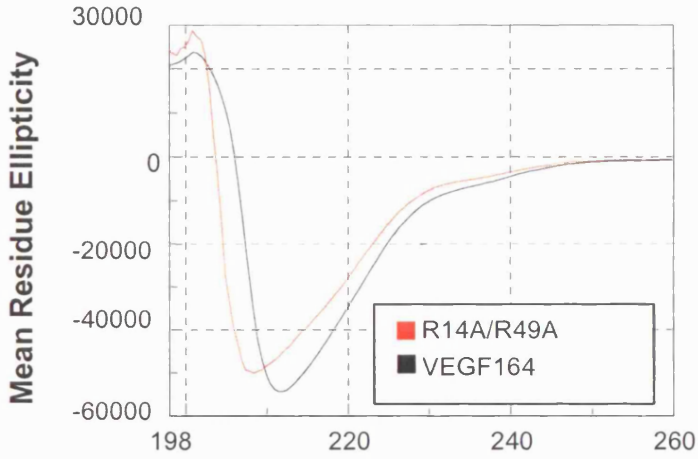
30000
0
-20000
-40000
-60000
Mean Residue Ellipticity
198
220
240
260
R14A/R49A
VEGF164

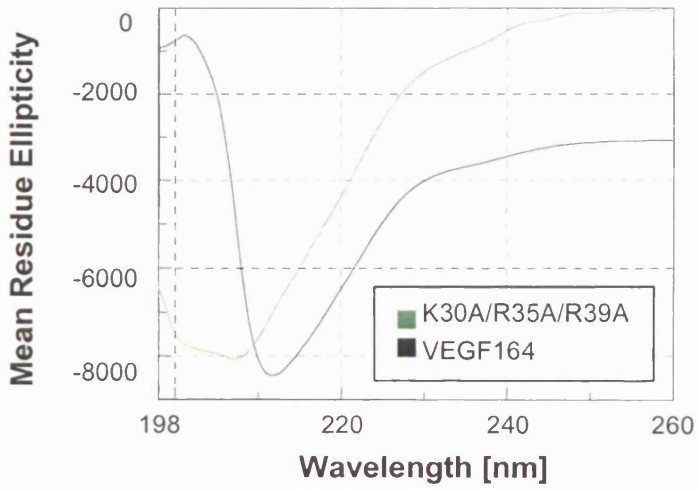
0
-2000
-4000
-6000
-8000
Mean Residue Ellipticity
198
220
240
260
Wavelength [nm]
K30A/R35A/R39A
VEGF164

Figure 3.8 Secondary structure analysis of VEGF164 variants by far-UV CD spectroscopy. CD spectra (198-260 nm) were obtained at room temperature for the VEGF164 HBD mutants R13A/R14A/R49A (top panel, pink line), R14A/R49A (central panel, red line) and K30A/R35A/R39A (bottom panel, green line) in comparison with VEGF164 (black line). The solvent spectrum was subtracted from the sample spectra and the subtracted spectra were converted from millidegrees of ellipticity (θ) to mean residue ellipticity [θ_{mrw}] (degrees x cm^2 x $dmol^{-1}$). The molar ellipticity of VEGF164 has a different magnitude in each panel due to normalization for protein concentration. Spectra were measured twice with identical results.

percentage of β-sheet structures [292]. The qualitative analysis also revealed a significant, albeit lower, α-helical content, characterized by a positive band at 192 nm and two negative bands at 208 nm and 222 nm. These results, although not quantitative due to the lack of a reference CD spectrum, are in good agreement with the secondary structure assignment derived from the solution structure of the VEGF (1-110) fragment and HBD (VEGF111-165) [112, 119]. Concerning mutant R14A/R49A, it was evident that the spectral shape and magnitude of this mutant is very similar to that of native VEGF, despite a slight shift of the curve between 198 nm and 210 nm (Figure 3.8, central panel). To determine whether the partial loss of heparin binding ability for mutant K30A/R35A/R39A resulted from structural abnormalities, fractions 2-4 (Figure 3.7) were collected, pooled and subjected to far-UV CD analysis. As shown in the bottom panel of Figure 3.8, the mutant spectrum was very different from that of the wild-type. Computer-aided secondary structure prediction revealed a high amount of random coil structures and a marked reduction in α-helical content (Table 3.2).

The lack of significant changes in secondary structures of R14A/R49A and R13A/R14A/R49A suggests that the impairment in heparin binding was not the result of a disrupted backbone structure. In contrast, the analysis of K30A/R35A/R39A strongly supports the view that any heparin-binding deficiency of this mutant was caused by major conformational changes, suggesting that the exchange of residues in this mutant may have rendered the protein susceptible to misfolding. The analysis of mutants K30A/R35A/R39A and K30A/R35A/R39A/R49A was therefore not further pursued.

Protein	Alpha-helix	Beta-strand	Random-coil
VEGF164	0.3	0.37	0.33
R13A/R14A/R49A	0.28	0.41	0.31
R14A/R49A	0.35	0.25	0.4
K30A/R35A/R39A	0.08	0.42	0.5

Table 3.2 Prediction of secondary structure content of VEGF164 variants based on far-UV CD data. Estimated percentages (shown as fractions) of helix, beta and random secondary structure of VEGF164 and HBD mutant proteins. Calculations were performed using the K2d program [293] by submitting 41 CD values ranging from 200 nm to 240 nm obtained from spectra depicted in Figure 3.8.

3.2.7 Quantitative analysis of the heparin-binding affinities of selected VEGF164 HBD mutants

While heparin-sepharose chromatography represents a valuable screening method, this technique is incapable of providing dissociation constants (K_d) and is biased towards electrostatic interactions due to the high concentration of heparin in the column. To better assess non-ionic interactions, such as hydrogen bonding and hydrophobic interactions, heparin-binding affinities of selected mutants were determined in a nitrocellulose filter trapping assay [239]. This assay involves incubation of tritium-labeled heparin with increasing concentrations of VEGF in solution. Nitrocellulose filters are then used to separate heparin-protein complexes from free molecules. The quantity of complex formed at equilibrium is determined by measuring the radioactivity retained by the filter. This assay is thought to better reflect the overall binding capacity of a given protein [294].

The saturation binding curves for VEGF164 and HBD mutants demonstrate that the K_d-value for VEGF164 binding to heparin was 0.157 ± 0.017 (mean ± SEM) μM (Figure 3.9), which is in good agreement with the dissociation constant of 0.165 μM reported in the literature [295]. As indicated by heparin-affinity chromatography, the single mutant K26A showed slightly reduced affinity (0.415 ± 0.08 μM) compared to VEGF164 (Figure 3.9). Binding of the two double mutants R13A/R14A (2.04 ± 1.01 μM) and R46A/R49A (1.98 ± 1.04 μM) was reduced approximately twelve-fold compared to wild-type VEGF164 (Figure 3.9). However, the large standard errors resulted in wide 95% confidence bands of the best fit curves, therefore the K_d values for these two mutants could not be accurately calculated. Nonetheless, this decrease in affinity was not observed in the column assay,

confirming the higher sensitivity of the filter trapping assay. Consistent with the previous assays, the quadruple mutant R13A/R14A/R46A/R49A did not show any detectable binding to heparin. The residual binding activity observed in the previous assay is likely attributable to non-specific interactions.

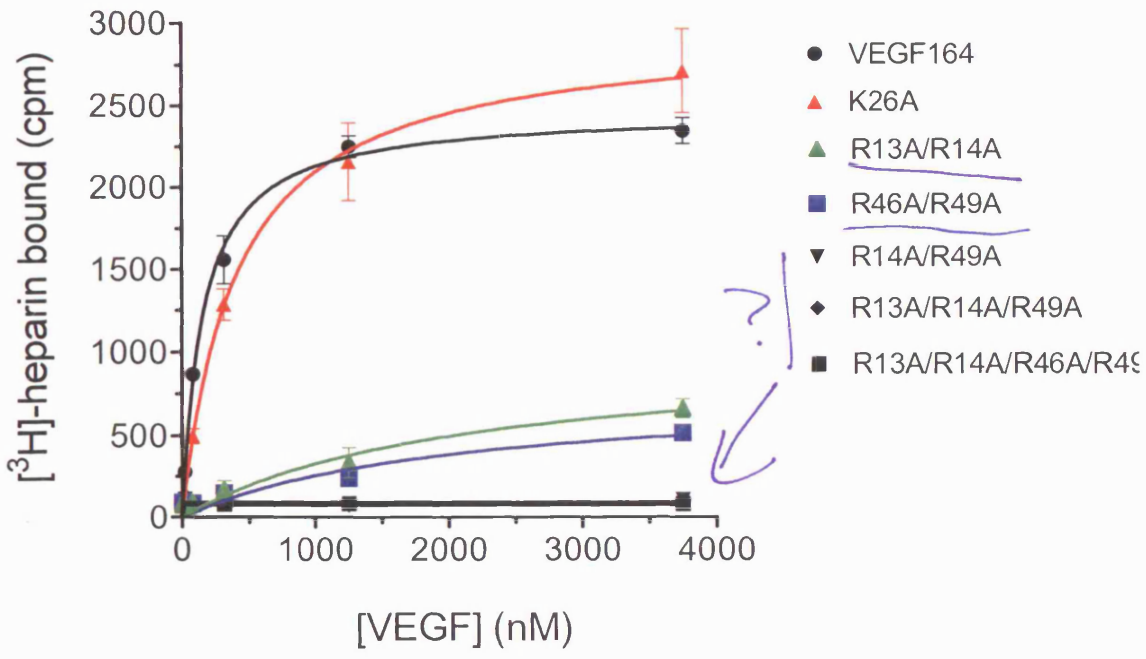

Figure 3.9 Binding of VEGF164 and HBD mutants to [^{3}H]-heparin. [^{3}H]-heparin (0.05 μM) was incubated with increasing amounts of VEGF variants in the presence of 0.15 M NaCl, and VEGF-heparin complexes were recovered using the nitrocellulose filter trapping assay [239]. Bound [^{3}H]-heparin was quantified in a liquid scintillation counter. The GraphPad Prism program was used to generate a logarithmic curve fit according to the one-site binding model and to calculate the dissociation constants. Mutants R14A/R49A, R13A/R14A/R49A, and R13A/R14A/R46A/R49A could not be fitted. Each data point represents the mean ± SEM of three independent experiments, with each experiment performed in triplicate.

As expected from the column assay, binding of mutant R13A/R14A/R49A to [^{3}H]-heparin was completely abolished in the presence of physiological salt concentration. Interestingly, the same effect was observed in mutant R14A/R49A. In this case, the result differs from the outcome of the heparin column assay, where residual, low-affinity binding was observed (Figure 3.7).

So far, this mutational analysis has identified critical amino acids residing in the C-terminal subdomain (R46 and R49) and an adjacent loop region (R13, R14), and indicates that Arg14 and Arg49 constitute a 'minimal' heparin-binding site. The data also provide evidence for a major electrostatic contribution to the binding energy and highlight the importance of an appropriate spatial conformation of the residues to ensure optimal affinity and specificity of the interaction.

3.2.8 Binding of VEGF164 HBD mutants to neuropilin-1

The VEGF isoform specific receptor neuropilin-1 binds to the exon 7-encoded region of VEGF164 [126], but the amino acids mediating this interaction have not yet been identified. To assess the effect of the HBD mutations on neuropilin-1 binding, a plate-based competition binding assay was performed in which increasing concentrations of VEGF164 dimers were mixed with ^{125}I-VEGF165 and added to immobilized neuropilin-1. The binding of ^{125}I-VEGF165 to neuropilin-1 was inhibited in a dose-dependent manner by VEGF164

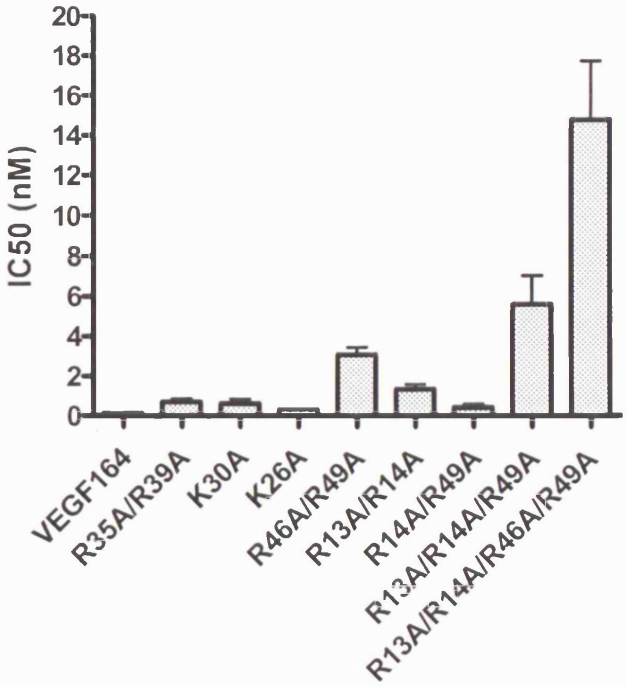

VEGF164	0.128 ± 0.02 nM
R35A/R39A	0.710 ± 0.16 nM
K30A	0.621 ± 0.24 nM
K26A	0.318 ± 0.03 nM
R46A/R49A	3.080 ± 0.37 nM
R13A/R14A	1.340 ± 0.24 nM
R14A/R49A	0.432 ± 0.18 nM
R13A/R14A/R49A	5.610 ± 1.42 nM
R13A/R14A/R46A/R49A	14.80 ± 1.72 nM

Figure 3.10 Competitive binding of VEGF164 HBD mutants to neuropilin-1. Binding of ^{125}I-VEGF165 to immobilized neuropilin-1/F_c was competed with increasing concentrations of VEGF164 or VEGF164 HBD mutants. Bound ^{125}I-VEGF165 was quantified in a liquid scintillation counter. (Top panel) The IC_{50} for each VEGF variant shown on the histogram were derived from three independent experiments performed in triplicates. The binding data were used to calculate the percent specific binding. Inhibition binding curves were generated by non-linear regression analysis using the one-site competition binding model. Binding curves and IC_{50} ± SEM values (bottom panel) for all mutants were generated using the GraphPad Prism program.

with a half-maximal inhibitory concentration (IC_{50}) of 0.128 ± 0.02 (mean ± SEM) nM, indicating that binding to neuropilin-1 occurs with relatively high affinity in the absence of heparin (Figure 3.11). The mutants were between 2.6-fold (K26A) and 120-fold (R13A/R14A/R46A/R49A) less effective in competing with ^{125}I-VEGF165, compared to VEGF164. Despite this reduction in binding affinity, all mutants were able to bind neuropilin-1. These results suggest that the binding sites for heparin and neuropilin-1 in VEGF164 cannot be completely separated by site-directed mutagenesis, since the mutation of residues that mediate heparin binding also appears to affect the interaction with neuropilin-1.

3.3 Discussion

3.3.1 Characterization of the VEGF164 heparin-binding site.

In this part of the study, I have identified residues that contribute to the interaction of VEGF164 with heparin by employing two *in vitro* heparin-binding assays. Relative heparin-binding affinities were differentially affected in all mutants. The degree of binding impairment appeared to be related to the number of substitutions and, therefore, the decrease of the total electropositive charge. Minor conformational perturbations may have also contributed to reductions in affinity. For example, the 2.6 fold decrease in affinity of the K26A mutant relative to wild-type VEGF164 likely resulted from the substitution of lysine with the smaller alanine, indirectly affecting the ability of heparin to access its binding groove. It is unlikely that Lys26 directly binds to heparin, as this basic residue is surrounded by negatively-charged amino acids, which have a repelling rather than attracting effect on heparin binding.

A basic cluster containing Lys30, Arg35 and Arg39 was expected to contribute significantly to the interaction with heparin [119]. Although this VEGF species retained the ability to induce TF expression, the mutation of these residues clearly had a detrimental effect on the secondary structure of mutant K30A/R35A/R39A, as demonstrated by circular dichroism (CD) analysis. Arg35 takes part in the formation of a short α-helix that packs against the two-stranded β-sheet in the C-terminal subdomain [119]. The substitution of Arg35, together with Lys30 and Arg39, may have disrupted the integrity of the helix, which is reflected by a significant reduction in α-helical content relative to VEGF164. Nevertheless, mutant K30A/R35A/R39A partially retained heparin-binding activity at

physiological salt concentration in the solid phase assay, indicating that this region does not constitute a major heparin-binding site. In contrast, mutants R13A/R14A and R14A/R49A displayed a marked decrease in heparin-binding affinity. The binding of R14A/R49A to soluble heparin in the presence of 0.15 M NaCl was reduced to a level where K_d values were not measurable, and the triple mutant R13A/R14A/R49A failed to bind heparin at physiological salt concentration in two independent *in vitro* heparin-binding assays. The observed binding at low salt concentration (0.1 M NaCl) and its elution at 0.52 M NaCl may be explained by non-specific electrostatic interactions with the matrix under low-stringency conditions. The lack of binding at higher ionic strength might have been due to the saturation or shielding of these sites.

Taken together, these data suggest the existence of a principal heparin-binding site consisting of Arg13, Arg14 and Arg49, with potential binding energy contributions from Arg46. Arg14 and Arg49 may constitute a 'minimal' binding site. The residues, although non-contiguous in sequence, are located along the interface of the clearly defined N-terminal and C-terminal subdomain and form a continuous binding surface. Support for this model comes from a recent publication presenting a refined NMR solution structure and a much-improved definition of the mutual orientation of the subdomains [120]. In contrast to the original structure [119], the refinement revealed that the heparin-binding residues (i.e. Arg13, Arg14 and Arg49) are in close contact with each other. Spatial proximity of heparin-binding residues in the three-dimensional structure is characteristic for many heparin-binding proteins [296-299]. The nature of basic residues appears to be an important factor for this interaction. Arginines bind more tightly than lysines because they have a higher potential to form hydrogen bonds. In addition, the guanidinium group may

form a stronger electrostatic interaction with the sulfate anion than the ammonium group [300]. It should be mentioned that other residues may also contribute to the free binding energy by providing non-electrostatic interactions with heparin and glycosaminoglycan chains, including hydrophobic contacts and hydrogen bonds.

3.3.2 Implications for neuropilin-1 binding by VEGF164

Based on the results from the competition binding assay, it was concluded that the interaction of VEGF164 with neuropilin-1 is of high-affinity. This was an unexpected result, considering that VEGF is thought to require heparin for efficient binding to neuropilin-1 [301]. The finding is also in striking contrast to the low affinity of VEGF165 to mouse neuropilin-1, which has been reported in a binding study using the BIAcore system [186]. This discrepancy may be explained by a lower affinity of mouse and rat neuropilin-1 (used in this study) for human VEGF compared to human neuropilin-1, although this has not been confirmed. In light of these findings, the IC_{50} numbers obtained with this approach should be regarded as relative values rather than absolute values. The binding affinity of all mutant VEGF proteins to immobilized neuropilin-1 was reduced between 2.5-fold (K26A) and 115-fold (R13A/R14A/R46A/R49A) compared to VEGF164, suggesting that the neuropilin-1 and the heparin-binding epitopes are overlapping. Still, all mutants retained significant neuropilin-binding activity.

Information regarding the requirements for VEGF binding to neuropilin-1 at a molecular level is mainly based on the observation that VEGF and semaphorin 3A compete for neuropilin-1 binding at the b1 domain. Since binding of semaphorin 3A is mediated by its

basic C-terminal tail, it has been hypothesized that competition between the two molecules results from binding of basic amino acids to a shared electronegative binding surface on neuropilin-1 [302, 303]. The data presented here suggest that electrostatic forces play a significant role, and that the neuropilin-1-binding site of VEGF164 may contain residues that also promote heparin binding. This hypothesis still agrees with the observation that heparin potentiates the binding of VEGF165 to the b1/b2 domain [173], because the heparin- and VEGF-binding sites of neuropilin-1 may be non-overlapping. In this context, it would be interesting to investigate whether heparin still has the ability to increase neuropilin binding of the heparin-binding-deficient VEGF mutants. On the other hand, since the electropositive b2 domain of neuropilin-1 also contributes to the binding energy [173], the participation of non-basic residues cannot be ruled out. Interestingly, a recent study showed that neuropilin-1 is able to bind strongly to the heparin-binding site of several other proteins, including FGF-1, -2, -4, and -7 as well as FGFR-1 and hepatocyte growth factor (HGF) [304]. The authors observed that these interactions could be diminished by competition with heparin and concluded that binding may occur through a 'heparin mimetic' site in neuropilin-1. This site might act as a scaffold for growth factor-receptor complexes and confer on certain proteins a general modulatory activity. Such a heparin-mimicking site might be non-specific and interact with its binding partners by means of charge-charge complementarity. It is not known whether VEGF falls into this class of binding partners.

The prediction that heparin and neuropilin-1 share partially overlapping binding sites within the exon 7-encoded domain implies that the generation of highly selective heparin-

or neuropilin-binding-deficient mutants, which could be used as tools to dissect the functions of the two binding properties of VEGF, may not be feasible.

Chapter 4: *In vitro* functional characterization of heparin-binding-deficient VEGF164 mutants

4.1 Introduction

In the previous chapter I described the design and production of VEGF164 HBD mutant forms and their characterization with respect to their heparin- and neuropilin-1-binding activity. For the investigations into the biological implications of the VEGF164 HBD, I selected two mutants, R14A/R49A and R13A/R14A/R49A to use as biochemical tools. The selection was made based on the following key experimental findings: both mutants lost their ability to bind heparin at physiological salt concentration *in vitro*; both displayed significant binding affinity for neuropilin-1; and both retained secondary-structure conformation and TF induction activity comparable to wild-type VEGF164.

In the studies described in this chapter, I further characterized R14A/R49A and R13A/R14A/R49A by assessing their interactions with cell-associated HSPGs using an assay that is better suited to simulate the *in vivo* heparin-binding capacities of these proteins than the heparin-sepharose column or the filter trapping assay. In addition, the effects of the mutations in the C-terminus on binding to VEGFR-1 and VEGFR-2 were studied in a cell-free binding assay. Finally, the potencies of the mutants to stimulate blood vessel growth in an *ex vivo* model of angiogenesis in comparison to VEGF120 and VEGF164 were also determined .

4.2 Results

4.2.1 Binding of VEGF164 HBD mutants to HSPGs on PAE cells

To further characterize the function of the mutants, I examined whether the loss of heparin binding displayed by R14A/R49A and R13A/R14A/R49A translates into an inability to interact with cell-associated HSPGs. For this experiment, native PAE cells were used because these cells lack expression of VEGFR-1, VEGFR-2 and neuropilin-1 [143, 256]. The amount of VEGF bound to HSPGs was determined by assaying the VEGF concentration in the medium after enzymatic treatment of the cells with heparinase I and III. VEGF120, which lacks the HBD, was released from PAE cells by heparinase treatment at a significantly lower level than was wild-type VEGF164 (1.67 ± 0.65 (mean ± SD) pM and 5.17 ± 0.81 pM, respectively; Figure 4.1). The values obtained for the mutants were not significantly different from those of VEGF120, at 1.9 ± 1.27 pM (R14A/R49A) and 1.17 ± 0.42 pM (R13A/R14A/R49A), suggesting that these mutations are as effective at disrupting HSPG binding as is complete loss of the HBD.

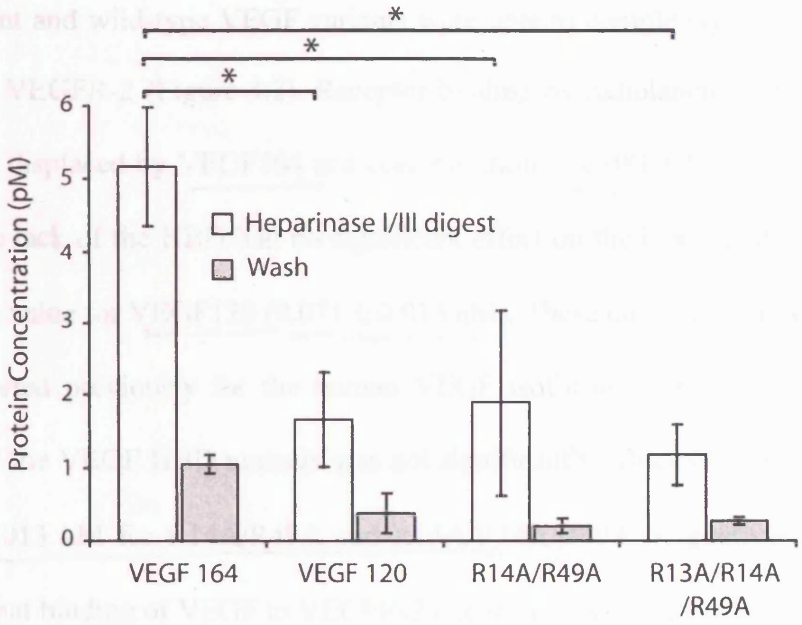

Figure 4.1 Interaction of R14A/R49A, R13A/R14A/R49A and wild-type VEGF isoforms with cell-associated HSPGs. Confluent porcine aortic endothelial (PAE) cells were incubated with purified VEGF variants (7.14 nM) in binding buffer (pH 7.5) and treated with heparinase I and III (0.5 U/ml). The supernatant containing dissociated VEGF (white bars) and the final wash fraction (grey bars) were collected and the amount of VEGF in both fractions was measured in a mouse VEGF-specific ELISA. Average values with standard deviations derived from three independent experiments are shown. Statistical significance (*P<0.05) was determined using the Bonferroni test.

4.2.2 Analysis of VEGFR-2 binding by VEGF164 HBD mutants

Next, I sought to establish whether the mutations in R14A/R49A and R13A/R14A/R49A have an impact on interactions with VEGFR-2. To this end, I assayed the ability of the mutants and wild-type isoforms to compete with ^{125}I-VEGF165 for binding to immobilized VEGFR-2 using a microtiter plate format. This inhibition binding assay was preferred to a direct binding assay as it does not require labeling of the mutant proteins.

Both mutant and wild-type VEGF variants were able to completely inhibit ^{125}I-VEGF165 binding to VEGFR-2 (Figure 4.2). Receptor binding by radiolabeled VEGF165 was half-maximally displaced by VEGF164 at a concentration of 0.081 ± 0.016 (mean ± SEM) nM (IC_{50}). The lack of the HBD had no significant effect on the binding affinity, as indicated by the IC_{50} value for VEGF120 (0.071 ± 0.013 nM). These data are in good agreement with those reported previously for the human VEGF isoforms [118]. As expected, receptor binding by the VEGF HBD mutants was not significantly affected (0.099 ± 0.013 nM and 0.064 ± 0.013 nM for R14A/R49A and R13A/R14A/R49A, respectively), which further confirms that binding of VEGF to VEGFR-2 occurs independently of a functional HBD.

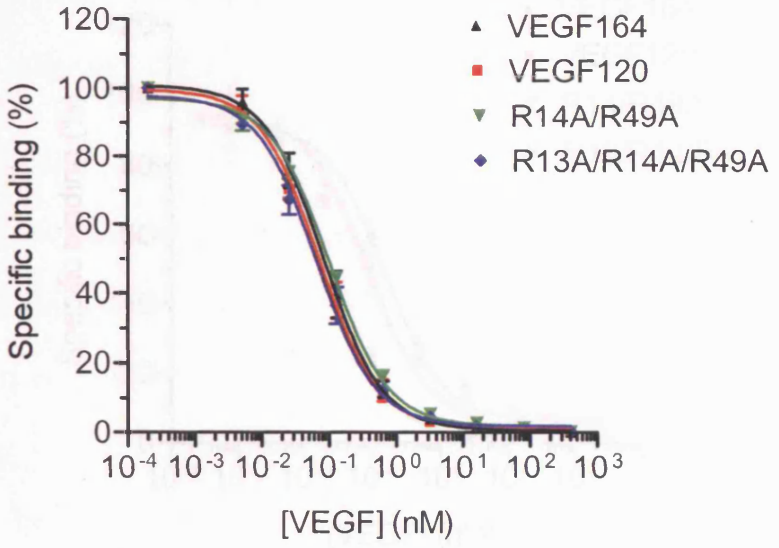

Figure 4.2 Binding of R14A/R49A, R13A/R14A/R49A and wild-type VEGF isoforms to VEGFR-2. Competitive displacement of ^{125}I-VEGF165 binding to immobilized mouse VEGFR-2/F_c with various concentrations of *Pichia*-derived VEGF164 (black), VEGF120 (red), R14A/R49A (green), and R13A/R14A/R49A (blue). Specific binding was determined by subtracting the background signal (non-specific signal obtained in the presence of 400 nM of VEGF164) from raw signal values. Non-linear regression and analysis of binding parameters using the one-site competition model were performed with GraphPad Prism software. Data (mean ± SEM) are representative of three independent experiments performed in triplicates.

4.2.3 Analysis of VEGFR-1 binding by VEGF164 HBD mutants

VEGFR-1 binding has been shown to differ significantly between VEGF165 and the shorter isoform VEGF121 [118]. Here, competition binding analysis demonstrated a 3.5-fold reduction in competitive binding activity of VEGF120 compared to VEGF164 (IC_{50}: 0.077 ± 0.018 (mean ± SEM) nM, and 0.022 ± 0.003 nM for VEGF120 and VEGF164, respectively; Figure 4.3). The mutants R14A/R49A and R13A/R14A/R49A, too,

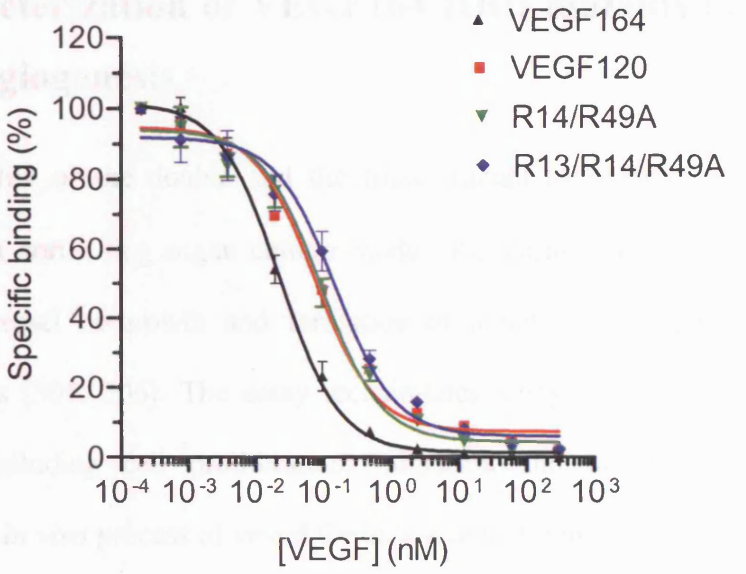

Figure 4.3 Binding of R14A/R49A, R13A/R14A/R49A, and wild-type VEGF isoforms to VEGFR-1. Competitive displacement of ^{125}I-VEGF165 binding to immobilized mouse VEGFR-1/F_c with the indicated concentrations of *Pichia*-derived VEGF164 (black), VEGF120 (red), R14A/R49A (green), and R13A/R14A/R49A (blue). Curve fitting and analysis of binding parameters were done as described in Figure 4.2. Data (mean ± SEM) are representative of three independent experiments performed in triplicates.

exhibited decreased binding to VEGFR-1, with IC_{50} values similar to those of VEGF120 (0.092 ± 0.024 nM and 0.151 ± 0.049 nM for R14A/R49A and R13A/R14A/R49A, respectively). These results indicate that both the loss of the HBD and mutations within this domain negatively affect VEGFR-1 binding by VEGF, with the triple mutant exhibiting an approximately 7-fold reduction in potency compared with VEGF164. The VEGF receptor binding assays were performed in the absence of heparin; thus, charged residues important for heparin binding appear to be directly contributing to the high affinity interaction with VEGFR-1.

4.2.4 Characterization of VEGF164 HBD mutants in an *ex vivo* model of angiogenesis

Next, the potential of the double and the triple mutant to promote angiogenesis was assessed in a rat aortic ring organ culture model. Rat aortic rings can be stimulated to generate microvessel outgrowth and formation of a network composed of branching endothelial tubes [305, 306]. The assay recapitulates many of the *in vivo* processes of angiogenesis, including cell proliferation, migration and lumen formation. It also recapitulates the *in vivo* process of vessel formation in that non-endothelial cells, including fibroblasts, smooth muscle cells and pericytes, also contribute to the differentiation and maturation of the microvasculature, and is therefore well suited to assess the angiogenic potency of VEGF variants [307, 308]. Segments of the aorta were embedded in collagen and equimolar amounts of VEGF120, VEGF164, R14A/R49A or R13A/R14A/R49A were added to the cultures every 48 hr. After 7 days in culture, branching microvessel networks extended mostly from the edges of the rings and were surrounded by elongated, fibroblast-like cells (Figure 4.4 A). Treatment with either VEGF120 or VEGF164 induced a 3.5-fold or 3.6-fold increase in total microvessel length, respectively, compared to PBS-treated rings (Figure 4.4 B). The R14A/R49A and R13A/R14A/R49A mutants were 5-fold and 4.6-fold more potent than PBS, respectively, at promoting sprouting angiogenesis. The HBD mutants therefore exhibited a comparable, if not more potent, activity to that observed for VEGF120 and VEGF164. No gross differences in sprout morphology were

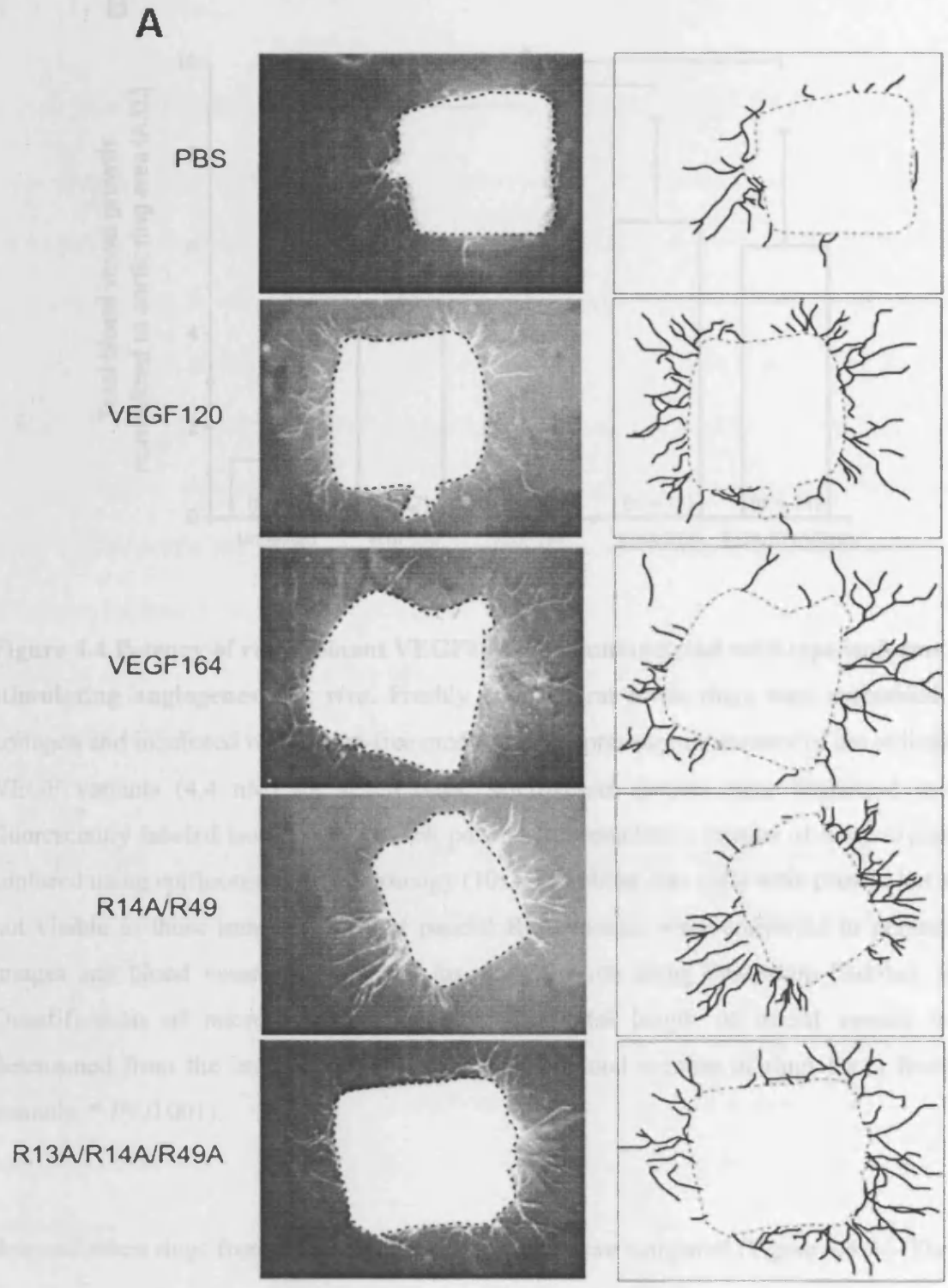
A
PBS
VEGF120
VEGF164
R14A/R49
R13A/R14A/R49A

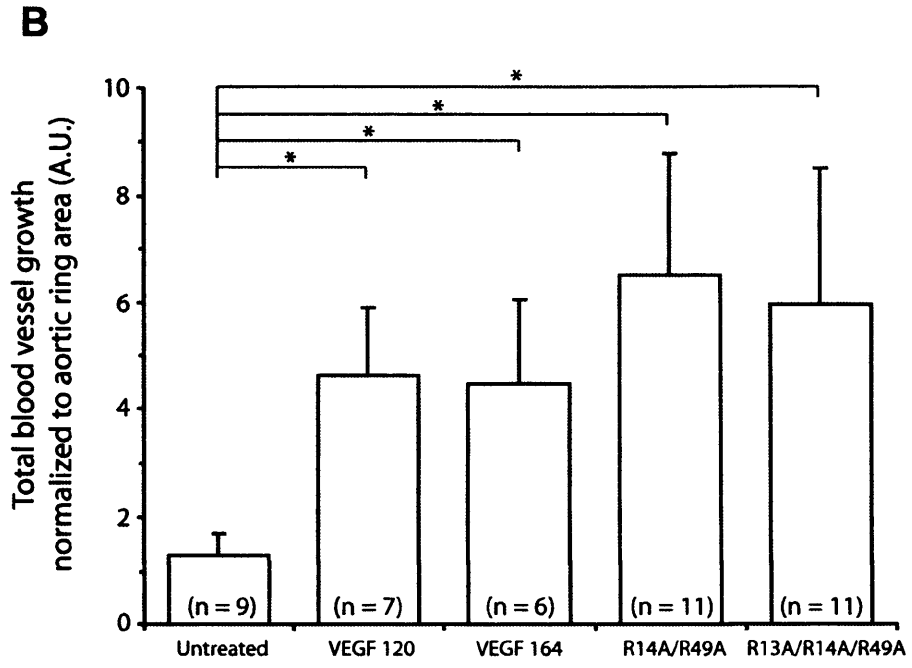

Figure 4.4 Potency of recombinant VEGF164 HBD mutants and wild-type isoforms at stimulating angiogenesis *ex vivo*. Freshly prepared rat aortic rings were embedded in collagen and incubated with serum-free medium in the presence or absence of the indicated VEGF variants (4.4 nM) for seven days. Microvessel sprouts were visualized using fluorescently labeled isolectin B. (A, left panels) Representative images of aorta explants captured using epifluorescence microscopy (10x). Fibroblast-like cells were present but are not visible in these images. (A, right panels) RGB images were converted to grayscale images and blood vessels were traced for quantification using Photoshop (Adobe). (B) Quantification of microvascular outgrowth. The total length of traced vessels was determined from the images obtained at day 7 (n = total number of rings taken from 4 animals, * $P< 0.001$).

detected when rings from different treatment groups were compared (Figure 4.4 A). These data demonstrate that heparin-binding activity of VEGF164 is not required for stimulation of *ex vivo* angiogenesis in this assay.

4.3 Discussion

4.3.1 Differential binding of VEGF variants to HSPGs *in vitro*

This study has shown that the lack of heparin-binding of VEGF120 and the VEGF164 HBD mutants observed in the previous chapter, correlated with a significant reduction in PAE cell-surface binding activity compared to VEGF164. Moreover, the lack of heparin-binding residues in the mutants had the same effect as complete loss of the HBD in VEGF120, indicating that association with these cells was mediated by a native HBD. This interaction was dependent on heparan sulfate proteoglycans, as shown by heparinase treatment to digest HS chains, and did not depend on the presence of VEGF receptors. Thus, the increased binding of VEGF164 in this assay reinforces a mechanism whereby VEGF is stored on the cell-surface and can be rapidly released from this site to initiate blood vessel growth and sprouting.

The interstitial matrix that is being produced by cultured endothelial cells also contains binding partners that act to sequester VEGF. In this extracellular matrix compartment, VEGF not only binds to HSPGs directly, but also indirectly through other ECM components, such as fibronectin, suggesting additional mechanisms for the retention of VEGF164 by PAE cells [309, 310]. Fibronectin-binding activity at neutral pH has also been shown for VEGF121 [311], which may explain the residual binding of this isoform and the heparin-binding-deficient mutants observed in the assay, as this interaction does not appear to be mediated by the HBD. Overall, these findings represent an indication of the differential ability of the VEGF variants to recognize and interact with matrix- and cell-surface-associated HS chains *in vivo*.

4.3.2 Mutations in the VEGF164 HBD affect binding of VEGFR-1 and VEGFR-2 differently

Because of the cardinal role of the two major VEGF receptors in VEGF biology, I resorted to a competition binding assay to gauge the receptor-binding potential of the VEGF164 HBD mutants. These assays were conducted in the absence of heparin, therefore all effects regarding receptor binding affinities are due directly to changes in ligand-receptor interaction. The finding that binding of R14A/R49A and R13A/R14A/R49A to VEGFR-2 was not compromised supports previous data suggesting that the VEGF C-terminal domain is not directly involved in receptor binding [118]. The HBD has, however, been implicated in control of endothelial cell proliferation, a response mediated by VEGFR-2 signaling. Keyt and colleagues noted that loss of the HBD in VEGF121 was associated with a 100-fold reduced potency in endothelial cell proliferation [118]. In my hands, VEGF120 showed no decrease in binding to VEGFR-2. Moreover, in the TF induction assay, but not in the aortic ring assay, VEGF120 was only slightly diminished in its potency compared with VEGF164. These data are consistent with a more recent report demonstrating that VEGF120 and VEGF164 have similar potency in endothelial cell proliferation assays [61] Thus, it is possible that the recombinant VEGF121 protein used by Keyt *et al.* had lost some of its activity during bacterial expression and subsequent refolding.

Unlike VEGFR-2, VEGFR-1 is bound by soluble VEGF120 and the heparin-binding VEGF164 with different affinities, though the variation observed in my experiment was less dramatic than the 16-fold difference reported by Keyt et al. [118] (for the same potential reason as mentioned above). The increased affinity of VEGF164 for VEGFR-1 compared to VEGF120 has been linked to the presence of the HBD in VEGF164 [118,

312]. The loss of wild-type affinity for this receptor in the double and triple mutant further supports this theory. Although the HBD peptide does not directly interact with VEGFR-1 [118], its conformation within VEGF164 appears to enhance receptor binding. It is conceivable that this domain is folded in such a way that it contributes directly or indirectly to the binding energy of the VEGFR-1-VEGF interaction, but not to the binding energy in the VEGFR-2-VEGF complex.

4.3.3 Heparin-binding-deficient VEGF164 mutants are potent stimulators of *ex vivo* angiogenesis

Blood vessel growth in the aortic ring assay approximates *in vivo* angiogenesis in that it involves microvascular sprouting, branching and capillary tube formation [305]. Measurement of total vessel length demonstrated that R14A/R49A and R13A/R14A/R49A possess an angiogenic activity similar to that of native VEGF164. The slightly enhanced potency of the mutants, although not significant, could be indicative of differential bioavailability of the VEGF variants in the extracellular environment. Whereas some VEGF164 may be sequestered in the matrix in an inactive form, requiring cleavage of extracellular matrix components for release from these stores [258], heparin-binding-deficient mutants may be more freely available for interaction with their receptors.

In view of the decreased VEGFR-1 binding activity of the HBD mutants, these data underline the considerable experimental evidence which shows that the growth and proliferative signals are predominantly mediated by VEGFR-2 [143, 160, 312]. Furthermore, the fact that both mutants exhibited significant reduction in binding to

heparan sulfate on endothelial cells implies that this activity of VEGF164 is not essential for VEGFR-2-mediated functions such as TF induction, VEGFR-2 binding, and vessel growth from *ex vivo* aortic tissue. These findings agree with observations that neither exogenous heparin nor cell surface-associated heparan sulfates are necessary for VEGF165 binding to cell surface-expressed VEGFR-2, and that heparin-binding ability of VEGF165 may only be required under conditions in which oxidative damage occurs [247]. Similarly VEGF-E, a VEGFR-2 specific ligand which lacks the HBD and only weakly interacts with neuropilin-1, promoted migration and sprouting of endothelial cells in HUVEC spheroids, and stimulated angiogenesis *in vivo* as potently as did VEGF165 [313]. These results do not imply that heparin binding has no role in vessel growth. Indeed, heparin-binding functions of VEGF are required for guiding developing vessels where precise and directed branching morphogenesis is critical [61]. Rather, these findings emphasize the need for more detailed studies examining the function of VEGF-heparin interactions at different stages during vessel development.

Chapter 5: *In vivo* functional analysis of the VEGF164 heparin-binding domain

5.1 Introduction

To investigate the effects of the VEGF164 HBD mutants on vessel growth *in vivo*, I chose to study angiogenesis in the context of the eye. The mouse or rat retina provides an excellent model tissue for studying angiogenesis as the progress of blood vessel growth can be monitored by angiography or fundoscopy and the entire retinal vasculature can be viewed in flat-mounted retinal preparations. The sequence of vascularization during postnatal development is well-characterized, and several murine models of retinopathies have been developed.

VEGF and its receptors are constitutively expressed in the retina of the normal eye [314, 315]. Blood vessels in the adult eye are relatively resistant to neovascular stimuli, but when the retina is made hypoxic or ischemic, VEGF levels increase and induce physiological vascular development or pathological neovascularization [87, 271]. Similarly, when VEGF levels are increased experimentally by intraocular injection or transgenic overexpression, this stimulus triggers the pathological neovascularization observed in ischemic retinopathies [316-318]. Pathological, but not physiological, retinal neovascularization is characterized by increased levels of the VEGF164 isoform [273]. The highly regulated expression pattern of the VEGF isoforms in normal development appears to be disrupted in certain disease conditions, leading to inflammation-associated invasion of retinal blood vessels into the vitreous. Both *in vitro* data and experiments using mouse models of diabetes demonstrated that VEGF164 is more potent than VEGF120 at inducing retinal and corneal inflammation [273, 275]. This isoform-specific inflammatory response is causally linked to the pathogenesis of vascular leakage and blood-retinal barrier

breakdown [278]. The 'pathological' activity of VEGF164 in the eye has not been investigated in greater detail, nor have the mechanisms underlying this isoform-specific effect been elucidated. Using genetically modified mice and the HBD mutants, I conducted *in vivo* structure-function studies testing the hypothesis that the heparin-binding function of VEGF164 is responsible for heightened inflammation in the retina and thereby contributes to the pathological role of the VEGF164 isoform in retinal neovascularization.

5.2 Results

5.2.1 Characterization of retinal neovascularization in $VEGF^{120/188}$ mice in a model of ischemic retinopathy

To further investigate the importance of VEGF164 in ocular disease, VEGF164-deficient mice ($VEGF^{120/188}$) were analyzed in a model of OIR, in which the process of retinal neovascularization can be recapitulated experimentally [254, 274, 284]. In this model, newborn mice on day P7 are exposed to an environment containing 75% oxygen for 5 days (Figure 5.1). During this time vessel regression occurs, most likely through apoptosis of

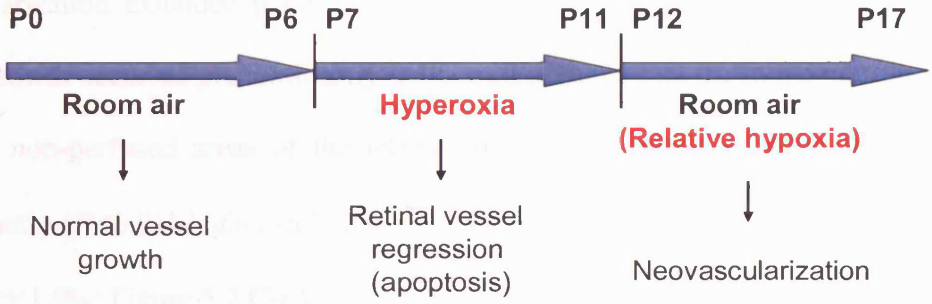

Figure 5.1 Timeline of vessel formation in a mouse model of oxygen-induced retinopathy (OIR). Schematic representation of the protocol developed by Smith et al. [274]. Experimental mice are exposed to a hyperoxic environment (75% O_2) on postnatal day 7 (P7) for a 5-day-period. The vessels respond by undergoing severe vasoconstriction. When normal oxygen is restored (P12), relative hypoxia triggers an ischemic condition in the retina, where tufts of vessels grow through the internal limiting membrane into the vitreous (from P14 onward). The hypoxia-induced neovascular response normally peaks at P17.

endothelial cells following cessation of VEGF production by neuroglial cells. After return to room air for an additional 5 days (relative hypoxia), prominent retinal neovascularization caused by increased VEGF production is observed in 100% of the animals between P17 and P21.

To determine whether lack of VEGF164 alters the retinal neovascular phenotype observed in the OIR model, retinal flat mounts of $VEGF^{120/188}$ littermates were examined at P12 and P17. Figure 5.2 shows the vaso-obliteration in the retina at the end of the hyperoxic phase at P12 in wild-type and $VEGF^{120/188}$ mice (A and B). At this time point (P12), the avascular, non-perfused area in the centre of the retina surrounding the optical nerve disc was similar in both wild-type (4.98 ± 0.52 (mean ± SEM) mm^2) and mutant mice (4.7 ± 0.32 mm^2; Figure 5.3 E, left panel). Upon return to normoxic conditions, physiological revascularization extended parallel to the retinal surface towards the optic nerve. New vessel growth occurred predominantly in the mid-periphery, at the junction of the perfused and the non-perfused areas of the retina. At P17, the extent of revascularization was significantly ($P<0.01$) higher in $VEGF^{120/188}$ retinas than in wild-type retinas (30.7 ± 1.3% vs. 22.9 ± 1.9%; Figure 5.2 C-E).

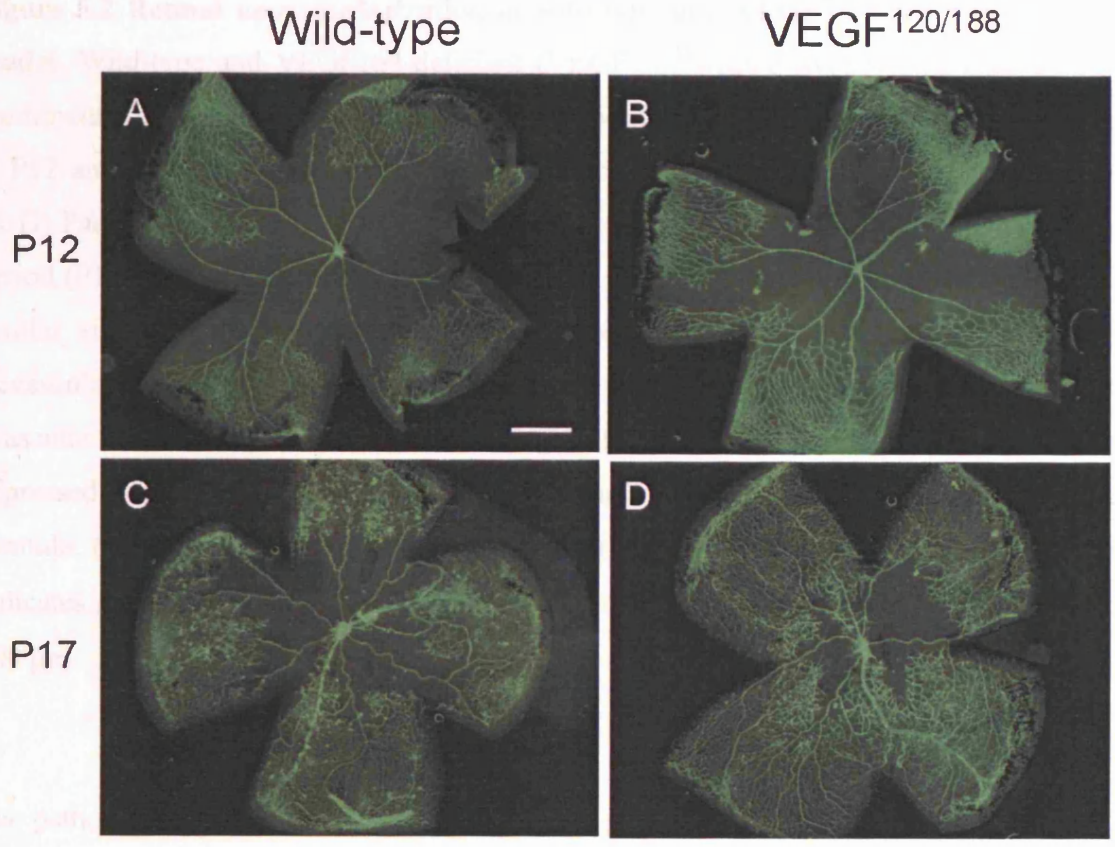
Wild-type
VEGF120/188
A
B
P12
C
D
P17

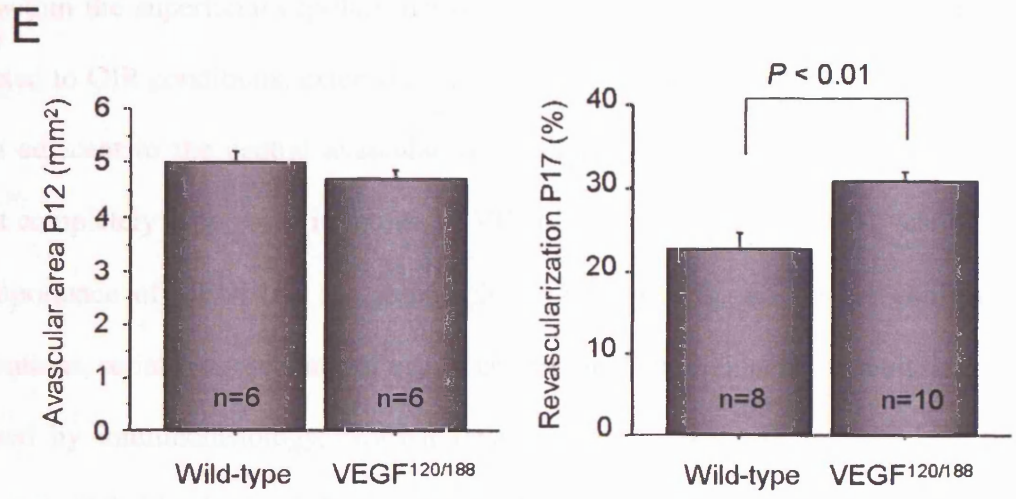
E
Avascular area P12 (mm²)
6
5
4
3
2
1
0
n=6
n=6
Wild-type
VEGF120/188
P < 0.01
Revascularization P17 (%)
40
30
20
10
0
n=8
n=10
Wild-type
VEGF120/188

Figure 5.2 Retinal neovascularization in wild-type and VEGF$^{120/188}$ mice in the OIR model. Wild-type and VEGF164-deficient (VEGF$^{120/188}$) mice were treated according to the timeline described in Figure 5.1. Mice were perfused with FITC-coupled Con A lectin at P12 and P17, then retinal whole mounts were examined by fluorescence microscopy. (A-D) Panels show representative images of each time point. At the end of the hyperoxic period (P12), obliteration of the central retinal vasculature resulted in an avascular area of similar size in both animals. At P17, the extent of physiological neovascularization (revascularization) was greater in VEGF$^{120/188}$ mice than in wild-type mice. (E) The avascular area at P12 was measured using NIH Image. The revascularized area was expressed as a percentage of the whole retinal surface and quantified using the following formula: (vascularized area at P17 – vascularized area at P12)/total retinal area at P17. N indicates number of animals analyzed and data are expressed as mean ± SEM. Scale bar, 200 μm.

The pathological neovascular response in the oxygen-injured retinas develops similarly to the physiological revascularization but is characterized by the formation of neovascular tufts within the superficial capillary network between P17 and P21. In wild-type retinas subjected to OIR conditions, extensive tuft formation was observed at P17 in the vascular region adjacent to the central avascular zone (Figure 5.3 A, arrows). This process was almost completely suppressed in retinas of VEGF$^{120/188}$ mice (Figure 5.3 B), demonstrating the importance of VEGF164 for pathological vessel growth. To further confirm these observations, serial cross sections of eyes were prepared and retinal neovascularization was analyzed by immunohistology. Normal revascularization was observed in both animal genotypes, with blood vessels branching out from the retinal surface toward the deeper layers (inner plexiform layer and inner nuclear layer, Figure 5.3 C and D). Wild-type OIR mice showed a robust neovascular response, with vessels breaking through the inner limiting membrane and extending into the vitreous cavity (Figure 5.3 C, arrows).

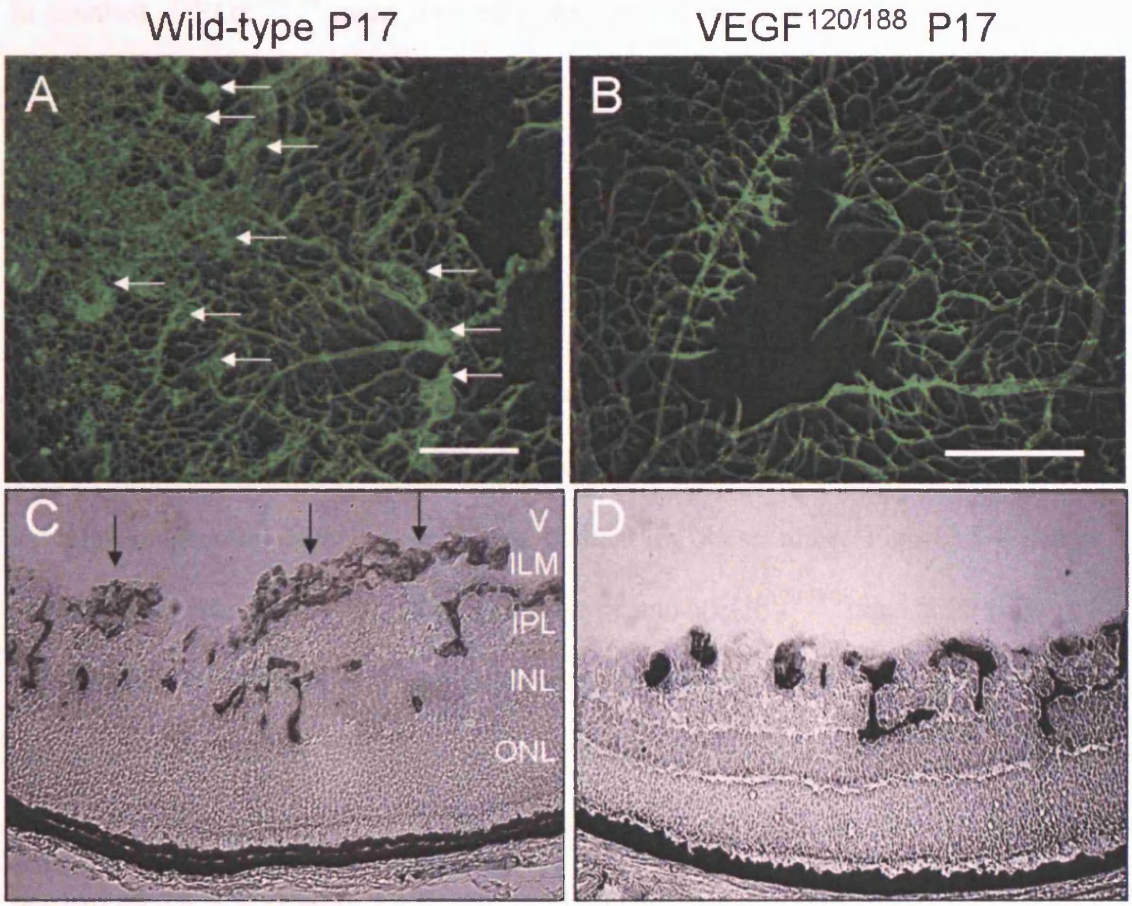

Figure 5.3 VEGF$^{120/188}$ mice with ischemic retinopathy show no significant signs of pathologic neovascularization. Wild-type and VEGF164-deficient (VEGF$^{120/188}$) mice were treated according to the timeline described in Figure 5.1 and euthanized on day P17. (A and B) Fluorescein angiography of retinal flat mounts and magnification of the leading edge of the growing vasculature. Arrows indicate neovascular tufts in the superficial layer of wild-type retinas, which are absent in the retinas of VEGF$^{120/188}$ mice. (C and D) Eyes of P17 animals were enucleated and cut in sections. Blood vessels in tissue sections were immunostained with an anti-PECAM antibody. Tuft formation (arrows) can be seen just anterior to the inner limiting membrane (ILM) of wild-type, but not mutant, retinas. V, vitreous; ILM, inner limiting membrane; IPL, inner plexiform layer; INL, inner nuclear layer; ONL, outer nuclear layer. Scale bar, 25 μm.

In contrast, $VEGF^{120/188}$ mice showed little or no tuft formation on the retinal surface (Figure 5.3 D).

5.2.2 $VEGF^{120/188}$ mice display normal physiological neovascularization

To exclude the possibility that the lack of pathological vessel growth in VEGF164-deficient mice is the result of a decreased angiogenic capacity, I examined the process of vascular outgrowth during retinal development in these mice. Figure 5.4 shows the physiological retinal vascularization of wild-type and $VEGF^{120/188}$ mice at P5 (Figure 5.4 A and B) and P10 (Figure 5.4 C and D) as monitored by perfusion-labeling and imaging of flat mount preparations. The outgrowth of retinal capillaries of $VEGF^{120/188}$ mice reached 51.3 ± 1.1 (mean ± SEM) % of the retinal radius at P5, whereas that of wild-type mice reached 49.5 ± 2 % (Figure 5.4 E, left panel). There was no significant difference in mean vascular density between wild-type (28.4 ± 0.3%) and $VEGF^{120/188}$ retinas (28.8 ± 0.4%) at P5 (Figure 5.4 E, right panel). These findings complement previous data showing vascular retinal development in these mice at P10 [273]. At P10, the superficial vessels had already reached the edge of the retina and the extensive vascular network in the VEGF164-deficient retina was essentially indistinguishable from that of the wild-type mice (Figure 5.4 C and D). In addition, no significant difference was observed in the formation of the deep vascular plexus between the two mouse strains (Figure 5.4 C and D, arrowheads).

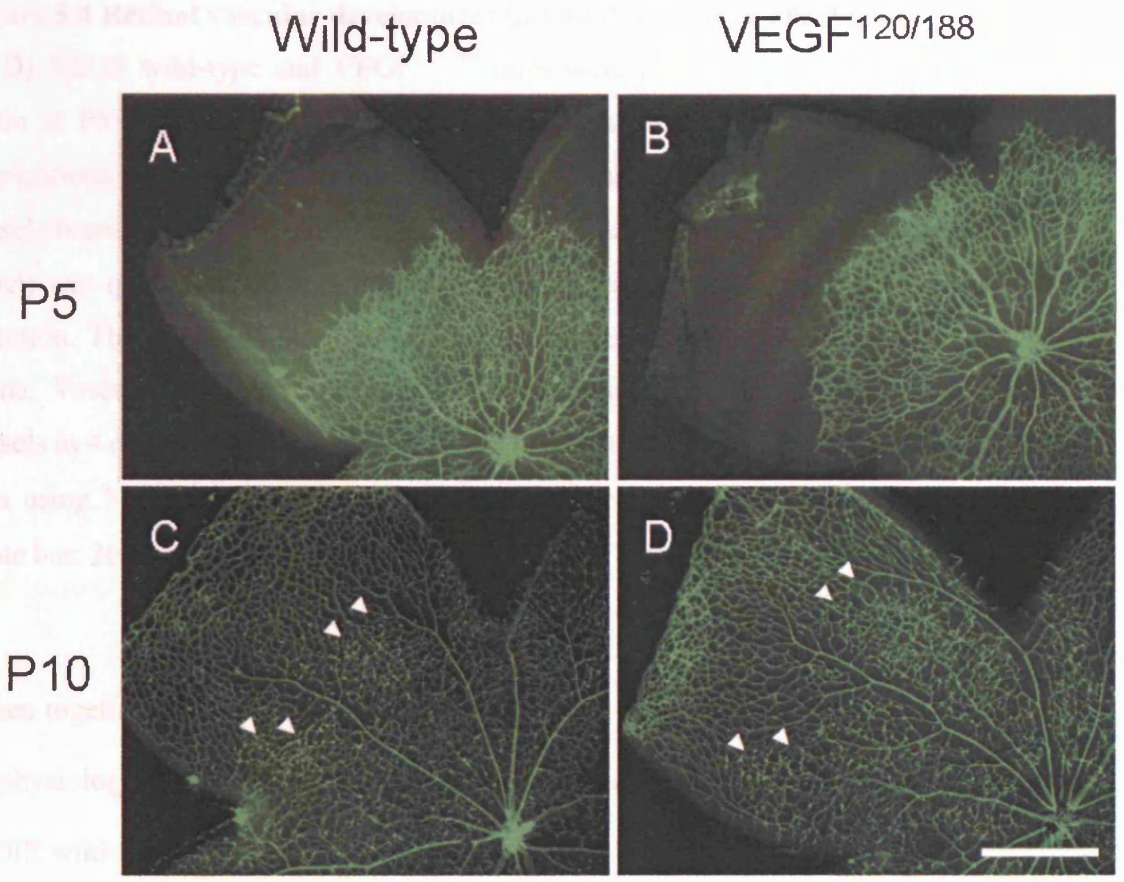
Wild-type
VEGF120/188
A
B
P5
C
D
P10

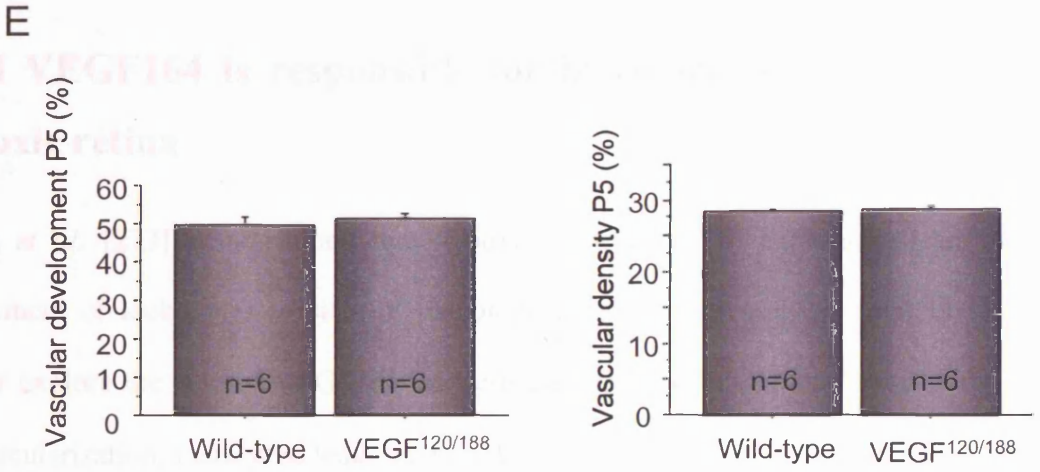
E
Vascular development P5 (%)
60
50
40
30
20
10
0
n=6
n=6
Wild-type
VEGF120/188
Vascular density P5 (%)
30
20
10
0
n=6
n=6
Wild-type
VEGF120/188

Figure 5.4 Retinal vascular development in VEGF wild-type and VEGF$^{120/188}$ mice
(A-D) VEGF wild-type and VEGF$^{120/188}$ mice were perfused with FITC-coupled Con A lectin at P5 and P10. The retinal vasculature was then visualized in retinal flat-mount preparations by fluorescence microscopy. Arrowheads indicate areas where superficial vessels branch out to form the deep vascular plexus. (E) Vascular development at P5 (left panel) was quantified by measuring the length of eight vessels, each going in a different direction. The length of these vessels was expressed as a percentage of the radius of the retina. Vascular density (right panel) was determined by measuring the total length of vessels in 4 different areas (each 200 pixel^2) and was expressed as a percentage of the total area using NIH image. Data are expressed as means ± SEM of 12 eyes (n=6 animals). Scale bar: 200 μm.

Taken together, these data demonstrate that VEGF164 deficiency has no significant effect on physiological neovascularization and suggest that the pathological phenotype observed in OIR wild-type mice is VEGF164 isoform-specific.

5.2.3 VEGF164 is responsible for increased leukostasis in the hypoxic retina

Ishida *et al.* [273] demonstrated that hypoxia-induced VEGF expression leads to the recruitment of leukocytes to sites of pathological retinal neovascularization in rats. To further explore the role of VEGF164 as a critical stimulus for leukocyte stasis in retinal neovascularization, I analyzed leukostasis in VEGF164-deficient (VEGF$^{120/188}$) mice using the OIR model. Leukocyte adhesion was examined in lectin-perfused retinas after 48 hr of relative hypoxia (P14).

In wild-type and $VEGF^{120/188}$ control mice, the number of adherent leukocytes per retina was 17.4 ± 2.1 (mean ± SEM) and 25.4 ± 2.2, respectively (Figure 5.5 A, B and F). Quantitative analysis of leukostasis in wild-type mice subjected to OIR conditions revealed a 4.3-fold increase in leukocyte adhesion over baseline levels. Only a 1.4-fold increase was observed in VEGF164-deficient OIR mice, suggesting that VEGF164 is responsible for the induction and amplification of leukostasis in this model (Figure 5.5 F). Adherent leukocytes were predominantly found in the revascularizing retina at the leading edge of the vascular zone. Interestingly, during the progression of retinal neovascularization in wild-type OIR mice, leukocytes were frequently found associated with vascular tufts (Figure 5.5 E).

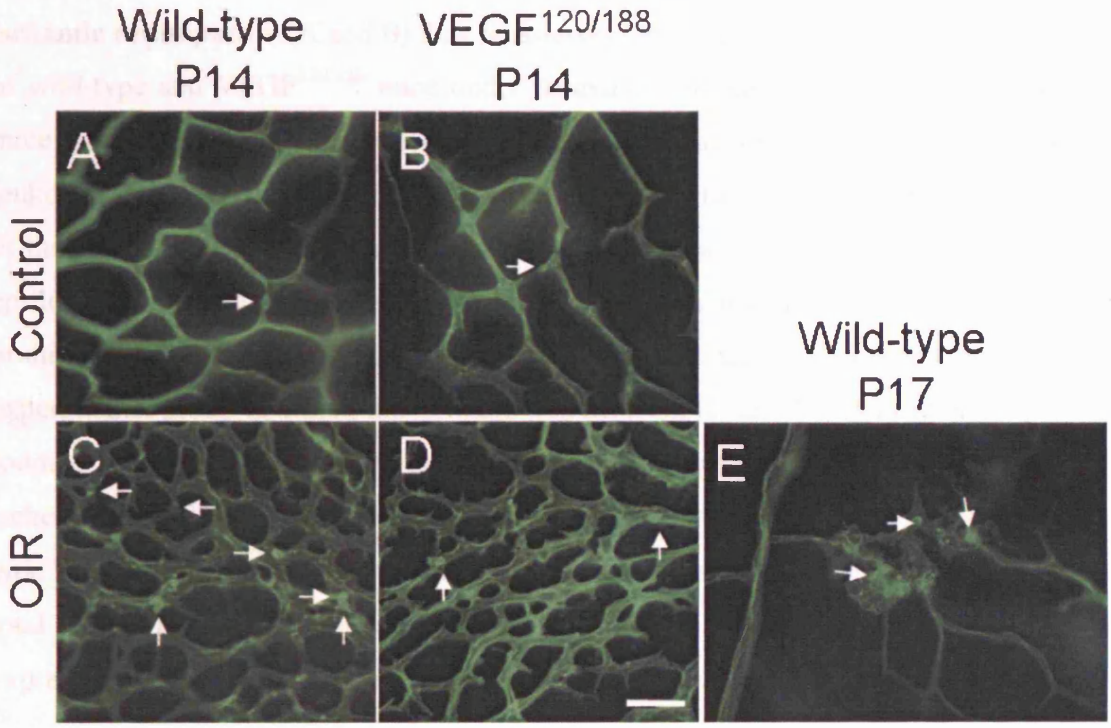
Wild-type
P14
VEGF120/188
P14
Wild-type
P17
Control
OIR
A
B
C
D
E

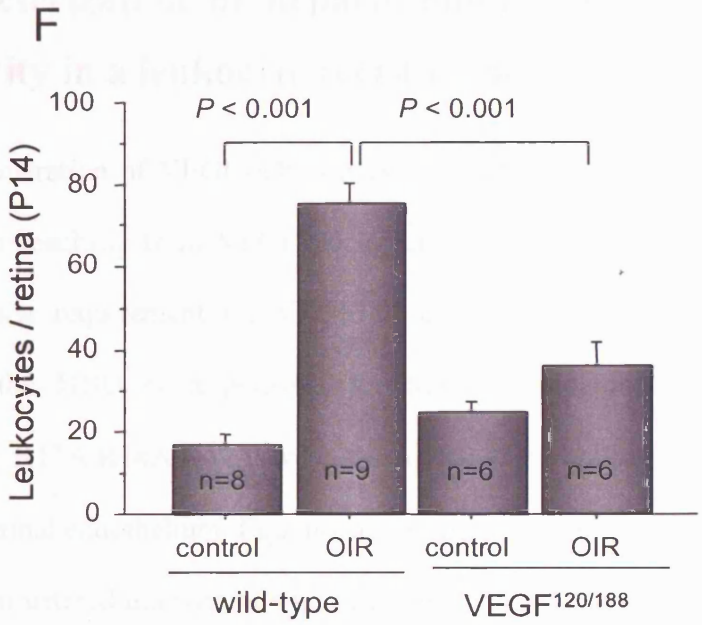
F
Leukocytes / retina (P14)
100
80
60
40
20
0
P < 0.001
P < 0.001
n=8
n=9
n=6
n=6
control
OIR
control
OIR
wild-type
VEGF120/188

Figure 5.5 Retinal leukocyte adhesion in wild-type and VEGF$^{120/188}$ mice with ischemic retinopathy. (A and B) Few leukocytes (arrows) adhere to the retinal vasculature of wild-type and VEGF$^{120/188}$ mice under normal conditions. On the indicated days, OIR mice and non-OIR control mice were perfused with PBS to remove non-adherent leukocytes, then perfused with FITC-coupled Con A lectin to identify adherent leukocytes in the retinal vasculature. Retinas were flat-mounted and images were captured using an epifluorescence microscope. Note that control animals had already undergone vascular pruning by P14, leaving behind a less dense and smaller-caliber vasculature than that of the experimental group in which this process was delayed. (C and D) 48 hr after the return to room air, leukocyte adhesion in ischemic wild-type mice was significantly higher than in ischemic VEGF$^{120/188}$ mice. (E) Leukocytes adhering to vascular tufts in ischemic wild-type mice during progression of retinal neovascularization (P17). (F) Quantification of total leukocyte adhesion per retina at P14. N indicates the number of animals. Data are expressed as mean ± SEM. Scale bar, 10 μm.

5.2.4 Characterization of heparin-binding-deficient VEGF164 mutant activity in a leukocyte recruitment assay

Intraocular administration of VEGF164 induces a specific inflammatory response that is stronger than that resulting from VEGF120 injection [275, 278]. This is not surprising, given the particular requirement for VEGF164 in pathological neovascularization. To assess whether the HBD is responsible for this inflammatory effect, the mutants R14A/R49A and R13A/R14A/R49A were tested for their ability to induce leukocyte adhesion to the retinal endothelium. Equimolar concentrations of purified, sterilized VEGF variants were administered intravitreally into rats, and leukocyte accumulation in the retina was analyzed after 24, 48, and 72 hr by *in vivo* leukocyte fluorography.

As shown in Figure 5.6 A, VEGF164-induced leukostasis in the retinal microvasculature peaked at 48 hr after injection (52.6 ± 8.3 (mean ± SEM) leukocytes/mm^2 retinal surface area) and was 3-fold higher than that induced by VEGF120 (17.7 ± 2.7 leukocytes/mm^2). When compared with control mice injected with inactivated VEGF164, these findings indicate that the effect was specific and directly caused by active VEGF. These data are comparable with results reported previously in which VEGF164 induced a 1.9-fold greater increase in leukostasis than did VEGF120 [278]. In contrast, the VEGF164 HBD mutants R14A/R49A and R13A/R14A/R49A were increasingly less effective at inducing leukocyte recruitment to the retinal capillary bed compared to VEGF164. Only 31.9 ± 5.1 leukocytes/mm^2 and 13.1 ± 1.6 leukocytes/mm^2 were counted 48 hr after injection of the double mutant and the triple mutant, respectively (Figure 5.6 A, F and G).

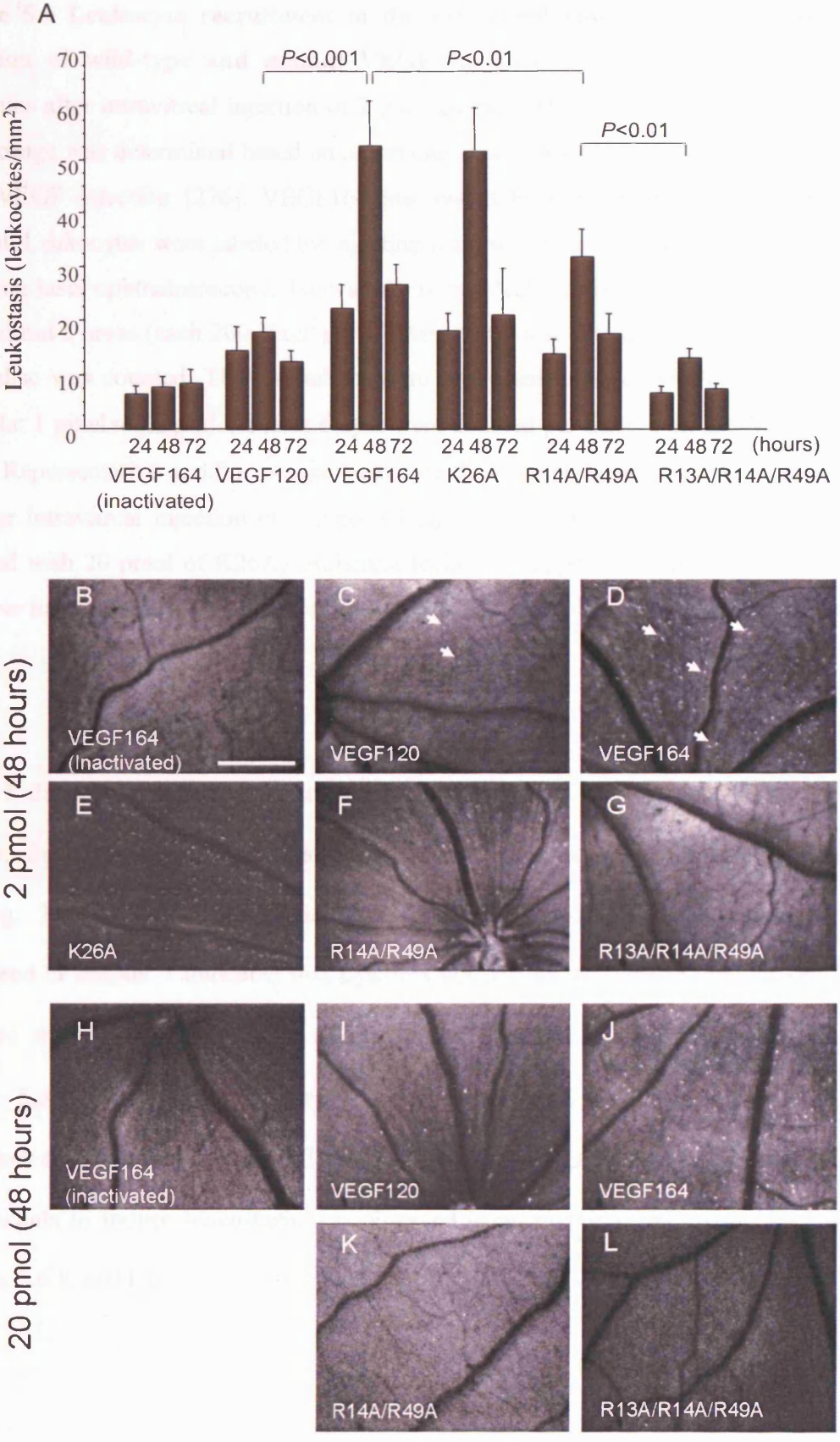
A
P<0.001
P<0.01
P<0.01
Leukostasis (leukocytes/mm²)
0
10
20
30
40
50
60
70
24 48 72 24 48 72 24 48 72 24 48 72 24 48 72 24 48 72 (hours)
VEGF164 (inactivated)
VEGF120
VEGF164
K26A
R14A/R49A
R13A/R14A/R49A
2 pmol (48 hours)
20 pmol (48 hours)
B
VEGF164 (Inactivated)
C
VEGF120
D
VEGF164
E
K26A
F
R14A/R49A
G
R13A/R14A/R49A
H
VEGF164 (inactivated)
I
VEGF120
J
VEGF164
K
R14A/R49A
L
R13A/R14A/R49A

Figure 5.6 Leukocyte recruitment to the rat retinal vasculature after intravitreal injection of wild-type and mutant VEGF variants. (A) Time course of leukocyte dynamics after intravitreal injection of 2 pmol of purified, *Pichia*-derived VEGF variants. The dosage was determined based on a previous report describing leukostasis in the retina after VEGF injection [276]. VEGF164 inactivated by boiling for 10 min served as a control. Leukocytes were labeled by injecting acridine orange intravenously 30 min before scanning laser ophthalmoscopy. To evaluate retinal leukostasis, the number of fluorescent dots within 8 areas (each 200 pixel^2) at a distance of 5 disc diameters from the edge of the optic disc was counted. These numbers were converted to leukocytes/mm^2 by using the formula: 1 pixel = 3.2 μm^2. At least 6 eyes were counted per time point and VEGF variant. (B-L) Representative acridine orange leukocyte fluorography images of the eye fundus 48 hr after intravitreal injection of 2 pmol (B-G) or 20 pmol (H-L) VEGF (Rats were not injected with 20 pmol of K26A). Adherent leukocytes appear as white dots (arrows). No increase in leukostasis was observed in 20 pmol vs. 2 pmol injected eyes. Scale bar: 500 μm.

Next, I determined whether the reduced potency of the two mutants with respect to leukostasis was specifically associated with alterations in the region implicated in heparin binding. The single mutant K26A was used for comparison, since binding studies described in chapter 3 indicated that Lys26 is not part of the heparin-binding site. K26A retained wild-type potency 48 hr after injection of 2 pmol (51 ± 7.9 leukocytes/mm^2; Figure 5.6A), suggesting that Arg13, Arg14 and Arg49 constitute residues that are important for mediating the pro-inflammatory activity of VEGF164. The reduced ability of the mutants to induce leukostasis was observed even after injecting 20 pmol of protein (Figure 5.6 K and L).

To identify the type of infiltrating leukocytes in the retinal vasculature, weight-matched mice were perfused with FITC-labeled Con A 24 hr after intravitreal injection of VEGF164, allowing visualization of the retinal vasculature and leukocytes. Double-labeling with the pan-macrophage marker F4/80, followed by superimposition of the images from Con A perfusion, identified the majority of the lectin-stained leukocytes inside blood vessels as F4/80-positive monocytes/macrophages (Figure 5.7, right panel, arrows). The F4/80-negative leukocyte population infiltrating the retinal vessels likely consists of neutrophils and lymphocytes.

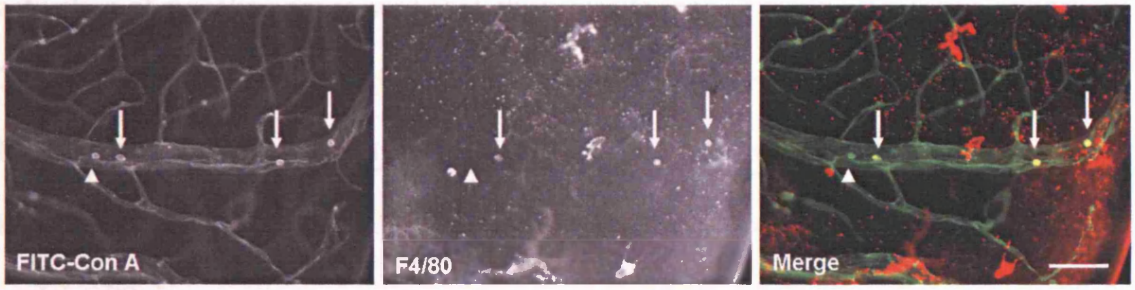

Figure 5.7 Identity of endothelium-associated leukocytes in the retina after VEGF164 injection. Mice were injected intravitreally with VEGF164 (2 pmol) and perfused with FITC-coupled Con A lectin (green fluorescence, left panel) 24 hr later. Retinal flat mounts were probed with an anti-F4/80 antibody (red fluorescence, middle panel). Arrows indicate F4/80/lectin-positive macrophages/monocytes, whereas F4/80-negative leukocytes are marked by arrowheads in the superimposed image (right panel). Scale bar: 50 μm.

5.2.5 Analysis of VEGF receptor involvement in VEGF164-induced leukostasis

In an attempt to examine the involvement of individual VEGF receptors in mediating VEGF164-induced leukostasis, rat eyes were injected with VEGF receptor-selective ligands of the VEGF family of growth factors. Both VEGFR-1-specific PlGF-1 and VEGFR-2-specific VEGF-E exhibited only a weak stimulatory effect on leukocyte recruitment, which was comparable to that of VEGF120 (Figure 5.8 A). A ten-fold increase in the injected dose (20 pmol) of either ligand did not result in an increase in leukocyte accumulation (data not shown). Since VEGF-E and VEGF have been shown to bind VEGFR-2 with similar affinity, resulting in receptor phosphorylation and subsequent activation of signaling processes [313], these results suggest that the activation of VEGFR-2 alone is not sufficient to elicit a potent inflammatory response in the retina. In contrast to PlGF-1, mouse PlGF-2 displayed similar kinetics to, and was as potent as, VEGF164 in inducing leukostasis (55.6 ± 7.3 (mean ± SEM) leukocytes/mm^2 at 48 hr). PlGF-2 is bound by VEGFR-1 and the neuropilins, and is the only PlGF splice form able to interact with heparin [127]. No macroscopic signs of inflammatory reactions, such as corneal opacity, were detected, indicating that the retinal inflammatory response induced by PlGF-2 was direct.

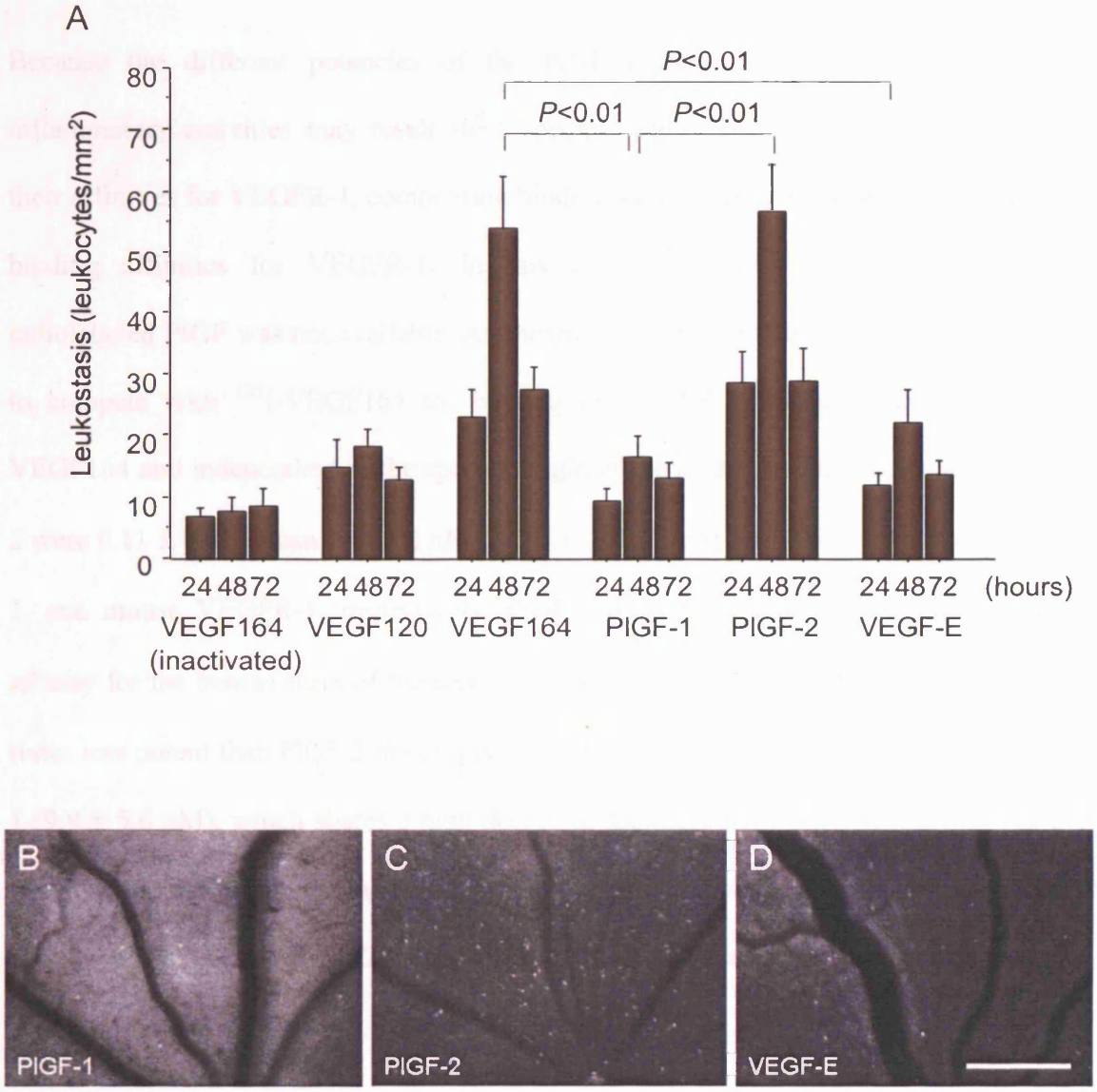

Figure 5.8 Induction of retinal leukostasis by VEGF receptor-selective ligands. (A) Time course of leukostasis after intravitreal injection of 2 pmol of PlGF-1 (human), PlGF-2 (mouse) or VEGF-E (ORF-virus) into rats. Values for VEGF164 (inactivated), VEGF120 and VEGF164 are shown for comparison. Analysis and quantification of leukostasis was conducted as described in Figure 5.6. Bars represent mean values ± SEM. At least 5 eyes were analyzed in each group. (B-D) Representative acridine orange leukocyte fluorography images of the retinal vasculature at 48 hr after injection. Leukocytes appear as white dots. Scale bar: 500 μm.

Because the different potencies of the PlGF isoforms with respect to their pro-inflammatory activities may result from species- and/or isoform-specific differences in their affinities for VEGFR-1, competition binding assays were conducted to assess relative binding affinities for VEGFR-1. In this assay, ^{125}I-VEGF165 was used because radiolabeled PlGF was not available. As shown in Figure 5.9, the ability of mouse PlGF-2 to compete with ^{125}I-VEGF165 for binding to VEGFR-1 was comparable to that of VEGF164 and independent of the species origin of the receptor. The IC_{50} values for PlGF-2 were 0.11 ± 0.02 (mean ± SEM) nM, and 0.11 ± 0.02 nM for binding to human VEGFR-1, and mouse VEGFR-1, respectively. PlGF-1 on the other hand, displayed a weaker affinity for the human form of the receptor (0.88 ± 0.37 nM), and was approximately 100 times less potent than PlGF-2 in competing with VEGF165 for binding to mouse VEGFR-1 (9.9 ± 5.6 nM), which shares a high degree of sequence homology with the rat receptor [319]. Thus, the difference in VEGFR-1-binding affinity may account for the differential potency of PlGF-1 and PlGF-2 in the leukocyte recruitment assay.

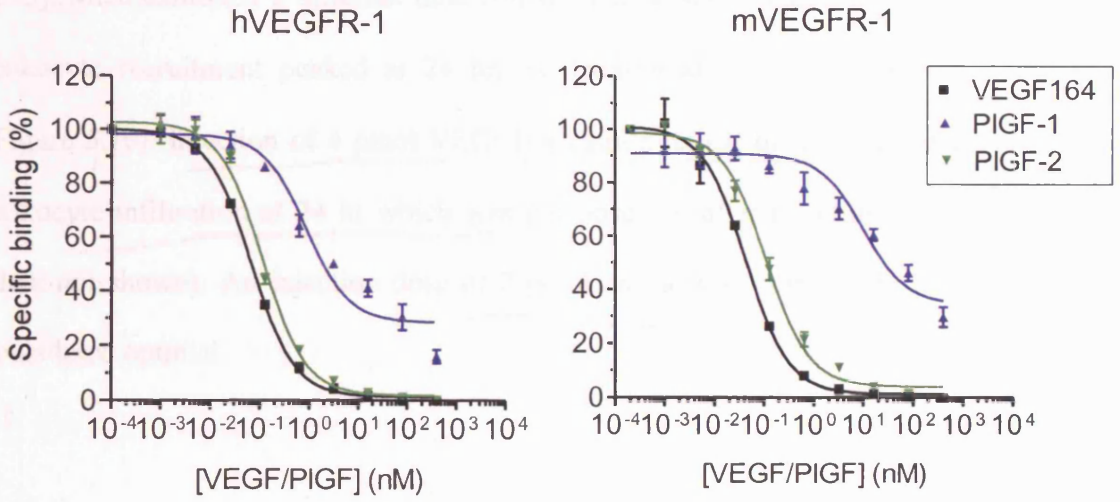

Figure 5.9 Characterization of PlGF-1 and PlGF-2 binding to immobilized VEGFR-1. Competitive displacement of ^{125}I-VEGF165 binding to immobilized human (h) VEGFR-1/F_c (left panel) and mouse (m) VEGFR-1/F_c (right panel) in the presence or absence of increasing concentrations of PlGF-1, mouse PlGF-2 or VEGF164 was carried out in a 96-well microtiter plate. Curve fitting and analysis of binding parameters using the one-site competition model were performed with GraphPad software. Specific binding was determined by subtracting the background signal (non-specific signal obtained in the presence of 400 nM VEGF164) from raw signal values. Data points (means ± SEM) are from triplicate wells and are representative of three independent experiments.

Previous studies have demonstrated that PlGF and VEGFR-1 are involved in a variety of inflammatory conditions [167, 168, 320], and that corneal inflammation after VEGF pellet implantation was suppressed by selectively blocking VEGFR-1 activity [275]. In combination with the finding that both VEGF164 HBD mutants show decreased VEGFR-1-binding affinity, the data presented here further point to a role for VEGFR-1 in VEGF164-induced retinal leukostasis. To test this hypothesis in mice, VEGFR-1 mediated responses were blocked *in vivo* using a mouse-specific VEGFR-1 neutralizing antibody

[275]. Mice exhibited a different time course of leukostasis than rats (Figure 5.6) in that leukocyte recruitment peaked at 24 hr, as determined in a dose-response experiment (Figure 5.10). Injection of 4 pmol VEGF164 caused retinal hemorrhage and non-specific leukocyte infiltration at 24 hr which was not observed after injecting 2 pmol VEGF164 (data not shown). An injection dose of 2 pmol and a time point of 24 hr was therefore considered optimal.

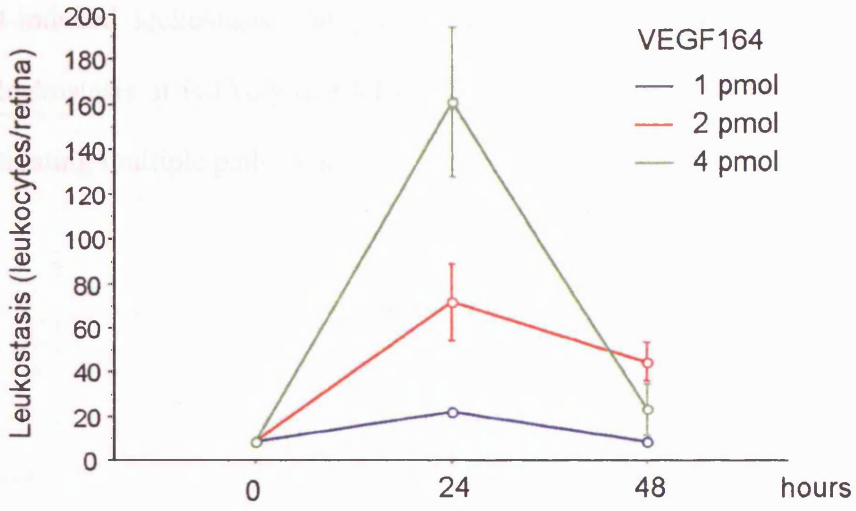

Figure 5.10 Time course and dose-response curve of VEGF-induced leukostasis in mice. C57BL/6J male mice received intravitreal injections of 1, 2, or 4 pmol of VEGF164, and were perfusion-labeled with FITC-coupled Con A immediately, 24 or 48 hr later. Retinal flat mounts were imaged with an epifluorescence microscope and the total number of adherent leukocytes per retina was determined. At least 5 eyes were analyzed in each group. Data points are represented as mean ± SEM.

Weight-matched mice received intraperitoneal injections of the antibody 3 hr before intravitreal injection of VEGF164. Systemic administration of the anti-VEGFR-1 antibody was necessary, as injection of the goat IgG control antibody into the mouse or rat vitreous induced an immune response in the eye. Neither control IgG nor neutralizing antibody caused local inflammation when injected into the mouse peritoneum. As shown in Figure 5.11, the VEGFR-1-blocking antibody suppressed VEGF164-induced retinal leukostasis by 51% compared to control IgG (28.5 ± 4.3 (mean ± SEM) vs. 57.7 ± 9.5 leukocytes/retina) when administered at a concentration of 1.5 mg/kg. A dose of 3 mg/kg of anti-VEGFR-1 did not further reduce the number of leukocytes recruited to the retinal vessels (29.2 ± 4.2 leukocytes/retina). These findings support a role for VEGFR-1 in VEGF164-induced leukostasis, but given that VEGFR-1 blockade did not completely abrogate leukostasis, it is likely that VEGF164 exerts its pro-inflammatory activity in the eye by activating multiple pathways.

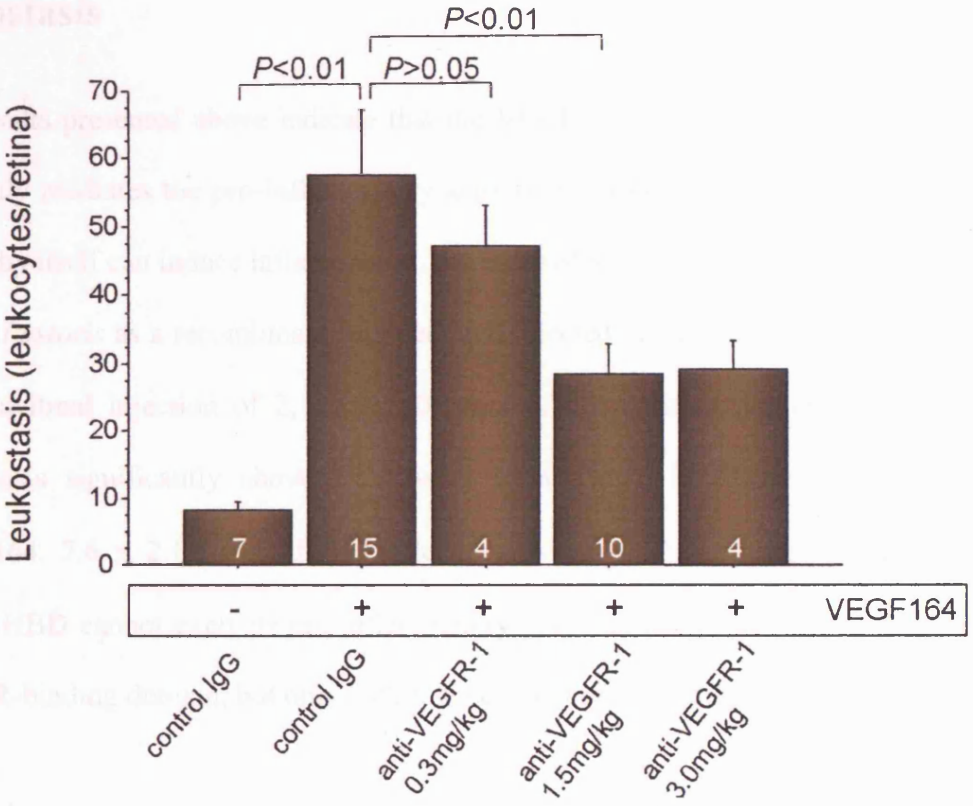

Figure 5.11 Suppression of VEGF164-induced retinal leukostasis by blocking VEGFR-1 activity. Mice received intraperitoneal injections of 0.3, 1.5, or 3 mg/kg of a goat anti-mouse VEGFR-1 neutralizing antibody (anti-VEGFR-1) or pre-immune control goat IgG (control IgG, 3 mg/kg) 3 hr before intravitreal injection of VEGF164 (2 pmol) or PBS. The dosage of anti-VEGFR-1 antibody was based on similar experiments reported previously [275]. 24 hr after VEGF injection, adherent leukocytes in the retinal vasculature were imaged by perfusion-labeling with FITC-coupled Con A lectin. The total number of static leukocytes per retina was determined using an epifluorescence microscope. Numbers inside bars represent the number of eyes analyzed. Data are represented as mean ± SEM.

5.2.6 Recombinant VEGF164 HBD inhibits VEGF164-induced leukostasis

The results presented above indicate that the VEGF C-terminal domain either directly or indirectly mediates the pro-inflammatory activity of VEGF164. To examine whether this region by itself can induce inflammation, the HBD of VEGF164 was expressed in the yeast *Pichia Pastoris* as a recombinant fragment and injected into rats. As shown in Figure 5.12 A, intravitreal injection of 2, 10 or 50 pmol of the purified peptide did not increase leukostasis significantly above the control level shown in Figure 5.6 A (inactivated VEGF164, 7.6 ± 2.1 (mean ± SEM) leukocytes/mm^2). This strongly suggests that the VEGF HBD cannot exert its pro-inflammatory potential independently of the N-terminal VEGFR-binding domain, but only within the context of the full-length protein.

Since the recombinant HBD lacks the ability to induce leukostasis, it may be able to interfere with the pro-inflammatory activity of VEGF. To investigate this possibility, 2, 10 or 50 pmol of recombinant HBD was injected intravitreally 2 min before VEGF164 using an injection-delay technique that does not require removal of the needle between the two injections. HBD potently inhibited VEGF164-induced leukocyte adhesion to the retinal microvasculature in a dose-dependent manner (Figure 5.12 A and C-E). A 25-fold molar excess of the HBD monomer (50 pmol) over the VEGF dimer (2 pmol) reduced VEGF164-induced leukostasis to background levels (8.8 ± 2.13 (mean ± SEM) leukocytes/mm^2 vs. 7.1 ± 2.6 leukocytes/mm^2). These data suggest that the VEGF HBD might act as an anti-inflammatory agent *in vivo* by interfering with VEGF164 activity in the eye.

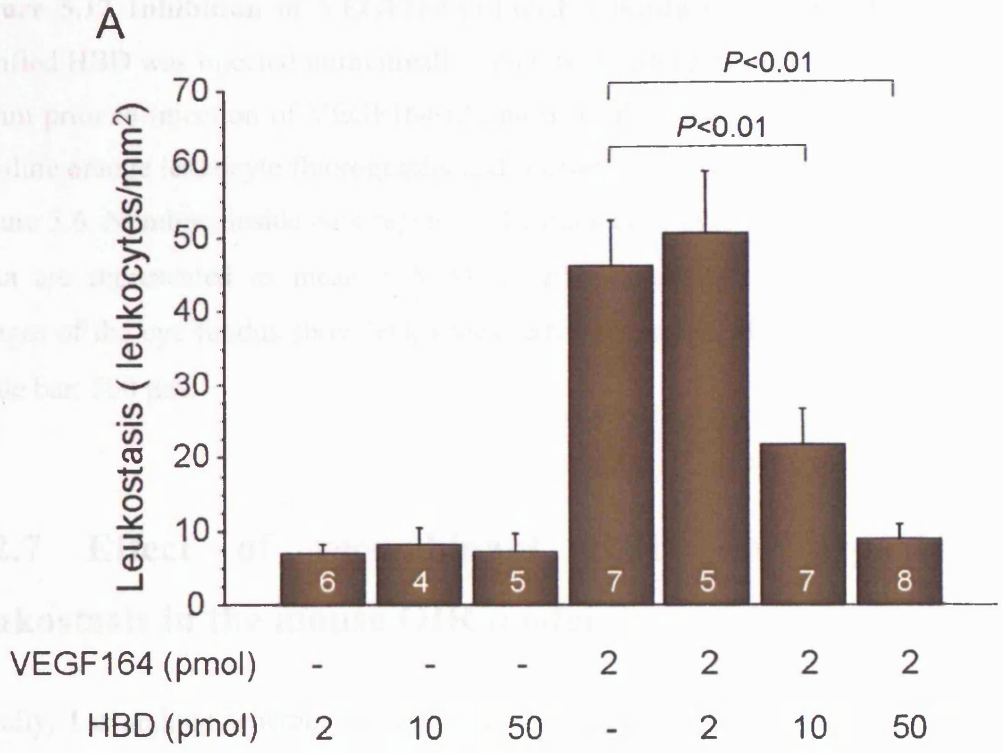
A
P<0.01
P<0.01
Leukostasis (leukocytes/mm2)
70
60
50
40
30
20
10
0
6
4
5
7
5
7
8
VEGF164 (pmol) - - - 2 2 2 2
HBD (pmol) 2 10 50 - 2 10 50

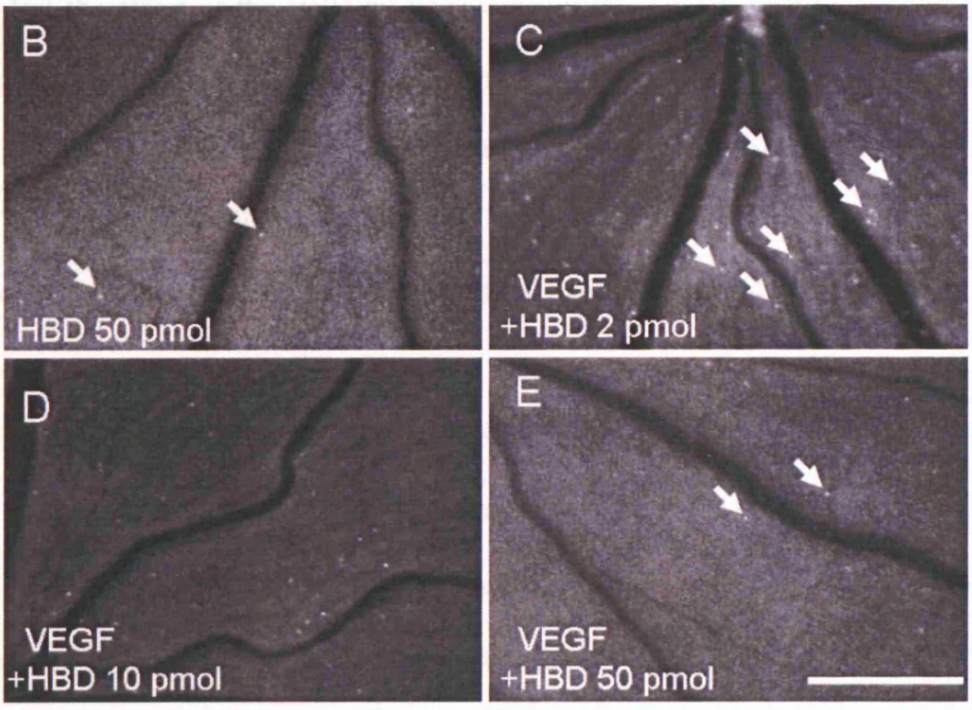
B
HBD 50 pmol
C
VEGF
+HBD 2 pmol
D
VEGF
+HBD 10 pmol
E
VEGF
+HBD 50 pmol

Figure 5.12 Inhibition of VEGF164-induced leukostasis by recombinant HBD. (A) Purified HBD was injected intravitreally into rats at different concentrations either alone or 2 min prior to injection of VEGF164 (2 pmol). Leukostasis was evaluated after 48 hr by acridine orange leukocyte fluorography and scanning laser ophthalmoscopy as described in Figure 5.6. Numbers inside bars represent the number of eyes analyzed for each condition. Data are represented as mean ± SEM. (B-E) Representative fluorescein angiography images of the eye fundus show leukocytes (arrows) associated with the microvasculature. Scale bar: 500 μm.

5.2.7 Effect of recombinant HBD on hypoxia-induced leukostasis in the mouse OIR model

Finally, I examined whether recombinant HBD is able to reduce leukocyte recruitment caused by hypoxia-induced upregulation of VEGF164 in the eye [273]. As shown earlier, leukocyte adhesion in the OIR model was elevated in wild-type but not in $VEGF^{120/188}$ mice. To test the effect of the HBD on leukostasis in this model, wild-type mouse pups were taken out of the oxygen chamber on P12 and injected intraperitoneally with 2 nmol of the VEGF HBD at P12 and P13 (hypoxic phase). In parallel, control groups received 5 mg/kg of anti-VEGF neutralizing antibody or 5 mg/kg of a goat IgG control. Inflammatory cell recruitment to retinal vessels was visualized and quantified at P14.

As summarized in Figure 5.13, P14 mice in the non-OIR control group exhibited low levels of leukostasis in the retina (16.1 ± 2 (mean ± SEM) leukocytes/retina). The number of leukocytes was increased 4.3-fold (70 ± 4.8 leukocytes/retina) in OIR mice injected with IgG from non-immunized goats, which served as an isotype control for the VEGF neutralizing antibody.

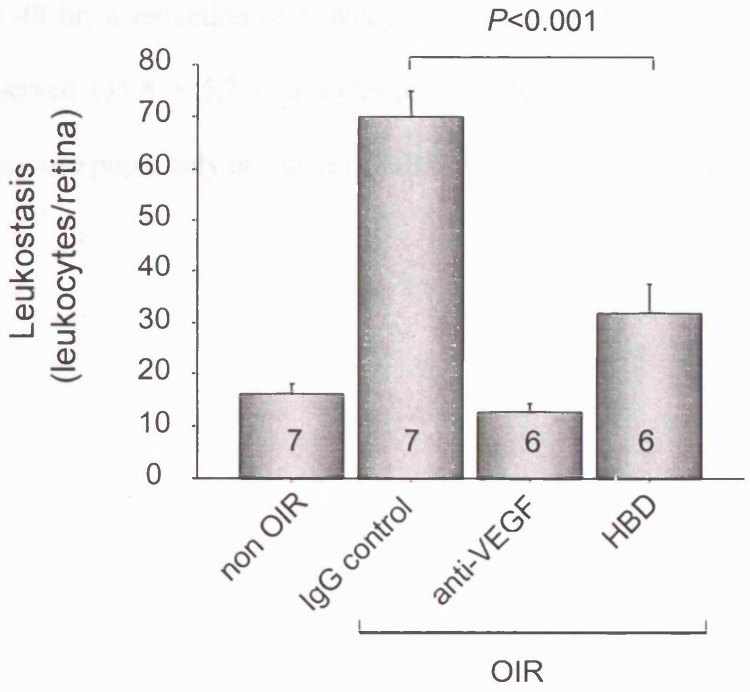

Figure 5.13 Suppression of retinal leukostasis by recombinant HBD in mice with oxygen-induced retinopathy. Oxygen-induced retinopathy (OIR) in mice was induced as described. The following injections were performed intravenously at P12 and P13: total goat IgG control (5 mg/kg), goat anti-mouse VEGF neutralizing antibody (5 mg/kg), and purified HBD (2 nmol). Adherent leukocytes inside retinal vessels were visualized by perfusion of P14 mouse pups with FITC-coupled Con A lectin and quantified. Note that the total number of retinal vessels in OIR mice is lower than in non-OIR mice due to vessel regression during the hyperoxic phase. Numbers inside the columns represent number of eyes analyzed. Data are presented as mean values ± SEM.

These levels are similar to those obtained in non-injected OIR mice (Figure 5.5) and demonstrate that the control antibody has no effect on leukocyte behaviour. The administration of an anti-VEGF neutralizing antibody further reduced disease-related inflammation in the mouse retina compared to the IgG control by a total of 81% (12.8 ± 1.5 leukocytes/retina). Strikingly, when OIR mice were injected with recombinant HBD

and analyzed at 48 hr, a reduction of leukocyte adhesion by 55% compared to the OIR control was observed (31.8 ± 5.7 leukocytes/retina). Due to the elevated mortality rate among the OIR mouse pups, only one dose of HBD was tested in this experiment.

5.3 Discussion

The functional importance of the heparin-binding forms of VEGF has been studied by several groups using a variety of strategies, such as overexpression of single isoforms in cell lines and tumors, proteolytic removal of the C-terminal domain and, most recently, transgenic expression of only one isoform in mice by 'knock-in' mutation of the endogenous gene [118, 124, 254, 260, 263, 284]. Here, by combining *in vitro* and *in vivo* analysis using biochemical tools, I have shown that the heparin-binding domain mediates VEGF164-induced retinal leukostasis and is critical for promoting the inflammatory activities of VEGF164 in ocular pathology.

5.3.1 The differential requirement of VEGF164 in retinal vascular development and in the response of the retina to ischemia

Hypoxia-induced VEGF governs both retinal vascular development and pathological retinal neovascularization [321]. The importance of the VEGF164 isoform for the pathogenesis of retinal neovascular diseases has been demonstrated in a number of studies [273, 275, 278]. Similar observations were made here by studying VEGF164-deficient mice in a well-characterized mouse model of proliferative retinopathy. The loss-of-function phenotype of these mice can be best summarized as a lack of neovascular tufts and a vastly reduced ability to recruit leukocytes to the ischemic retina. The absence of the pathological phenotype in VEGF164-deficient mice is unlikely to be the result of a decrease in total VEGF expression levels compared to those in wild-type mice, since

VEGF transcription levels in $VEGF^{120/120}$, $VEGF^{188/188}$ and $VEGF^{+/+}$ mice are comparable [254, 284]. Although other factors may contribute to the pathologic phenotype described here, VEGF appears to be the only endothelial cell mitogen that is upregulated in the hypoxic retina [322]. Previously published VEGF isoform expression data are consistent with a major role of VEGF164 in oxygen-induced retinopathies. In the rat OIR model, repeated cycles of hyperoxic and hypoxic episodes were shown to result in significantly elevated VEGF164 mRNA levels relative to other isoforms, and this upregulation was maintained through the time of maximal neovascularization [272, 273]. Whereas angiopathic changes were not analyzed in the present study, Tolentino *et al.* showed that intravitreal delivery of VEGF165 into non-human primates stimulates aberrant blood vessel formation. The newly formed vessels showed features of proliferative retinopathy, including vessel dilation and tortuousity as well as preretinal neovascularization originating from superficial veins and venules [323].

In contrast to the tightly regulated expression of VEGF164 during development, hypoxic conditions result in exaggerated VEGF164 levels sufficient to generate the observed pathologic phenotype. Here, the inflammatory response observed in the OIR model could be similarly reproduced by intravitreal injections of VEGF164 into normal rats. Using scanning laser ophthalmoscopy, a technique that allows the observation and quantification of leukocyte dynamics *in vivo*, a reliable and dramatic increase in leukocyte adhesion was observed after intravitreal delivery of *Pichia*-derived VEGF164. VEGF120 did not exert this effect. Taken together with the observations made in $VEGF^{120/188}$ transgenic mice, these data suggest that VEGF164 is both required and sufficient for induction of retinal inflammation. Because inflammatory cells clearly play an important role in promoting

neovascularization [324, 325], these data further substantiate the essential role of the VEGF164 isoform in pathological angiogenesis. I therefore expect that the R14A/R49A and R13A/R14A/R49A mutants would be less potent than wild-type VEGF164 at inducing pathological neovascularization. It would also be interesting to see whether injection of HBD in the OIR model will have a normalizing effect on aberrant blood vessel growth in addition to its anti-inflammatory effect.

Physiological vascular development of the retina does not appear to be a VEGF164-dependent process as development of superficial and deep retinal capillary beds were not compromised in VEGF164-deficient mice. This observation supports previous data [273] and suggests that VEGF164 function in normal vessel development can be replaced by the simultaneous expression of soluble (VEGF120) and cell-associated (VEGF188) isoforms. While VEGF164 may not be required for normal vascular development of the retina, a recent study showed that the retinal vasculature of mice solely expressing this isoform ($VEGF^{164/164}$) developed normally [254]. These findings may appear contradictory at first glance, but they suggest a certain degree of functional redundancy between the VEGF variants in normal retinal angiogenesis. The observation that anti-VEGFR-2 antibody treatment does not affect developmental vessel morphology and growth also indicates that interaction of VEGF with this receptor is not an absolute requirement for vascular development in the neonatal retina [326]. Normal retinal vascularization is likely to be more complex than pathological angiogenesis, and may require hypoxia-dependent and -independent stimuli and/or stimuli derived from non-endothelial cells, such as neuroglia, pericytes, and the retinal pigment epithelium [22].

5.3.2 VEGF164 HBD encodes determinants that enhance its pro-inflammatory properties

The results presented here reinforce the presence of HBD-encoded determinants that are indispensable for promoting VEGF-induced leukostasis. The leukostasis-inducing activities of the two VEGF164 HBD mutants were not only severely impaired but also correlated with their respective heparin-binding potential, suggesting that binding to cell-associated glycosaminoglycans is essential for this function. Two major glycosaminoglycans, heparan-sulfate and chondroitin-sulfate, are expressed in distinct spatiotemporal patterns in the retina during postnatal development and in the adult rat [327]. Heparan sulfate is consistently found in the ganglion cell layer at the vitreoretinal interface and in the inner nuclear layer [328, 329]. In the ganglion cell layer, heparan sulfate chains are likely components of the basal lamina and/or the cell surface of endothelial cells in the superficial retinal vessels.

Upon injection, VEGF164 is expected to penetrate the vitreoretinal membrane because of its low molecular weight and diffuse into the ganglion cell layer, where it may interact with HSPGs on the superficial vasculature [330, 331]. Low-affinity binding of VEGF by HSPGs, rather than the less abundant high-affinity signaling receptors, may result in increased levels of VEGF around the endothelium that would be available to stimulate target cells. Compared to wild-type VEGF164, which binds to HSPGs, the mutants R14A/R49A and R13A/R14A/R49A may therefore be more rapidly cleared from the retina. Efforts to determine the diffusion rate of the VEGF variants after injection by comparing their concentrations in the vitreous humor and the retina failed due to difficulties in

separating these intimately attached compartments. Future work will seek to address the anatomical distribution of these VEGF variants within the retina and the type of cells involved.

Recombinant HBD potently inhibited VEGF164-induced leukostasis in a concentration-dependent manner but did not exert a visible effect on leukocyte recruitment when injected alone. Thus, it appears that the receptor-binding domain and the HBD of VEGF164 represent two domains that act interdependently to amplify leukostasis and inflammation-driven neovascularization in the retina. Given the complexity of interactions between VEGF and its receptors in the presence of heparin-like molecules, one could imagine several mechanisms that could explain the enhanced activity of VEGF164 relative to its HBD alone. In addition to facilitating the retention of VEGF164 on cell surfaces, the interaction with glycosaminoglycans of certain chain length and subtype may lead to quantitative and qualitative differences in receptor engagement and signaling output. Although it is not clear whether VEGF is able to oligomerize on glycosaminoglycans, the formation of such oligomeric structures may result in the activation of receptor-mediated and specific 'pro-inflammatory' signal transduction pathways. In this model, reduced activity of the mutants would be explained by the inability of the glycosaminoglycan chains to link the mutants into higher-order oligomers, due to the lack of heparin-binding epitopes. It follows, then, that recombinant HBD would antagonize VEGF164-induced leukostasis by competing with VEGF for binding to heparan-sulfate proteoglycans and/or neuropilin-1, without engaging signaling receptors. The importance of oligomerization for *in vivo* function of certain chemokines has been demonstrated by analyzing heparin-binding-deficient versions of RANTES/CCL5, MIP-1β/CCL4, and MCP-1/CCL2. These

mutants, which did not form glycosaminoglycan-associated oligomeric complexes, activated receptors but were unable to induce inflammatory cell recruitment in a peritoneal recruitment assay [239, 332].

The type of proteoglycan involved, too, might influence signaling events. For example, the two cell-surface HSPGs syndecan and glypican are equally capable of forming ternary complexes with FGF-2 and FGFR-1. Yet only glypican-1, which is also known to modulate the binding of VEGF165 to VEGFR-2, is able to sensitize brain endothelial cells to FGF-2-induced mitogenesis [229, 333]. HSPG-mediated association of VEGF164 with VEGF receptors may also induce biologically relevant changes in auto-phosphorylation patterns of intracellular receptor domains as has been shown for FGF-2. While not essential for receptor dimerization and kinase activation, heparan sulfate is required for the phosphorylation of specific receptor substrates in response to FGF-2 [334, 335]. Similar roles for HSPGs in VEGF signaling, particularly with regard to the pro-inflammatory activity of VEGF164, have yet to be investigated.

Other mechanisms that may be operative in the generation of VEGF-induced leukostasis are the expression or translocation of endothelial cell adhesion molecules, including ICAM-1, VCAM-1, E-selectin, or P-selectin, and chemokines such as MCP-1, IL-8, and MIP-1α [276, 336-342]. A comparison of VEGF120 with VEGF164 demonstrated that VEGF164 more potently induces both expression of ICAM-1 and translocation of P-selectin to the surface of cultured HUVEC [275, 336, 338]. *In vivo*, VEGF164 is known to induce ICAM-1 expression in the murine retinal vasculature [343] and increased levels of VEGF and ICAM-1 were shown to coincide with elevated leukocyte counts in the retina

during experimental diabetes, where the VEGF164 isoform accounts for 80% of total VEGF [279, 344]. ICAM interacts with activated CD11a-CD18 (LFA-1) and CD11b-CD18 (Mac-1) integrins on rolling leukocytes which then firmly bind to the endothelium before transmigrating into the underlying tissue [345], indicating that increased leukocyte adhesiveness secondary to ICAM-1 upregulation may in part be responsible for the pro-inflammatory activity of VEGF164.

Recent in vitro data suggest a pivotal role for VEGFR-2 in mediating VEGF-induced ICAM-1 expression [275, 336]. VEGFR-2 expression in rodents during normal development has mostly been detected in the neural retina outside the microvasculature and, to a lower degree, in retinal vessels [151, 346, 347]. After hyperoxic insult, VEGFR-2 immuno-reactivity is strongly elevated in intravitreal neovascular growth correlating with the high proliferative activity associated with this condition [326, 346]. While VEGFR-2-mediated upregulation of adhesion molecules may play a role in VEGF164-induced retinal leukostasis, the reduced ability of VEGF-E (isolate D1701) and the HBD mutants to induce leukocyte recruitment *in vivo* suggests that activation of VEGFR-2 alone is not sufficient. Given the fact that VEGF164 and mutant R13A/R14A/R49A are equally active in stimulating VEGFR-2-driven processes, such as endothelial cell proliferative pathways *in vitro* and microvessel growth *ex vivo*, it is possible that the HBD-dependent pro-inflammatory pathway induced by VEGF164 is distinct and different from its HBD-independent mitogenic pathway. Therefore, the increased capacity of the VEGF164 isoform to induce leukostasis does not originate from an elevated proliferative activity of VEGF164.

Because recombinant HBD does not interact with VEGFR-1 and VEGFR-2 directly [118], competition of HBD with VEGF164 for binding to heparan sulfate and/or neuropilin-1 may also have indirectly limited its access to one or both of the VEGF receptors. The blockade of VEGF-neuropilin-1 interaction may impede VEGFR-2 downstream signaling by interfering with receptor coupling and/or the formation of a ternary complex [126, 187]. A similar mechanism has been proposed by Soker et al., who showed that a GST-fusion protein corresponding to the amino acid sequence of VEGF exon 7 and 8 not only inhibited cross-linking of ^{125}I-VEGF165 to neuropilin-1, but also to VEGFR-2, without directly binding to VEGFR-2 [348]. Reports about an involvement of neuropilins in inflammation are limited. VEGF165 may contribute to neutrophil adhesion to activated endothelial cells by inducing the translocation of P-Selectin to the endothelial cell surface primarily through activation of VEGFR-2. Binding of VEGF165 to neuropilin-1 is thought to potentiate this effect as compared to VEGF121 [338]. In the eye, high transcript levels and a strong co-localization of neuropilin-1 with VEGFR-2 mRNA can be detected in neovascularized vessels and fibrovascular tissue in two mouse models of proliferative retinopathy suggesting a role for neuropilin-1 in regulating vascular density [280, 349]. On the other hand, a role for neuropilin-1 in retinal leukostasis may be difficult to reconcile with the fact that the adult quiescent retina expresses very low levels of neuropilin-1 [349]. Furthermore, mutant R13A/R14A/R49A was inactive in the leukocyte recruitment assay, despite retaining considerable binding affinity for neuropilin-1 *in vitro*. In the current study, a PlGF-2-derived peptide that blocks VEGF binding to neuropilin-1 [185] was used *in vivo* to assess the role of neuropilin-1 in VEGF-induced leukostasis but yielded inconclusive results because it was found to also inhibit VEGF binding to heparin (data not shown). Further studies regarding the functional aspects of neuropilin-1 binding by VEGF in the

eye as well as a possible involvement of neuropilin-2 in this process using more selective receptor antagonists are warranted.

The findings presented in this chapter are consistent with a significant role for VEGFR-1 in VEGF-induced leukocyte recruitment and are in line with previous reports showing anti-inflammatory effects of anti-VEGFR-1 treatment in a variety of tissues other than the retina [168, 275, 350]. In the present study, retinal leukostasis induced by VEGF164 was maximally reduced by 51% after systemic administration of an anti-VEGFR-1 neutralizing antibody. The incomplete inhibition of leukocyte infiltration may be partially attributed to the limited access of the antibody to the retinal tissue but also indicates the involvement of other pathways activated by VEGF. While the latter is likely the case, it begs an explanation for the apparently contradictory finding that both VEGF164 and VEGFR-1-selective PlGF-2 exhibit a similar dose-response profile in the leukostasis assay. This discrepancy may be explained by the reported ability of PlGF-2 to activate VEGFR-1 differently than VEGF, resulting in the expression of distinct downstream target genes [169]. PlGF-2 may also recruit a different subset of leukocytes.

VEGFR-1 is constitutively expressed in the normal retina, where it is associated with both microvascular and non-vascular structures in the inner nuclear layer as well as the ganglion cell layer and the basement membrane-rich inner limiting membrane [315, 351, 352]. VEGFR-1 expression has been detected in arteries and veins and has been shown to be stimulated by hypoxia-inducible factors *in vitro* [254, 353]. Using the mouse OIR model, Carmeliet et al. reported that expression of membrane-bound VEGFR-1 was significantly upregulated in retinal vessels during ischemia [163], thus providing further support for an

involvement of VEGFR-1 in mediating the inflammatory response in the hypoxic eye and after VEGF injection. VEGF may act as a chemoattractant for inflammatory cells by ligating and stimulating VEGFR-1, which is expressed on the monocyte/macrophage subpopulation [154, 165]. Indeed, immunostaining of retinal flat mounts using the macrophage marker F4/80 indicated that the majority of leukocytes that adhere to the vessels after VEGF injection are of the monocyte/macrophage lineage. Elevated local VEGF concentrations thus provide recruitment signals for differentiated Flt-1^+ inflammatory cells to home to future or ongoing inflammation. During the recruitment process, monocytes/macrophages become activated and secrete more VEGF and other pro-inflammatory factors, as well as integrins which in turn further promote inflammation [354-356]. The migration of monocytes in response to VEGF has been shown to require a functional VEGFR-1 tyrosine kinase domain [161]. Whether stimulation of this receptor subunit triggers a signaling cascade that results in *de novo* synthesis of gene products which are linked to the migratory activity of these cells has yet to be demonstrated.

From this discussion, it follows that the selective recruitment of leukocytes to VEGF164 may lie in the greater affinity of VEGF164 for VEGFR-1 compared to VEGF120, R14A/R49A and R13A/R14A/R49A. More importantly, the examination of heparin-binding-deficient mutants suggests that, irrespective of the exact mechanism, the ability of VEGF164 to bind to HSPGs in addition to VEGFR-1 is essential for its leukostasis-inducing activity. By binding to these low-affinity receptors on endothelial cells, VEGF164 may provide matrix- or cell-surface-associated guidance cues that facilitate the recruitment and retention of VEGFR-1-positive monocytes to the vessel-wall endothelium. The non-heparin binding VEGF forms would be unable to provide such cues because of

their increased diffusibility. Interestingly, VEGF121 is able to cross-link to VEGFR-2 on HUVE cells but, unlike VEGF164, not to VEGFR-1 [247]. This effect may be due to a lack of a heparin-binding domain which may be required to crosslink with the receptor via cell surface HSPGs. *In vivo*, VEGFR-1 activation by VEGF120 or HBD mutants may therefore only be transient and insufficient to reach a critical threshold level necessary to elicit a certain effect. Lasting VEGFR-1 stimulation able to overcome the weak intrinsic kinase activity [143] may not be attained until the VEGF/VEGFR-1 complex is stabilized by heparan sulfate. VEGF164-induced VEGFR-1 signaling thus sustained can be quantitatively or qualitatively different leading to specific yet unknown effects on gene expression in endothelial cells or monocytes relevant to leukostasis.

Given the above discussion, it is becoming clear that the interaction of VEGF with HSPGs represents a significant component of VEGF biology. With regard to therapeutic intervention, interference with heparin binding of VEGF164/165 may create a viable anti-inflammatory strategy. Agents that specifically target the subdomain within VEGF that has been shown here to amplify inflammation and disease progression in the eye may prove beneficial for patients with ocular vascular disease in which VEGF165 expression predominates. Possible ways of intervention can be the inhibition of VEGF-binding epitopes on glycosaminoglycans by peptide derivatives, or the blockade of residues within the VEGF HBD by small molecule inhibitors and selective glycosaminoglycan mimetics. These alternative approaches may have the benefit of avoiding side effects resulting from pan-VEGF inhibition used in classical anti-VEGF therapies; a feature that may be desirable considering the role of VEGF in survival and homeostasis.

In conclusion, I have shown here evidence indicating that the VEGF164 HBD and its association with heparin-like molecules are required for mediating the pro-inflammatory potential of this isoform. This finding is surprising as glycosaminoglycans are obligate binding partners of several growth factors implicated in developmental rather than pathological processes. Although a link between VEGFR-1 and VEGF-induced leukostasis has been established in this study, contributions from other receptor systems, such as the neuropilins or VEGFR-2, are likely and need to be investigated in more detail. Future studies will also have to address whether heparin binding is relevant to other inflammatory disorders related to VEGF. The present data also provide new insights into the mechanisms regulating the activity of VEGF in ocular disease.

Chapter 6: References

1. Garlanda, C. and E. Dejana, *Heterogeneity of endothelial cells. Specific markers.* Arterioscler Thromb Vasc Biol, 1997. **17**(7): p. 1193-202.
2. Carmeliet, P., *Mechanisms of angiogenesis and arteriogenesis.* Nat Med, 2000. **6**(4): p. 389-95.
3. Thorin, E. and S.M. Shreeve, *Heterogeneity of vascular endothelial cells in normal and disease states.* Pharmacol Ther, 1998. **78**(3): p. 155-66.
4. Abbott, N.J., *Astrocyte-endothelial interactions and blood-brain barrier permeability.* J Anat, 2002. **200**(6): p. 629-38.
5. Kmiec, Z., *Cooperation of liver cells in health and disease.* Adv Anat Embryol Cell Biol, 2001. **161**: p. III-XIII, 1-151.
6. Jain, R.K., *Molecular regulation of vessel maturation.* Nat Med, 2003. **9**(6): p. 685-93.
7. Hellstrom, M., et al., *Lack of pericytes leads to endothelial hyperplasia and abnormal vascular morphogenesis.* J Cell Biol, 2001. **153**(3): p. 543-53.
8. Sottile, J., *Regulation of angiogenesis by extracellular matrix.* Biochim Biophys Acta, 2004. **1654**(1): p. 13-22.
9. Hirschi, K.K. and P.A. D'Amore, *Pericytes in the microvasculature.* Cardiovasc Res, 1996. **32**(4): p. 687-98.
10. Risau, W. and I. Flamme, *Vasculogenesis.* Annu Rev Cell Dev Biol, 1995. **11**: p. 73-91.
11. Risau, W., *Mechanisms of angiogenesis.* Nature, 1997. **386**(6626): p. 671-4.
12. Ferrara, N., *Molecular and biological properties of vascular endothelial growth factor.* J Mol Med, 1999. **77**(7): p. 527-43.
13. Hanahan, D. and J. Folkman, *Patterns and emerging mechanisms of the angiogenic switch during tumorigenesis.* Cell, 1996. **86**(3): p. 353-64.
14. Hudlicka, O., M. Brown, and S. Egginton, *Angiogenesis in skeletal and cardiac muscle.* Physiol Rev, 1992. **72**(2): p. 369-417.
15. Hudlicka, O., *Mechanical factors involved in the growth of the heart and its blood vessels.* Cell Mol Biol Res, 1994. **40**(2): p. 143-52.
16. Bergers, G. and L.E. Benjamin, *Tumorigenesis and the angiogenic switch.* Nat Rev Cancer, 2003. **3**(6): p. 401-10.
17. Carmeliet, P., *Angiogenesis in health and disease.* Nat Med, 2003. **9**(6): p. 653-60.

18. Fruttiger, M., *Development of the mouse retinal vasculature: angiogenesis versus vasculogenesis.* Invest Ophthalmol Vis Sci, 2002. **43**(2): p. 522-7.

19. Claxton, S. and M. Fruttiger, *Role of arteries in oxygen induced vaso-obliteration.* Exp Eye Res, 2003. **77**(3): p. 305-11.

20. Ishida, S., et al., *Leukocytes mediate retinal vascular remodeling during development and vaso-obliteration in disease.* Nat Med, 2003. **9**(6): p. 781-8.

21. Uemura, A., et al., *Angiogenesis in the mouse retina: a model system for experimental manipulation.* Exp Cell Res, 2006. **312**(5): p. 676-83.

22. Gariano, R.F. and T.W. Gardner, *Retinal angiogenesis in development and disease.* Nature, 2005. **438**(7070): p. 960-6.

23. Ferrara, N., H.P. Gerber, and J. LeCouter, *The biology of VEGF and its receptors.* Nat Med, 2003. **9**(6): p. 669-76.

24. Breier, G., et al., *Expression of vascular endothelial growth factor during embryonic angiogenesis and endothelial cell differentiation.* Development, 1992. **114**(2): p. 521-32.

25. Millauer, B., et al., *High affinity VEGF binding and developmental expression suggest Flk-1 as a major regulator of vasculogenesis and angiogenesis.* Cell, 1993. **72**(6): p. 835-46.

26. Peters, K.G., C. De Vries, and L.T. Williams, *Vascular endothelial growth factor receptor expression during embryogenesis and tissue repair suggests a role in endothelial differentiation and blood vessel growth.* Proc Natl Acad Sci U S A, 1993. **90**(19): p. 8915-9.

27. Carmeliet, P., et al., *Abnormal blood vessel development and lethality in embryos lacking a single VEGF allele.* Nature, 1996. **380**(6573): p. 435-9.

28. Ferrara, N., et al., *Heterozygous embryonic lethality induced by targeted inactivation of the VEGF gene.* Nature, 1996. **380**(6573): p. 439-42.

29. Fong, G.H., et al., *Role of the Flt-1 receptor tyrosine kinase in regulating the assembly of vascular endothelium.* Nature, 1995. **376**(6535): p. 66-70.

30. Shalaby, F., et al., *Failure of blood-island formation and vasculogenesis in Flk-1-deficient mice.* Nature, 1995. **376**(6535): p. 62-6.

31. Dumont, D.J., et al., *Cardiovascular failure in mouse embryos deficient in VEGF receptor-3.* Science, 1998. **282**(5390): p. 946-9.

32. Miquerol, L., B.L. Langille, and A. Nagy, *Embryonic development is disrupted by modest increases in vascular endothelial growth factor gene expression.* Development, 2000. **127**(18): p. 3941-6.

33. Ferrara, N., *Vascular endothelial growth factor: basic science and clinical progress.* Endocr Rev, 2004. **25**(4): p. 581-611.

34. Adamis, A.P., et al., *Inhibition of vascular endothelial growth factor prevents retinal ischemia-associated iris neovascularization in a nonhuman primate.* Arch Ophthalmol, 1996. **114**(1): p. 66-71.

35. Gragoudas, E.S., et al., *Pegaptanib for neovascular age-related macular degeneration.* N Engl J Med, 2004. **351**(27): p. 2805-16.

36. Kim, K.J., et al., *Inhibition of vascular endothelial growth factor-induced angiogenesis suppresses tumour growth in vivo.* Nature, 1993. **362**(6423): p. 841-4.

37. Kondo, S., M. Asano, and H. Suzuki, *Significance of vascular endothelial growth factor/vascular permeability factor for solid tumor growth, and its inhibition by the antibody.* Biochem Biophys Res Commun, 1993. **194**(3): p. 1234-41.

38. Millauer, B., et al., *Glioblastoma growth inhibited in vivo by a dominant-negative Flk-1 mutant.* Nature, 1994. **367**(6463): p. 576-9.

39. Ferrara, N., *VEGF and the quest for tumour angiogenesis factors.* Nat Rev Cancer, 2002. **2**(10): p. 795-803.

40. Leung, D.W., et al., *Vascular endothelial growth factor is a secreted angiogenic mitogen.* Science, 1989. **246**(4935): p. 1306-9.

41. Keck, P.J., et al., *Vascular permeability factor, an endothelial cell mitogen related to PDGF.* Science, 1989. **246**(4935): p. 1309-12.

42. Mesri, E.A., H.J. Federoff, and M. Brownlee, *Expression of vascular endothelial growth factor from a defective herpes simplex virus type 1 amplicon vector induces angiogenesis in mice.* Circ Res, 1995. **76**(2): p. 161-7.

43. Phillips, G.D., et al., *Vascular endothelial growth factor (rhVEGF165) stimulates direct angiogenesis in the rabbit cornea.* In Vivo, 1994. **8**(6): p. 961-5.

44. Wu, L.W., et al., *Utilization of distinct signaling pathways by receptors for vascular endothelial cell growth factor and other mitogens in the induction of endothelial cell proliferation.* J Biol Chem, 2000. **275**(7): p. 5096-103.

45. Meadows, K.N., P. Bryant, and K. Pumiglia, *Vascular endothelial growth factor induction of the angiogenic phenotype requires Ras activation.* J Biol Chem, 2001. **276**(52): p. 49289-98.

46. Takahashi, T., et al., *A single autophosphorylation site on KDR/Flk-1 is essential for VEGF-A-dependent activation of PLC-gamma and DNA synthesis in vascular endothelial cells.* EMBO J, 2001. **20**(11): p. 2768-78.

47. Takahashi, T., H. Ueno, and M. Shibuya, *VEGF activates protein kinase C-dependent, but Ras-independent Raf-MEK-MAP kinase pathway for DNA synthesis in primary endothelial cells.* Oncogene, 1999. **18**(13): p. 2221-30.

48. Gliki, G., et al., *Vascular endothelial growth factor-induced prostacyclin production is mediated by a protein kinase C (PKC)-dependent activation of extracellular signal-regulated protein kinases 1 and 2 involving PKC-delta and by mobilization of intracellular Ca2+.* Biochem J, 2001. **353**(Pt 3): p. 503-12.

49. Gerber, H.P., et al., *Vascular endothelial growth factor regulates endothelial cell survival through the phosphatidylinositol 3'-kinase/Akt signal transduction pathway. Requirement for Flk-1/KDR activation.* J Biol Chem, 1998. **273**(46): p. 30336-43.

50. Thakker, G.D., et al., *The role of phosphatidylinositol 3-kinase in vascular endothelial growth factor signaling.* J Biol Chem, 1999. **274**(15): p. 10002-7.

51. Hermann, C., et al., *Insulin-mediated stimulation of protein kinase Akt: A potent survival signaling cascade for endothelial cells.* Arterioscler Thromb Vasc Biol, 2000. **20**(2): p. 402-9.

52. Sugimoto, H., et al., *Neutralization of circulating vascular endothelial growth factor (VEGF) by anti-VEGF antibodies and soluble VEGF receptor 1 (sFlt-1) induces proteinuria.* J Biol Chem, 2003. **278**(15): p. 12605-8.

53. Gerber, H.P., et al., *VEGF is required for growth and survival in neonatal mice.* Development, 1999. **126**(6): p. 1149-59.

54. Ostendorf, T., et al., *VEGF(165) mediates glomerular endothelial repair.* J Clin Invest, 1999. **104**(7): p. 913-23.

55. Mayr-Wohlfart, U., et al., *Vascular endothelial growth factor stimulates chemotactic migration of primary human osteoblasts.* Bone, 2002. **30**(3): p. 472-7.

56. Senger, D.R., et al., *Stimulation of endothelial cell migration by vascular permeability factor/vascular endothelial growth factor through cooperative mechanisms involving the alphavbeta3 integrin, osteopontin, and thrombin.* Am J Pathol, 1996. **149**(1): p. 293-305.

57. Shalaby, F., et al., *A requirement for Flk1 in primitive and definitive hematopoiesis and vasculogenesis.* Cell, 1997. **89**(6): p. 981-90.

58. Clauss, M., et al., *Vascular permeability factor: a tumor-derived polypeptide that induces endothelial cell and monocyte procoagulant activity, and promotes monocyte migration.* J Exp Med, 1990. **172**(6): p. 1535-45.

59. Schwarz, Q., et al., *Vascular endothelial growth factor controls neuronal migration and cooperates with Sema3A to pattern distinct compartments of the facial nerve.* Genes Dev, 2004. **18**(22): p. 2822-34.

60. Cho, N.K., et al., *Developmental control of blood cell migration by the Drosophila VEGF pathway.* Cell, 2002. **108**(6): p. 865-76.

61. Ruhrberg, C., et al., *Spatially restricted patterning cues provided by heparin-binding VEGF-A control blood vessel branching morphogenesis.* Genes Dev, 2002. **16**(20): p. 2684-98.

62. Gerhardt, H., et al., *VEGF guides angiogenic sprouting utilizing endothelial tip cell filopodia.* J Cell Biol, 2003. **161**(6): p. 1163-77.

63. Dobrogowska, D.H., et al., *Increased blood-brain barrier permeability and endothelial abnormalities induced by vascular endothelial growth factor.* J Neurocytol, 1998. **27**(3): p. 163-73.

64. Risau, W., *Development and differentiation of endothelium.* Kidney Int Suppl, 1998. **67**: p. S3-6.

65. Roberts, W.G. and G.E. Palade, *Increased microvascular permeability and endothelial fenestration induced by vascular endothelial growth factor.* J Cell Sci, 1995. **108 (Pt 6)**: p. 2369-79.

66. Rhodin, J.A., *The diaphragm of capillary endothelial fenestrations.* J Ultrastruct Res, 1962. **6**: p. 171-85.

67. Esser, S., et al., *Vascular endothelial growth factor induces endothelial fenestrations in vitro.* J Cell Biol, 1998. **140**(4): p. 947-59.

68. Neufeld, G., et al., *Vascular endothelial growth factor (VEGF) and its receptors.* FASEB J, 1999. **13**(1): p. 9-22.

69. Robinson, C.J. and S.E. Stringer, *The splice variants of vascular endothelial growth factor (VEGF) and their receptors.* J Cell Sci, 2001. **114**(Pt 5): p. 853-65.

70. Goldman, C.K., et al., *Epidermal growth factor stimulates vascular endothelial growth factor production by human malignant glioma cells: a model of glioblastoma multiforme pathophysiology.* Mol Biol Cell, 1993. **4**(1): p. 121-33.

71. Pertovaara, L., et al., *Vascular endothelial growth factor is induced in response to transforming growth factor-beta in fibroblastic and epithelial cells.* J Biol Chem, 1994. **269**(9): p. 6271-4.

72. Finkenzeller, G., et al., *Sp1 recognition sites in the proximal promoter of the human vascular endothelial growth factor gene are essential for platelet-derived growth factor-induced gene expression.* Oncogene, 1997. **15**(6): p. 669-76.

73. Goad, D.L., et al., *Enhanced expression of vascular endothelial growth factor in human SaOS-2 osteoblast-like cells and murine osteoblasts induced by insulin-like growth factor I.* Endocrinology, 1996. **137**(6): p. 2262-8.

74. Kijowski, J., et al., *The SDF-1-CXCR4 axis stimulates VEGF secretion and activates integrins but does not affect proliferation and survival in lymphohematopoietic cells.* Stem Cells, 2001. **19**(5): p. 453-66.

75. Cohen, T., et al., *Interleukin 6 induces the expression of vascular endothelial growth factor.* J Biol Chem, 1996. **271**(2): p. 736-41.

76. Li, J., et al., *Induction of vascular endothelial growth factor gene expression by interleukin-1 beta in rat aortic smooth muscle cells.* J Biol Chem, 1995. **270**(1): p. 308-12.

77. Ryuto, M., et al., *Induction of vascular endothelial growth factor by tumor necrosis factor alpha in human glioma cells. Possible roles of SP-1.* J Biol Chem, 1996. **271**(45): p. 28220-8.

78. Siemeister, G., et al., *Reversion of deregulated expression of vascular endothelial growth factor in human renal carcinoma cells by von Hippel-Lindau tumor suppressor protein.* Cancer Res, 1996. **56**(10): p. 2299-301.

79. Stratmann, R., et al., *Putative control of angiogenesis in hemangioblastomas by the von Hippel-Lindau tumor suppressor gene.* J Neuropathol Exp Neurol, 1997. **56**(11): p. 1242-52.

80. Kieser, A., et al., *Mutant p53 potentiates protein kinase C induction of vascular endothelial growth factor expression.* Oncogene, 1994. **9**(3): p. 963-9.

81. Rak, J., et al., *Oncogenes as inducers of tumor angiogenesis.* Cancer Metastasis Rev, 1995. **14**(4): p. 263-77.

82. Grugel, S., et al., *Both v-Ha-Ras and v-Raf stimulate expression of the vascular endothelial growth factor in NIH 3T3 cells.* J Biol Chem, 1995. **270**(43): p. 25915-9.

83. Plate, K.H., et al., *Vascular endothelial growth factor is a potential tumour angiogenesis factor in human gliomas in vivo.* Nature, 1992. **359**(6398): p. 845-8.

84. Shweiki, D., et al., *Vascular endothelial growth factor induced by hypoxia may mediate hypoxia-initiated angiogenesis.* Nature, 1992. **359**(6398): p. 843-5.

85. Guillemin, K. and M.A. Krasnow, *The hypoxic response: huffing and HIFing.* Cell, 1997. **89**(1): p. 9-12.

86. Dor, Y., R. Porat, and E. Keshet, *Vascular endothelial growth factor and vascular adjustments to perturbations in oxygen homeostasis.* Am J Physiol Cell Physiol, 2001. **280**(6): p. C1367-74.

87. Stone, J., et al., *Development of retinal vasculature is mediated by hypoxia-induced vascular endothelial growth factor (VEGF) expression by neuroglia.* J Neurosci, 1995. **15**(7 Pt 1): p. 4738-47.

88. Ema, M., et al., *A novel bHLH-PAS factor with close sequence similarity to hypoxia-inducible factor 1alpha regulates the VEGF expression and is potentially involved in lung and vascular development.* Proc Natl Acad Sci U S A, 1997. **94**(9): p. 4273-8.

89. Forsythe, J.A., et al., *Activation of vascular endothelial growth factor gene transcription by hypoxia-inducible factor 1.* Mol Cell Biol, 1996. **16**(9): p. 4604-13.

90. Ikeda, E., et al., *Hypoxia-induced transcriptional activation and increased mRNA stability of vascular endothelial growth factor in C6 glioma cells.* J Biol Chem, 1995. **270**(34): p. 19761-6.

91. Shima, D.T., U. Deutsch, and P.A. D'Amore, *Hypoxic induction of vascular endothelial growth factor (VEGF) in human epithelial cells is mediated by increases in mRNA stability.* FEBS Lett, 1995. **370**(3): p. 203-8.

92. Maxwell, P.H., et al., *The tumour suppressor protein VHL targets hypoxia-inducible factors for oxygen-dependent proteolysis.* Nature, 1999. **399**(6733): p. 271-5.

93. Carmeliet, P., et al., *Role of HIF-1alpha in hypoxia-mediated apoptosis, cell proliferation and tumour angiogenesis.* Nature, 1998. **394**(6692): p. 485-90.

94. Iyer, N.V., et al., *Cellular and developmental control of O2 homeostasis by hypoxia-inducible factor 1 alpha.* Genes Dev, 1998. **12**(2): p. 149-62.

95. Shima, D.T., et al., *The mouse gene for vascular endothelial growth factor. Genomic structure, definition of the transcriptional unit, and characterization of transcriptional and post-transcriptional regulatory sequences.* J Biol Chem, 1996. **271**(7): p. 3877-83.

96. Stein, I., et al., *Stabilization of vascular endothelial growth factor mRNA by hypoxia and hypoglycemia and coregulation with other ischemia-induced genes.* Mol Cell Biol, 1995. **15**(10): p. 5363-8.

97. Li, X. and U. Eriksson, *Novel VEGF family members: VEGF-B, VEGF-C and VEGF-D.* Int J Biochem Cell Biol, 2001. **33**(4): p. 421-6.

98. Yamazaki, Y., et al., *Snake venom vascular endothelial growth factors (VEGFs) exhibit potent activity through their specific recognition of KDR (VEGF receptor 2).* J Biol Chem, 2003. **278**(52): p. 51985-8.

99. Lyttle, D.J., et al., *Homologs of vascular endothelial growth factor are encoded by the poxvirus orf virus.* J Virol, 1994. **68**(1): p. 84-92.

100. Gong, B., et al., *Characterization of the zebrafish vascular endothelial growth factor A gene: comparison with vegf-A genes in mammals and Fugu.* Biochim Biophys Acta, 2004. **1676**(1): p. 33-40.

101. Cleaver, O. and P.A. Krieg, *VEGF mediates angioblast migration during development of the dorsal aorta in Xenopus.* Development, 1998. **125**(19): p. 3905-14.

102. Traver, D. and L.I. Zon, *Walking the walk: migration and other common themes in blood and vascular development.* Cell, 2002. **108**(6): p. 731-4.

103. Houck, K.A., et al., *The vascular endothelial growth factor family: identification of a fourth molecular species and characterization of alternative splicing of RNA.* Mol Endocrinol, 1991. **5**(12): p. 1806-14.

104. Tischer, E., et al., *The human gene for vascular endothelial growth factor. Multiple protein forms are encoded through alternative exon splicing.* J Biol Chem, 1991. **266**(18): p. 11947-54.

105. Tischer, E., et al., *Vascular endothelial growth factor: a new member of the platelet-derived growth factor gene family.* Biochem Biophys Res Commun, 1989. **165**(3): p. 1198-206.

106. Poltorak, Z., et al., *VEGF145, a secreted vascular endothelial growth factor isoform that binds to extracellular matrix.* J Biol Chem, 1997. **272**(11): p. 7151-8.

107. Lei, J., A. Jiang, and D. Pei, *Identification and characterization of a new splicing variant of vascular endothelial growth factor: VEGF183.* Biochim Biophys Acta, 1998. **1443**(3): p. 400-6.

108. Bates, D.O., et al., *VEGF165b, an inhibitory splice variant of vascular endothelial growth factor, is down-regulated in renal cell carcinoma.* Cancer Res, 2002. **62**(14): p. 4123-31.

109. Woolard, J., et al., *VEGF165b, an inhibitory vascular endothelial growth factor splice variant: mechanism of action, in vivo effect on angiogenesis and endogenous protein expression.* Cancer Res, 2004. **64**(21): p. 7822-35.

110. Lange, T., et al., *VEGF162, a new heparin-binding vascular endothelial growth factor splice form that is expressed in transformed human cells.* J Biol Chem, 2003. **278**(19): p. 17164-9.

111. McDonald, N.Q. and W.A. Hendrickson, *A structural superfamily of growth factors containing a cystine knot motif.* Cell, 1993. **73**(3): p. 421-4.

112. Muller, Y.A., et al., *The crystal structure of vascular endothelial growth factor (VEGF) refined to 1.93 A resolution: multiple copy flexibility and receptor binding.* Structure, 1997. **5**(10): p. 1325-38.

113. Murray-Rust, J., et al., *Topological similarities in TGF-beta 2, PDGF-BB and NGF define a superfamily of polypeptide growth factors.* Structure, 1993. **1**(2): p. 153-9.

114. Muller, Y.A., et al., *Vascular endothelial growth factor: crystal structure and functional mapping of the kinase domain receptor binding site.* Proc Natl Acad Sci U S A, 1997. **94**(14): p. 7192-7.

115. Siemeister, G., D. Marme, and G. Martiny-Baron, *The alpha-helical domain near the amino terminus is essential for dimerization of vascular endothelial growth factor.* J Biol Chem, 1998. **273**(18): p. 11115-20.

116. Wiesmann, C., et al., *Crystal structure at 1.7 A resolution of VEGF in complex with domain 2 of the Flt-1 receptor.* Cell, 1997. **91**(5): p. 695-704.

117. Siemeister, G., et al., *An antagonistic vascular endothelial growth factor (VEGF) variant inhibits VEGF-stimulated receptor autophosphorylation and proliferation of human endothelial cells.* Proc Natl Acad Sci U S A, 1998. **95**(8): p. 4625-9.

118. Keyt, B.A., et al., *The carboxyl-terminal domain (111-165) of vascular endothelial growth factor is critical for its mitogenic potency.* J Biol Chem, 1996. **271**(13): p. 7788-95.

119. Fairbrother, W.J., et al., *Solution structure of the heparin-binding domain of vascular endothelial growth factor.* Structure, 1998. **6**(5): p. 637-48.

120. Stauffer, M.E., N.J. Skelton, and W.J. Fairbrother, *Refinement of the solution structure of the heparin-binding domain of vascular endothelial growth factor using residual dipolar couplings.* J Biomol NMR, 2002. **23**(1): p. 57-61.

121. Keck, R.G., et al., *Disulfide structure of the heparin binding domain in vascular endothelial growth factor: characterization of posttranslational modifications in VEGF.* Arch Biochem Biophys, 1997. **344**(1): p. 103-13.

122. Anthony, F.W., et al., *Short report: identification of a specific pattern of vascular endothelial growth factor mRNA expression in human placenta and cultured placental fibroblasts.* Placenta, 1994. **15**(5): p. 557-61.

123. Cheung, C.Y., et al., *Vascular endothelial growth factor gene expression in ovine placenta and fetal membranes.* Am J Obstet Gynecol, 1995. **173**(3 Pt 1): p. 753-9.

124. Houck, K.A., et al., *Dual regulation of vascular endothelial growth factor bioavailability by genetic and proteolytic mechanisms.* J Biol Chem, 1992. **267**(36): p. 26031-7.

125. Park, J.E., G.A. Keller, and N. Ferrara, *The vascular endothelial growth factor (VEGF) isoforms: differential deposition into the subepithelial extracellular matrix*

and bioactivity of extracellular matrix-bound VEGF. Mol Biol Cell, 1993. **4**(12): p. 1317-26.

126. Soker, S., et al., *Neuropilin-1 is expressed by endothelial and tumor cells as an isoform-specific receptor for vascular endothelial growth factor.* Cell, 1998. **92**(6): p. 735-45.

127. Gluzman-Poltorak, Z., et al., *Neuropilin-2 is a receptor for the vascular endothelial growth factor (VEGF) forms VEGF-145 and VEGF-165 [corrected].* J Biol Chem, 2000. **275**(24): p. 18040-5.

128. Ferrara, N. and W.J. Henzel, *Pituitary follicular cells secrete a novel heparin-binding growth factor specific for vascular endothelial cells.* Biochem Biophys Res Commun, 1989. **161**(2): p. 851-8.

129. Gospodarowicz, D., J.A. Abraham, and J. Schilling, *Isolation and characterization of a vascular endothelial cell mitogen produced by pituitary-derived folliculo stellate cells.* Proc Natl Acad Sci U S A, 1989. **86**(19): p. 7311-5.

130. Plouet, J., J. Schilling, and D. Gospodarowicz, *Isolation and characterization of a newly identified endothelial cell mitogen produced by AtT-20 cells.* Embo J, 1989. **8**(12): p. 3801-6.

131. Plouet, J., et al., *Extracellular cleavage of the vascular endothelial growth factor 189-amino acid form by urokinase is required for its mitogenic effect.* J Biol Chem, 1997. **272**(20): p. 13390-6.

132. Mott, J.D. and Z. Werb, *Regulation of matrix biology by matrix metalloproteinases.* Curr Opin Cell Biol, 2004. **16**(5): p. 558-64.

133. Lee, S., et al., *Processing of VEGF-A by matrix metalloproteinases regulates bioavailability and vascular patterning in tumors.* J Cell Biol, 2005. **169**(4): p. 681-91.

134. Terman, B.I., et al., *Identification of the KDR tyrosine kinase as a receptor for vascular endothelial cell growth factor.* Biochem Biophys Res Commun, 1992. **187**(3): p. 1579-86.

135. de Vries, C., et al., *The fms-like tyrosine kinase, a receptor for vascular endothelial growth factor.* Science, 1992. **255**(5047): p. 989-91.

136. Shibuya, M., et al., *Nucleotide sequence and expression of a novel human receptor-type tyrosine kinase gene (flt) closely related to the fms family.* Oncogene, 1990. **5**(4): p. 519-24.

137. Terman, B.I., et al., *Identification of a new endothelial cell growth factor receptor tyrosine kinase.* Oncogene, 1991. **6**(9): p. 1677-83.

138. Pajusola, K., et al., *FLT4 receptor tyrosine kinase contains seven immunoglobulin-like loops and is expressed in multiple human tissues and cell lines.* Cancer Res, 1992. **52**(20): p. 5738-43.

139. Finnerty, H., et al., *Molecular cloning of murine FLT and FLT4.* Oncogene, 1993. **8**(8): p. 2293-8.

140. Fuh, G., et al., *Requirements for binding and signaling of the kinase domain receptor for vascular endothelial growth factor.* J Biol Chem, 1998. **273**(18): p. 11197-204.

141. Davis-Smyth, T., et al., *The second immunoglobulin-like domain of the VEGF tyrosine kinase receptor Flt-1 determines ligand binding and may initiate a signal transduction cascade.* EMBO J, 1996. **15**(18): p. 4919-27.

142. Barleon, B., et al., *Mapping of the sites for ligand binding and receptor dimerization at the extracellular domain of the vascular endothelial growth factor receptor FLT-1.* J Biol Chem, 1997. **272**(16): p. 10382-8.

143. Waltenberger, J., et al., *Different signal transduction properties of KDR and Flt1, two receptors for vascular endothelial growth factor.* J Biol Chem, 1994. **269**(43): p. 26988-95.

144. Matsumoto, T. and L. Claesson-Welsh, *VEGF receptor signal transduction.* Sci STKE, 2001. **2001**(112): p. RE21.

145. Guo, D., et al., *Vascular endothelial cell growth factor promotes tyrosine phosphorylation of mediators of signal transduction that contain SH2 domains. Association with endothelial cell proliferation.* J Biol Chem, 1995. **270**(12): p. 6729-33.

146. Kabrun, N., et al., *Flk-1 expression defines a population of early embryonic hematopoietic precursors.* Development, 1997. **124**(10): p. 2039-48.

147. Quinn, T.P., et al., *Fetal liver kinase 1 is a receptor for vascular endothelial growth factor and is selectively expressed in vascular endothelium.* Proc Natl Acad Sci U S A, 1993. **90**(16): p. 7533-7.

148. Schuh, A.C., et al., *In vitro hematopoietic and endothelial potential of flk-1(-/-) embryonic stem cells and embryos.* Proc Natl Acad Sci U S A, 1999. **96**(5): p. 2159-64.

149. Gitay-Goren, H., R. Halaban, and G. Neufeld, *Human melanoma cells but not normal melanocytes express vascular endothelial growth factor receptors.* Biochem Biophys Res Commun, 1993. **190**(3): p. 702-8.

150. Dias, S., et al., *Autocrine stimulation of VEGFR-2 activates human leukemic cell growth and migration.* J Clin Invest, 2000. **106**(4): p. 511-21.

151. Yang, K. and C.L. Cepko, *Flk-1, a receptor for vascular endothelial growth factor (VEGF), is expressed by retinal progenitor cells.* J Neurosci, 1996. **16**(19): p. 6089-99.

152. Sondell, M., G. Lundborg, and M. Kanje, *Vascular endothelial growth factor has neurotrophic activity and stimulates axonal outgrowth, enhancing cell survival and Schwann cell proliferation in the peripheral nervous system.* J Neurosci, 1999. **19**(14): p. 5731-40.

153. Hattori, K., et al., *Placental growth factor reconstitutes hematopoiesis by recruiting VEGFR1(+) stem cells from bone-marrow microenvironment.* Nat Med, 2002. **8**(8): p. 841-9.

154. Sawano, A., et al., *Flt-1, vascular endothelial growth factor receptor 1, is a novel cell surface marker for the lineage of monocyte-macrophages in humans.* Blood, 2001. **97**(3): p. 785-91.

155. Fong, G.H., et al., *Increased hemangioblast commitment, not vascular disorganization, is the primary defect in flt-1 knock-out mice.* Development, 1999. **126**(13): p. 3015-25.

156. Olofsson, B., et al., *Vascular endothelial growth factor B (VEGF-B) binds to VEGF receptor-1 and regulates plasminogen activator activity in endothelial cells.* Proc Natl Acad Sci U S A, 1998. **95**(20): p. 11709-14.

157. Landgren, E., et al., *Placenta growth factor stimulates MAP kinase and mitogenicity but not phospholipase C-gamma and migration of endothelial cells expressing Flt 1.* Oncogene, 1998. **16**(3): p. 359-67.

158. Park, J.E., et al., *Placenta growth factor. Potentiation of vascular endothelial growth factor bioactivity, in vitro and in vivo, and high affinity binding to Flt-1 but not to Flk-1/KDR.* J Biol Chem, 1994. **269**(41): p. 25646-54.

159. Gille, H., et al., *A repressor sequence in the juxtamembrane domain of Flt-1 (VEGFR-1) constitutively inhibits vascular endothelial growth factor-dependent phosphatidylinositol 3'-kinase activation and endothelial cell migration.* EMBO J, 2000. **19**(15): p. 4064-73.

160. Gille, H., et al., *Analysis of biological effects and signaling properties of Flt-1 (VEGFR-1) and KDR (VEGFR-2). A reassessment using novel receptor-specific vascular endothelial growth factor mutants.* J Biol Chem, 2001. **276**(5): p. 3222-30.

161. Hiratsuka, S., et al., *Flt-1 lacking the tyrosine kinase domain is sufficient for normal development and angiogenesis in mice.* Proc Natl Acad Sci U S A, 1998. **95**(16): p. 9349-54.

162. Zeng, H., H.F. Dvorak, and D. Mukhopadhyay, *Vascular permeability factor (VPF)/vascular endothelial growth factor (VEGF) peceptor-1 down-modulates VPF/VEGF receptor-2-mediated endothelial cell proliferation, but not migration, through phosphatidylinositol 3-kinase-dependent pathways.* J Biol Chem, 2001. **276**(29): p. 26969-79.

163. Carmeliet, P., et al., *Synergism between vascular endothelial growth factor and placental growth factor contributes to angiogenesis and plasma extravasation in pathological conditions.* Nat Med, 2001. **7**(5): p. 575-83.

164. Kendall, R.L. and K.A. Thomas, *Inhibition of vascular endothelial cell growth factor activity by an endogenously encoded soluble receptor.* Proc Natl Acad Sci U S A, 1993. **90**(22): p. 10705-9.

165. Barleon, B., et al., *Migration of human monocytes in response to vascular endothelial growth factor (VEGF) is mediated via the VEGF receptor flt-1.* Blood, 1996. **87**(8): p. 3336-43.

166. Clauss, M., et al., *The vascular endothelial growth factor receptor Flt-1 mediates biological activities. Implications for a functional role of placenta growth factor in monocyte activation and chemotaxis.* J Biol Chem, 1996. **271**(30): p. 17629-34.

167. Selvaraj, S.K., et al., *Mechanism of monocyte activation and expression of proinflammatory cytochemokines by placenta growth factor.* Blood, 2003. **102**(4): p. 1515-24.

168. Luttun, A., et al., *Revascularization of ischemic tissues by PlGF treatment, and inhibition of tumor angiogenesis, arthritis and atherosclerosis by anti-Flt1.* Nat Med, 2002. **8**(8): p. 831-40.

169. Autiero, M., et al., *Role of PlGF in the intra- and intermolecular cross talk between the VEGF receptors Flt1 and Flk1.* Nat Med, 2003. **9**(7): p. 936-43.

170. Davis-Smyth, T., L.G. Presta, and N. Ferrara, *Mapping the charged residues in the second immunoglobulin-like domain of the vascular endothelial growth factor/placenta growth factor receptor Flt-1 required for binding and structural stability.* J Biol Chem, 1998. **273**(6): p. 3216-22.

171. Christinger, H.W., et al., *The crystal structure of placental growth factor in complex with domain 2 of vascular endothelial growth factor receptor-1.* J Biol Chem, 2004. **279**(11): p. 10382-8.

172. Hiratsuka, S., et al., *Involvement of Flt-1 tyrosine kinase (vascular endothelial growth factor receptor-1) in pathological angiogenesis.* Cancer Res, 2001. **61**(3): p. 1207-13.

173. Mamluk, R., et al., *Neuropilin-1 binds vascular endothelial growth factor 165, placenta growth factor-2, and heparin via its b1b2 domain.* J Biol Chem, 2002. **277**(27): p. 24818-25.

174. Neufeld, G., et al., *The neuropilins: multifunctional semaphorin and VEGF receptors that modulate axon guidance and angiogenesis.* Trends Cardiovasc Med, 2002. **12**(1): p. 13-9.

175. He, Z. and M. Tessier-Lavigne, *Neuropilin is a receptor for the axonal chemorepellent Semaphorin III.* Cell, 1997. **90**(4): p. 739-51.

176. Kolodkin, A.L., et al., *Neuropilin is a semaphorin III receptor.* Cell, 1997. **90**(4): p. 753-62.

177. Tamagnone, L., et al., *Plexins are a large family of receptors for transmembrane, secreted, and GPI-anchored semaphorins in vertebrates.* Cell, 1999. **99**(1): p. 71-80.

178. Takahashi, T., et al., *Plexin-neuropilin-1 complexes form functional semaphorin-3A receptors.* Cell, 1999. **99**(1): p. 59-69.

179. Kitsukawa, T., et al., *Overexpression of a membrane protein, neuropilin, in chimeric mice causes anomalies in the cardiovascular system, nervous system and limbs.* Development, 1995. **121**(12): p. 4309-18.

180. Kawasaki, T., et al., *A requirement for neuropilin-1 in embryonic vessel formation.* Development, 1999. **126**(21): p. 4895-902.

181. Lee, P., et al., *Neuropilin-1 is required for vascular development and is a mediator of VEGF-dependent angiogenesis in zebrafish.* Proc Natl Acad Sci U S A, 2002. **99**(16): p. 10470-5.

182. Migdal, M., et al., *Neuropilin-1 is a placenta growth factor-2 receptor.* J Biol Chem, 1998. **273**(35): p. 22272-8.

183. Makinen, T., et al., *Differential binding of vascular endothelial growth factor B splice and proteolytic isoforms to neuropilin-1.* J Biol Chem, 1999. **274**(30): p. 21217-22.

184. Wise, L.M., et al., *Vascular endothelial growth factor (VEGF)-like protein from orf virus NZ2 binds to VEGFR2 and neuropilin-1.* Proc Natl Acad Sci U S A, 1999. **96**(6): p. 3071-6.

185. Whitaker, G.B., B.J. Limberg, and J.S. Rosenbaum, *Vascular endothelial growth factor receptor-2 and neuropilin-1 form a receptor complex that is responsible for the differential signaling potency of VEGF(165) and VEGF(121).* J Biol Chem, 2001. **276**(27): p. 25520-31.

186. Fuh, G., K.C. Garcia, and A.M. de Vos, *The interaction of neuropilin-1 with vascular endothelial growth factor and its receptor flt-1.* J Biol Chem, 2000. **275**(35): p. 26690-5.

187. Mac Gabhann, F. and A.S. Popel, *Differential binding of VEGF isoforms to VEGF receptor 2 in the presence of neuropilin-1: a computational model.* Am J Physiol Heart Circ Physiol, 2005. **288**(6): p. H2851-60.

188. Chiang, M.K. and J.G. Flanagan, *Interactions between the Flk-1 receptor, vascular endothelial growth factor, and cell surface proteoglycan identified with a soluble receptor reagent.* Growth Factors, 1995. **12**(1): p. 1-10.

189. Dougher, A.M., et al., *Identification of a heparin binding peptide on the extracellular domain of the KDR VEGF receptor.* Growth Factors, 1997. **14**(4): p. 257-68.

190. Bagnard, D., et al., *Semaphorin 3A-vascular endothelial growth factor-165 balance mediates migration and apoptosis of neural progenitor cells by the recruitment of shared receptor.* J Neurosci, 2001. **21**(10): p. 3332-41.

191. Gu, C., et al., *Neuropilin-1 conveys semaphorin and VEGF signaling during neural and cardiovascular development.* Dev Cell, 2003. **5**(1): p. 45-57.

192. Bernfield, M., et al., *Biology of the syndecans: a family of transmembrane heparan sulfate proteoglycans.* Annu Rev Cell Biol, 1992. **8**: p. 365-93.

193. Iozzo, R.V., *Heparan sulfate proteoglycans: intricate molecules with intriguing functions.* J Clin Invest, 2001. **108**(2): p. 165-7.

194. Bernfield, M., et al., *Functions of cell surface heparan sulfate proteoglycans.* Annu Rev Biochem, 1999. **68**: p. 729-77.

195. Esko, J.D. and U. Lindahl, *Molecular diversity of heparan sulfate.* J Clin Invest, 2001. **108**(2): p. 169-73.

196. Esko, J.D. and S.B. Selleck, *Order out of chaos: assembly of ligand binding sites in heparan sulfate.* Annu Rev Biochem, 2002. **71**: p. 435-71.

197. Mulloy, B. and R.J. Linhardt, *Order out of complexity--protein structures that interact with heparin.* Curr Opin Struct Biol, 2001. **11**(5): p. 623-8.

198. Lindahl, U. and L. Kjellen, *Heparin or heparan sulfate--what is the difference?* Thromb Haemost, 1991. **66**(1): p. 44-8.

199. Merry, C.L., et al., *Highly sensitive sequencing of the sulfated domains of heparan sulfate.* J Biol Chem, 1999. **274**(26): p. 18455-62.

200. Hacker, U., K. Nybakken, and N. Perrimon, *Heparan sulphate proteoglycans: the sweet side of development.* Nat Rev Mol Cell Biol, 2005. **6**(7): p. 530-41.

201. Turnbull, J.E. and J.T. Gallagher, *Distribution of iduronate 2-sulphate residues in heparan sulphate. Evidence for an ordered polymeric structure.* Biochem J, 1991. **273 (Pt 3)**: p. 553-9.

202. Lortat-Jacob, H., J.E. Turnbull, and J.A. Grimaud, *Molecular organization of the interferon gamma-binding domain in heparan sulphate.* Biochem J, 1995. **310 (Pt 2)**: p. 497-505.

203. Spillmann, D., D. Witt, and U. Lindahl, *Defining the interleukin-8-binding domain of heparan sulfate.* J Biol Chem, 1998. **273**(25): p. 15487-93.

204. Stringer, S.E. and J.T. Gallagher, *Specific binding of the chemokine platelet factor 4 to heparan sulfate.* J Biol Chem, 1997. **272**(33): p. 20508-14.

205. Capila, I. and R.J. Linhardt, *Heparin-protein interactions.* Angew Chem Int Ed Engl, 2002. **41**(3): p. 391-412.

206. Whisstock, J.C., et al., *Conformational changes in serpins: II. The mechanism of activation of antithrombin by heparindagger.* J Mol Biol, 2000. **301**(5): p. 1287-305.

207. Capila, I., et al., *Annexin V--heparin oligosaccharide complex suggests heparan sulfate--mediated assembly on cell surfaces.* Structure (Camb), 2001. **9**(1): p. 57-64.

208. Faham, S., et al., *Heparin structure and interactions with basic fibroblast growth factor.* Science, 1996. **271**(5252): p. 1116-20.

209. Cardin, A.D. and H.J. Weintraub, *Molecular modeling of protein-glycosaminoglycan interactions.* Arteriosclerosis, 1989. **9**(1): p. 21-32.

210. Margalit, H., N. Fischer, and S.A. Ben-Sasson, *Comparative analysis of structurally defined heparin binding sequences reveals a distinct spatial distribution of basic residues.* J Biol Chem, 1993. **268**(26): p. 19228-31.

211. Powell, A.K., et al., *Interactions of heparin/heparan sulfate with proteins: appraisal of structural factors and experimental approaches.* Glycobiology, 2004. **14**(4): p. 17R-30R.

212. Plante, O.J., E.R. Palmacci, and P.H. Seeberger, *Automated synthesis of polysaccharides.* Methods Enzymol, 2003. **369**: p. 235-48.

213. Turnbull, J., A. Powell, and S. Guimond, *Heparan sulfate: decoding a dynamic multifunctional cell regulator.* Trends Cell Biol, 2001. **11**(2): p. 75-82.

214. Sasisekharan, R. and G. Venkataraman, *Heparin and heparan sulfate: biosynthesis, structure and function.* Curr Opin Chem Biol, 2000. **4**(6): p. 626-31.

215. Nakato, H. and K. Kimata, *Heparan sulfate fine structure and specificity of proteoglycan functions.* Biochim Biophys Acta, 2002. **1573**(3): p. 312-8.

216. Pye, D.A., et al., *Heparan sulfate oligosaccharides require 6-O-sulfation for promotion of basic fibroblast growth factor mitogenic activity.* J Biol Chem, 1998. **273**(36): p. 22936-42.

217. Guimond, S., et al., *Activating and inhibitory heparin sequences for FGF-2 (basic FGF). Distinct requirements for FGF-1, FGF-2, and FGF-4.* J Biol Chem, 1993. **268**(32): p. 23906-14.

218. Rusnati, M., et al., *Distinct role of 2-O-, N-, and 6-O-sulfate groups of heparin in the formation of the ternary complex with basic fibroblast growth factor and soluble FGF receptor-1.* Biochem Biophys Res Commun, 1994. **203**(1): p. 450-8.

219. Ono, K., et al., *Structural features in heparin that interact with VEGF165 and modulate its biological activity.* Glycobiology, 1999. **9**(7): p. 705-11.

220. Ornitz, D.M., et al., *Heparin is required for cell-free binding of basic fibroblast growth factor to a soluble receptor and for mitogenesis in whole cells.* Mol Cell Biol, 1992. **12**(1): p. 240-7.

221. Soker, S., et al., *Variations in the size and sulfation of heparin modulate the effect of heparin on the binding of VEGF165 to its receptors.* Biochem Biophys Res Commun, 1994. **203**(2): p. 1339-47.

222. Robinson, C.J., et al., *VEGF165-binding sites within heparan sulfate encompass two highly sulfated domains and can be liberated by K5 lyase.* J Biol Chem, 2006. **281**(3): p. 1731-40.

223. Baeg, G.H., et al., *The Wingless morphogen gradient is established by the cooperative action of Frizzled and Heparan Sulfate Proteoglycan receptors.* Dev Biol, 2004. **276**(1): p. 89-100.

224. Binari, R.C., et al., *Genetic evidence that heparin-like glycosaminoglycans are involved in wingless signaling.* Development, 1997. **124**(13): p. 2623-32.

225. The, I., Y. Bellaiche, and N. Perrimon, *Hedgehog movement is regulated through tout velu-dependent synthesis of a heparan sulfate proteoglycan.* Mol Cell, 1999. **4**(4): p. 633-9.

226. Kamimura, K., et al., *Regulation of Notch signaling by Drosophila heparan sulfate 3-O sulfotransferase.* J Cell Biol, 2004. **166**(7): p. 1069-79.

227. Kirkpatrick, C.A., et al., *Spatial regulation of Wingless morphogen distribution and signaling by Dally-like protein.* Dev Cell, 2004. **7**(4): p. 513-23.

228. Inatani, M., et al., *Mammalian brain morphogenesis and midline axon guidance require heparan sulfate.* Science, 2003. **302**(5647): p. 1044-6.

229. Gengrinovitch, S., et al., *Glypican-1 is a VEGF165 binding proteoglycan that acts as an extracellular chaperone for VEGF165.* J Biol Chem, 1999. **274**(16): p. 10816-22.

230. Iozzo, R.V. and J.D. San Antonio, *Heparan sulfate proteoglycans: heavy hitters in the angiogenesis arena.* J Clin Invest, 2001. **108**(3): p. 349-55.

231. Whitelock, J.M., et al., *The degradation of human endothelial cell-derived perlecan and release of bound basic fibroblast growth factor by stromelysin, collagenase, plasmin, and heparanases.* J Biol Chem, 1996. **271**(17): p. 10079-86.

232. Zatterstrom, U.K., et al., *Collagen XVIII/endostatin structure and functional role in angiogenesis.* Cell Struct Funct, 2000. **25**(2): p. 97-101.

233. Yayon, A., et al., *Cell surface, heparin-like molecules are required for binding of basic fibroblast growth factor to its high affinity receptor.* Cell, 1991. **64**(4): p. 841-8.

234. Linhardt, R.J., *2003 Claude S. Hudson Award address in carbohydrate chemistry. Heparin: structure and activity.* J Med Chem, 2003. **46**(13): p. 2551-64.

235. Schlessinger, J., I. Lax, and M. Lemmon, *Regulation of growth factor activation by proteoglycans: what is the role of the low affinity receptors?* Cell, 1995. **83**(3): p. 357-60.

236. Lander, A.D., *Proteoglycans: master regulators of molecular encounter?* Matrix Biol, 1998. **17**(7): p. 465-72.

237. Walker, A., J.E. Turnbull, and J.T. Gallagher, *Specific heparan sulfate saccharides mediate the activity of basic fibroblast growth factor.* J Biol Chem, 1994. **269**(2): p. 931-5.

238. Gallagher, J.T., *Heparan sulfate: growth control with a restricted sequence menu.* J Clin Invest, 2001. **108**(3): p. 357-61.

239. Proudfoot, A.E., et al., *Glycosaminoglycan binding and oligomerization are essential for the in vivo activity of certain chemokines.* Proc Natl Acad Sci U S A, 2003. **100**(4): p. 1885-90.

240. Handel, T.M., et al., *Regulation of protein function by glycosaminoglycans--as exemplified by chemokines.* Annu Rev Biochem, 2005. **74**: p. 385-410.

241. Shriver, Z., D. Liu, and R. Sasisekharan, *Emerging views of heparan sulfate glycosaminoglycan structure/activity relationships modulating dynamic biological functions.* Trends Cardiovasc Med, 2002. **12**(2): p. 71-7.

242. Middleton, J., et al., *Leukocyte extravasation: chemokine transport and presentation by the endothelium.* Blood, 2002. **100**(12): p. 3853-60.

243. Witt, D.P. and A.D. Lander, *Differential binding of chemokines to glycosaminoglycan subpopulations.* Curr Biol, 1994. **4**(5): p. 394-400.

244. Mertens, G., et al., *Cell surface heparan sulfate proteoglycans from human vascular endothelial cells. Core protein characterization and antithrombin III binding properties.* J Biol Chem, 1992. **267**(28): p. 20435-43.

245. Kinsella, M.G. and T.N. Wight, *Structural characterization of heparan sulfate proteoglycan subclasses isolated from bovine aortic endothelial cell cultures.* Biochemistry, 1988. **27**(6): p. 2136-44.

246. Kojima, T., et al., *Isolation and characterization of heparan sulfate proteoglycans produced by cloned rat microvascular endothelial cells.* J Biol Chem, 1992. **267**(7): p. 4859-69.

247. Gitay-Goren, H., et al., *Selective binding of VEGF121 to one of the three vascular endothelial growth factor receptors of vascular endothelial cells.* J Biol Chem, 1996. **271**(10): p. 5519-23.

248. Gitay-Goren, H., et al., *The binding of vascular endothelial growth factor to its receptors is dependent on cell surface-associated heparin-like molecules.* J Biol Chem, 1992. **267**(9): p. 6093-8.

249. Ashikari-Hada, S., et al., *Heparin Regulates Vascular Endothelial Growth Factor165-dependent Mitogenic Activity, Tube Formation, and Its Receptor Phosphorylation of Human Endothelial Cells: COMPARISON OF THE EFFECTS OF HEPARIN AND MODIFIED HEPARINS.* J Biol Chem, 2005. **280**(36): p. 31508-15.

250. Tessler, S., et al., *Heparin modulates the interaction of VEGF165 with soluble and cell associated flk-1 receptors.* J Biol Chem, 1994. **269**(17): p. 12456-61.

251. Terman, B., et al., *VEGF receptor subtypes KDR and FLT1 show different sensitivities to heparin and placenta growth factor.* Growth Factors, 1994. **11**(3): p. 187-95.

252. Cohen, T., et al., *VEGF121, a vascular endothelial growth factor (VEGF) isoform lacking heparin binding ability, requires cell-surface heparan sulfates for efficient binding to the VEGF receptors of human melanoma cells.* J Biol Chem, 1995. **270**(19): p. 11322-6.

253. Ito, N. and L. Claesson-Welsh, *Dual effects of heparin on VEGF binding to VEGF receptor-1 and transduction of biological responses.* Angiogenesis, 1999. **3**(2): p. 159-66.

254. Stalmans, I., et al., *Arteriolar and venular patterning in retinas of mice selectively expressing VEGF isoforms.* J Clin Invest, 2002. **109**(3): p. 327-36.

255. Hutchings, H., N. Ortega, and J. Plouet, *Extracellular matrix-bound vascular endothelial growth factor promotes endothelial cell adhesion, migration, and survival through integrin ligation.* FASEB J, 2003. **17**(11): p. 1520-2.

256. Bernatchez, P.N., et al., *Relative effects of VEGF-A and VEGF-C on endothelial cell proliferation, migration and PAF synthesis: Role of neuropilin-1.* J Cell Biochem, 2002. **85**(3): p. 629-39.

257. Ferrara, N., *The role of VEGF in the regulation of physiological and pathological angiogenesis.* EXS, 2005(94): p. 209-31.

258. Bergers, G., et al., *Matrix metalloproteinase-9 triggers the angiogenic switch during carcinogenesis.* Nat Cell Biol, 2000. **2**(10): p. 737-44.

259. Guo, P., et al., *Vascular endothelial growth factor isoforms display distinct activities in promoting tumor angiogenesis at different anatomic sites.* Cancer Res, 2001. **61**(23): p. 8569-77.

260. Cheng, S.Y., et al., *Intracerebral tumor-associated hemorrhage caused by overexpression of the vascular endothelial growth factor isoforms VEGF121 and VEGF165 but not VEGF189.* Proc Natl Acad Sci U S A, 1997. **94**(22): p. 12081-7.

261. Mori, A., et al., *Vascular endothelial growth factor-induced tumor angiogenesis and tumorigenicity in relation to metastasis in a HT1080 human fibrosarcoma cell model.* Int J Cancer, 1999. **80**(5): p. 738-43.

262. Zhang, H.T., et al., *The 121 amino acid isoform of vascular endothelial growth factor is more strongly tumorigenic than other splice variants in vivo.* Br J Cancer, 2000. **83**(1): p. 63-8.

263. Grunstein, J., et al., *Isoforms of vascular endothelial growth factor act in a coordinate fashion To recruit and expand tumor vasculature.* Mol Cell Biol, 2000. **20**(19): p. 7282-91.

264. Cressey, R., et al., *Alteration of protein expression pattern of vascular endothelial growth factor (VEGF) from soluble to cell-associated isoform during tumourigenesis.* BMC Cancer, 2005. **5**: p. 128.

265. Lee, Y.H., et al., *Cell-retained isoforms of vascular endothelial growth factor (VEGF) are correlated with poor prognosis in osteosarcoma.* Eur J Cancer, 1999. **35**(7): p. 1089-93.

266. Tokunaga, T., et al., *Vascular endothelial growth factor (VEGF) mRNA isoform expression pattern is correlated with liver metastasis and poor prognosis in colon cancer.* Br J Cancer, 1998. **77**(6): p. 998-1002.

267. Aiello, L.P., et al., *Vascular endothelial growth factor in ocular fluid of patients with diabetic retinopathy and other retinal disorders.* N Engl J Med, 1994. **331**(22): p. 1480-7.

268. Aiello, L.P., et al., *Suppression of retinal neovascularization in vivo by inhibition of vascular endothelial growth factor (VEGF) using soluble VEGF-receptor chimeric proteins.* Proc Natl Acad Sci U S A, 1995. **92**(23): p. 10457-61.

269. Krzystolik, M.G., et al., *Prevention of experimental choroidal neovascularization with intravitreal anti-vascular endothelial growth factor antibody fragment.* Arch Ophthalmol, 2002. **120**(3): p. 338-46.

270. Adamis, A.P., L.P. Aiello, and R.A. D'Amato, *Angiogenesis and ophthalmic disease.* Angiogenesis, 1999. **3**(1): p. 9-14.

271. Stone, J., et al., *Roles of vascular endothelial growth factor and astrocyte degeneration in the genesis of retinopathy of prematurity.* Invest Ophthalmol Vis Sci, 1996. **37**(2): p. 290-9.

272. McColm, J.R., P. Geisen, and M.E. Hartnett, *VEGF isoforms and their expression after a single episode of hypoxia or repeated fluctuations between hyperoxia and hypoxia: relevance to clinical ROP.* Mol Vis, 2004. **10**: p. 512-20.

273. Ishida, S., et al., *VEGF164-mediated inflammation is required for pathological, but not physiological, ischemia-induced retinal neovascularization.* J Exp Med, 2003. **198**(3): p. 483-9.

274. Smith, L.E., et al., *Oxygen-induced retinopathy in the mouse.* Invest Ophthalmol Vis Sci, 1994. **35**(1): p. 101-11.

275. Usui, T., et al., *VEGF164(165) as the pathological isoform: differential leukocyte and endothelial responses through VEGFR1 and VEGFR2.* Invest Ophthalmol Vis Sci, 2004. **45**(2): p. 368-74.

276. Miyamoto, K., et al., *Vascular endothelial growth factor (VEGF)-induced retinal vascular permeability is mediated by intercellular adhesion molecule-1 (ICAM-1).* Am J Pathol, 2000. **156**(5): p. 1733-9.

277. Tordjman, R., et al., *A neuronal receptor, neuropilin-1, is essential for the initiation of the primary immune response.* Nat Immunol, 2002. **3**(5): p. 477-82.

278. Ishida, S., et al., *VEGF164 is proinflammatory in the diabetic retina.* Invest Ophthalmol Vis Sci, 2003. **44**(5): p. 2155-62.

279. Qaum, T., et al., *VEGF-initiated blood-retinal barrier breakdown in early diabetes.* Invest Ophthalmol Vis Sci, 2001. **42**(10): p. 2408-13.

280. Ishida, S., et al., *Coexpression of VEGF receptors VEGF-R2 and neuropilin-1 in proliferative diabetic retinopathy.* Invest Ophthalmol Vis Sci, 2000. **41**(7): p. 1649-56.

281. Wung, J.L. and N.R. Gascoigne, *Antibody screening for secreted proteins expressed in Pichia pastoris.* Biotechniques, 1996. **21**(5): p. 808, 810, 812.

282. Linder, S., M. Schliwa, and E. Kube-Granderath, *Direct PCR screening of Pichia pastoris clones.* Biotechniques, 1996. **20**(6): p. 980-2.

283. Livak, K.J. and T.D. Schmittgen, *Analysis of relative gene expression data using real-time quantitative PCR and the 2(-Delta Delta C(T)) Method.* Methods, 2001. **25**(4): p. 402-8.

284. Carmeliet, P., et al., *Impaired myocardial angiogenesis and ischemic cardiomyopathy in mice lacking the vascular endothelial growth factor isoforms VEGF164 and VEGF188.* Nat Med, 1999. **5**(5): p. 495-502.

285. Edgington, T.S., et al., *The molecular biology of initiation of coagulation by tissue factor.* Curr Stud Hematol Blood Transfus, 1991(58): p. 15-21.

286. Carmeliet, P., et al., *Role of tissue factor in embryonic blood vessel development.* Nature, 1996. **383**(6595): p. 73-5.

287. Zhang, Y., et al., *Tissue factor controls the balance of angiogenic and antiangiogenic properties of tumor cells in mice.* J Clin Invest, 1994. **94**(3): p. 1320-7.

288. Mackman, N., *Regulation of the tissue factor gene.* FASEB J, 1995. **9**(10): p. 883-9.

289. Mechtcheriakova, D., et al., *Vascular endothelial cell growth factor-induced tissue factor expression in endothelial cells is mediated by EGR-1.* Blood, 1999. **93**(11): p. 3811-23.

290. Shen, B.Q., et al., *Vascular endothelial growth factor KDR receptor signaling potentiates tumor necrosis factor-induced tissue factor expression in endothelial cells.* J Biol Chem, 2001. **276**(7): p. 5281-6.

291. Pelton, J.T. and L.R. McLean, *Spectroscopic methods for analysis of protein secondary structure.* Anal Biochem, 2000. **277**(2): p. 167-76.

292. Sreerama, N. and R.W. Woody, *Computation and analysis of protein circular dichroism spectra.* Methods Enzymol, 2004. **383**: p. 318-51.

293. Andrade, M.A., et al., *Evaluation of secondary structure of proteins from UV circular dichroism spectra using an unsupervised learning neural network.* Protein Eng, 1993. **6**(4): p. 383-90.

294. Kuschert, G.S., et al., *Identification of a glycosaminoglycan binding surface on human interleukin-8.* Biochemistry, 1998. **37**(32): p. 11193-201.

295. Ashikari-Hada, S., et al., *Characterization of growth factor-binding structures in heparin/heparan sulfate using an octasaccharide library.* J Biol Chem, 2004. **279**(13): p. 12346-54.

296. Mourey, L., et al., *Crystal structure of cleaved bovine antithrombin III at 3.2 A resolution.* J Mol Biol, 1993. **232**(1): p. 223-41.

297. Lander, A.D., *Targeting the glycosaminoglycan-binding sites on proteins.* Chem Biol, 1994. **1**(2): p. 73-8.

298. van Tilbeurgh, H., et al., *Lipoprotein lipase. Molecular model based on the pancreatic lipase x-ray structure: consequences for heparin binding and catalysis.* J Biol Chem, 1994. **269**(6): p. 4626-33.

299. Eriksson, A.E., L.S. Cousens, and B.W. Matthews, *Refinement of the structure of human basic fibroblast growth factor at 1.6 A resolution and analysis of presumed heparin binding sites by selenate substitution.* Protein Sci, 1993. **2**(8): p. 1274-84.

300. Mascotti, D.P. and T.M. Lohman, *Thermodynamics of charged oligopeptide-heparin interactions.* Biochemistry, 1995. **34**(9): p. 2908-15.

301. Soker, S., et al., *Characterization of novel vascular endothelial growth factor (VEGF) receptors on tumor cells that bind VEGF165 via its exon 7-encoded domain.* J Biol Chem, 1996. **271**(10): p. 5761-7.

302. Giger, R.J., et al., *Neuropilin-2 is a receptor for semaphorin IV: insight into the structural basis of receptor function and specificity.* Neuron, 1998. **21**(5): p. 1079-92.

303. Lee, C.C., et al., *Crystal structure of the human neuropilin-1 b1 domain.* Structure (Camb), 2003. **11**(1): p. 99-108.

304. West, D.C., et al., *Interactions of multiple heparin binding growth factors with neuropilin-1 and potentiation of the activity of fibroblast growth factor-2.* J Biol Chem, 2005. **280**(14): p. 13457-64.

305. Nicosia, R.F. and A. Ottinetti, *Growth of microvessels in serum-free matrix culture of rat aorta. A quantitative assay of angiogenesis in vitro.* Lab Invest, 1990. **63**(1): p. 115-22.

306. Auerbach, R., et al., *Angiogenesis assays: a critical overview.* Clin Chem, 2003. **49**(1): p. 32-40.

307. Auerbach, R., W. Auerbach, and I. Polakowski, *Assays for angiogenesis: a review.* Pharmacol Ther, 1991. **51**(1): p. 1-11.

308. Nicosia, R.F. and S. Villaschi, *Rat aortic smooth muscle cells become pericytes during angiogenesis in vitro.* Lab Invest, 1995. **73**(5): p. 658-66.

309. Saunders, S. and M. Bernfield, *Cell surface proteoglycan binds mouse mammary epithelial cells to fibronectin and behaves as a receptor for interstitial matrix.* J Cell Biol, 1988. **106**(2): p. 423-30.

310. Wijelath, E.S., et al., *Novel vascular endothelial growth factor binding domains of fibronectin enhance vascular endothelial growth factor biological activity.* Circ Res, 2002. **91**(1): p. 25-31.

311. Goerges, A.L. and M.A. Nugent, *pH regulates vascular endothelial growth factor binding to fibronectin: a mechanism for control of extracellular matrix storage and release.* J Biol Chem, 2004. **279**(3): p. 2307-15.

312. Keyt, B.A., et al., *Identification of vascular endothelial growth factor determinants for binding KDR and FLT-1 receptors. Generation of receptor-selective VEGF variants by site-directed mutagenesis.* J Biol Chem, 1996. **271**(10): p. 5638-46.

313. Meyer, M., et al., *A novel vascular endothelial growth factor encoded by Orf virus, VEGF-E, mediates angiogenesis via signalling through VEGFR-2 (KDR) but not VEGFR-1 (Flt-1) receptor tyrosine kinases.* EMBO J, 1999. **18**(2): p. 363-74.

314. de Winter, F., et al., *Expression of class-3 semaphorins and their receptors in the neonatal and adult rat retina.* Invest Ophthalmol Vis Sci, 2004. **45**(12): p. 4554-62.

315. Kim, I., et al., *Constitutive expression of VEGF, VEGFR-1, and VEGFR-2 in normal eyes.* Invest Ophthalmol Vis Sci, 1999. **40**(9): p. 2115-21.

316. Tolentino, M.J., et al., *Vascular endothelial growth factor is sufficient to produce iris neovascularization and neovascular glaucoma in a nonhuman primate.* Arch Ophthalmol, 1996. **114**(8): p. 964-70.

317. Tolentino, M.J., et al., *Intravitreous injections of vascular endothelial growth factor produce retinal ischemia and microangiopathy in an adult primate.* Ophthalmology, 1996. **103**(11): p. 1820-8.

318. Okamoto, N., et al., *Transgenic mice with increased expression of vascular endothelial growth factor in the retina: a new model of intraretinal and subretinal neovascularization.* Am J Pathol, 1997. **151**(1): p. 281-91.

319. Shibuya, M., *Vascular endothelial growth factor receptor family genes: when did the three genes phylogenetically segregate?* Biol Chem, 2002. **383**(10): p. 1573-9.

320. Oura, H., et al., *A critical role of placental growth factor in the induction of inflammation and edema formation.* Blood, 2003. **101**(2): p. 560-7.

321. Adamis, A.P. and D.T. Shima, *The role of vascular endothelial growth factor in ocular health and disease.* Retina, 2005. **25**(2): p. 111-8.

322. Shima, D.T., et al., *Hypoxic induction of endothelial cell growth factors in retinal cells: identification and characterization of vascular endothelial growth factor (VEGF) as the mitogen.* Mol Med, 1995. **1**(2): p. 182-93.

323. Tolentino, M.J., et al., *Pathologic features of vascular endothelial growth factor-induced retinopathy in the nonhuman primate.* Am J Ophthalmol, 2002. **133**(3): p. 373-85.

324. Sunderkotter, C., et al., *Macrophages and angiogenesis.* J Leukoc Biol, 1994. **55**(3): p. 410-22.

325. Jackson, J.R., et al., *The codependence of angiogenesis and chronic inflammation.* FASEB J, 1997. **11**(6): p. 457-65.

326. McLeod, D.S., et al., *Localization of VEGF receptor-2 (KDR/Flk-1) and effects of blocking it in oxygen-induced retinopathy.* Invest Ophthalmol Vis Sci, 2002. **43**(2): p. 474-82.

327. Erlich, R.B., et al., *Major glycosaminoglycan species in the developing retina: synthesis, tissue distribution and effects upon cell death.* Exp Eye Res, 2003. **77**(2): p. 157-65.

328. Bollineni, J.S., I. Alluru, and A.S. Reddi, *Heparan sulfate proteoglycan synthesis and its expression are decreased in the retina of diabetic rats.* Curr Eye Res, 1997. **16**(2): p. 127-30.

329. Koga, T., et al., *Expression of glycosaminoglycans during development of the rat retina.* Curr Eye Res, 2003. **27**(2): p. 75-83.

330. Marmor, M.F., A. Negi, and D.M. Maurice, *Kinetics of macromolecules injected into the subretinal space.* Exp Eye Res, 1985. **40**(5): p. 687-96.

331. Jakeman, L.B., et al., *Binding sites for vascular endothelial growth factor are localized on endothelial cells in adult rat tissues.* J Clin Invest, 1992. **89**(1): p. 244-53.

332. Johnson, Z., et al., *Interference with heparin binding and oligomerization creates a novel anti-inflammatory strategy targeting the chemokine system.* J Immunol, 2004. **173**(9): p. 5776-85.

333. Qiao, D., et al., *Heparan sulfate proteoglycans as regulators of fibroblast growth factor-2 signaling in brain endothelial cells. Specific role for glypican-1 in glioma angiogenesis.* J Biol Chem, 2003. **278**(18): p. 16045-53.

334. Lundin, L., et al., *Differential tyrosine phosphorylation of fibroblast growth factor (FGF) receptor-1 and receptor proximal signal transduction in response to FGF-2 and heparin.* Exp Cell Res, 2003. **287**(1): p. 190-8.

335. Lundin, L., et al., *Selectively desulfated heparin inhibits fibroblast growth factor-induced mitogenicity and angiogenesis.* J Biol Chem, 2000. **275**(32): p. 24653-60.

336. Kim, I., et al., *Vascular endothelial growth factor expression of intercellular adhesion molecule 1 (ICAM-1), vascular cell adhesion molecule 1 (VCAM-1), and E-selectin through nuclear factor-kappa B activation in endothelial cells.* J Biol Chem, 2001. **276**(10): p. 7614-20.

337. Melder, R.J., et al., *During angiogenesis, vascular endothelial growth factor and basic fibroblast growth factor regulate natural killer cell adhesion to tumor endothelium.* Nat Med, 1996. **2**(9): p. 992-7.

338. Rollin, S., et al., *VEGF-mediated endothelial P-selectin translocation: role of VEGF receptors and endogenous PAF synthesis.* Blood, 2004. **103**(10): p. 3789-97.

339. Marumo, T., V.B. Schini-Kerth, and R. Busse, *Vascular endothelial growth factor activates nuclear factor-kappaB and induces monocyte chemoattractant protein-1 in bovine retinal endothelial cells.* Diabetes, 1999. **48**(5): p. 1131-7.

340. Lee, T.H., et al., *Vascular endothelial growth factor modulates neutrophil transendothelial migration via up-regulation of interleukin-8 in human brain microvascular endothelial cells.* J Biol Chem, 2002. **277**(12): p. 10445-51.

341. Croll, S.D., et al., *VEGF-mediated inflammation precedes angiogenesis in adult brain.* Exp Neurol, 2004. **187**(2): p. 388-402.

342. Yoshida, S., et al., *Role of MCP-1 and MIP-1alpha in retinal neovascularization during postischemic inflammation in a mouse model of retinal neovascularization.* J Leukoc Biol, 2003. **73**(1): p. 137-44.

343. Lu, M., et al., *VEGF increases retinal vascular ICAM-1 expression in vivo.* Invest Ophthalmol Vis Sci, 1999. **40**(8): p. 1808-12.

344. Miyamoto, K., et al., *Prevention of leukostasis and vascular leakage in streptozotocin-induced diabetic retinopathy via intercellular adhesion molecule-1 inhibition.* Proc Natl Acad Sci U S A, 1999. **96**(19): p. 10836-41.

345. Meerschaert, J. and M.B. Furie, *The adhesion molecules used by monocytes for migration across endothelium include CD11a/CD18, CD11b/CD18, and VLA-4 on monocytes and ICAM-1, VCAM-1, and other ligands on endothelium.* J Immunol, 1995. **154**(8): p. 4099-112.

346. Robbins, S.G., V.S. Rajaratnam, and J.S. Penn, *Evidence for upregulation and redistribution of vascular endothelial growth factor (VEGF) receptors flt-1 and flk-1 in the oxygen-injured rat retina.* Growth Factors, 1998. **16**(1): p. 1-9.

347. Gariano, R.F., D. Hu, and J. Helms, *Expression of angiogenesis-related genes during retinal development.* Gene Expr Patterns, 2006. **6**(2): p. 187-92.

348. Soker, S., et al., *Inhibition of vascular endothelial growth factor (VEGF)-induced endothelial cell proliferation by a peptide corresponding to the exon 7-encoded domain of VEGF165.* J Biol Chem, 1997. **272**(50): p. 31582-8.

349. Ishihama, H., et al., *Colocalization of neuropilin-1 and Flk-1 in retinal neovascularization in a mouse model of retinopathy.* Invest Ophthalmol Vis Sci, 2001. **42**(6): p. 1172-8.

350. Kunstfeld, R., et al., *Induction of cutaneous delayed-type hypersensitivity reactions in VEGF-A transgenic mice results in chronic skin inflammation associated with persistent lymphatic hyperplasia.* Blood, 2004. **104**(4): p. 1048-57.

351. Witmer, A.N., et al., *Altered expression patterns of VEGF receptors in human diabetic retina and in experimental VEGF-induced retinopathy in monkey.* Invest Ophthalmol Vis Sci, 2002. **43**(3): p. 849-57.

352. Witmer, A.N., et al., *Expression of vascular endothelial growth factor receptors 1, 2, and 3 in quiescent endothelia.* J Histochem Cytochem, 2002. **50**(6): p. 767-77.

353. Gerber, H.P., et al., *Differential transcriptional regulation of the two vascular endothelial growth factor receptor genes. Flt-1, but not Flk-1/KDR, is up-regulated by hypoxia.* J Biol Chem, 1997. **272**(38): p. 23659-67.

354. Iijima, K., et al., *Human mesangial cells and peripheral blood mononuclear cells produce vascular permeability factor.* Kidney Int, 1993. **44**(5): p. 959-66.

355. Moldovan, L. and N.I. Moldovan, *Role of monocytes and macrophages in angiogenesis.* EXS, 2005(94): p. 127-46.

356. Heil, M., et al., *Vascular endothelial growth factor (VEGF) stimulates monocyte migration through endothelial monolayers via increased integrin expression.* Eur J Cell Biol, 2000. **79**(11): p. 850-7.

357. Wise, L.M., et al., ***Viral vascular endothelial growth factors vary extensively in amino acid sequence, receptor-binding specificities, and the ability to induce vascular permeability yet are uniformly active mitogens.*** J Biol Chem, 2003. **278**(39): p. 38004-14.